ATR1 effectors versus RPP1 receptors: From natural variation to functional diversity

Dissertation

der Mathematisch-Naturwissenschaftlichen Fakultät

der Eberhard Karls Universität Tübingen

zur Erlangung des Grades eines

Doktors der Naturwissenschaften

(Dr. rer. nat.)

vorgelegt von

Miriam Lucke

aus Tuttlingen

Tübingen

2025

Gedruckt mit Genehmigung der Mathematisch-Naturwissenschaftlichen Fakultät der Eberhard Karls Universität Tübingen.

Tag der mündlichen Qualifikation:	02.10.2025
Dekan:	Prof. Dr. Thilo Stehle
1. Berichterstatter/-in:	Prof. Dr. Detlef Weigel
2. Berichterstatter/-in:	Prof. Dr. Heike Brötz-Oesterhelt

Summary

The ability to adapt rapidly to changes in their biotic environment is essential for any organism. While plants host many different strains of bacteria, they also carry other organisms, such as viruses and filamentous eukaryotic organisms. Some of these may be pathogenic to their host, including oomycetes, which cause drastic disease outbreaks in many crops (Kamoun et al., 2014). An example is *Phytophthora infestans*, responsible for devastating late blight on tomato and potato (Dong & Zhou, 2022). To prevent such outbreaks, we must first understand the exact nature of the relationship between pathogen and host. An excellent model for oomycete-plant interactions is the *Hyaloperonospora arabidopsidis - Arabidopsis thaliana* pathosystem. The oomycete *H. arabidopsidis* is an obligate biotroph that is highly specific to *A. thaliana*, being unable to colonize other hosts (Coates & Beynon 2010).

Like many other pathogens, *H. arabidopsidis* transfers so-called effectors into the plant, proteins that can manipulate plant immunity and physiology. The plant has in turn developed mechanisms to deploy intracellular receptors that recognize the effectors and counter the suppression of the immune response. This interaction between pathogen effectors and host receptors is crucial for understanding the co-evolution between both organisms. The sequences of both receptors and effectors can vary significantly among different *A. thaliana* individuals and *H. arabidopsidis* isolates, as the interaction between these proteins often hinges on single amino acid substitutions. Both effector and receptor sequences thus are subject to strong selection pressures, resulting in high diversity across genomes. A prominent example of a highly variable effector-receptor pair in the *H. arabidopsidis - A. thaliana* pathosystem is the effector ARABIDOPSIS THALIANA RECOGNIZED 1 (ATR1) and its receptor RECOGNITION OF PERONOSPORA PARASITICA 1 (RPP1) (Botella et al., 1998). Upon ATR1 binding, RPP1 forms tetramers, now known as resistosomes. Their structure was solved only in 2020, by cryo-EM (Ma et al., 2020). Despite the ATR1/RPP1 interaction having been studied for more than 20 years, only four host RPP1 variants and four *H. arabidopsidis* ATR1 variants have been characterized in depth, and another 12 *ATR1* alleles were identified through population genomics and ecotype screens.

This thesis focuses on ATR1/RPP1 co-evolution by systematic annotation of *ATR1* and *RPP1* alleles in large-scale samples of over 100 European-wide collected

H. arabidopsidis strains and over 200 long-read sequenced *A. thaliana* genomes. I highlight the locus-wide similarities and differences in *RPP1*. I also predict ATR1-interacting RPP1 receptor variants and test a subset of these by co-expressing them with different ATR1 alleles. To understand the biological relevance of the highly-diverse *RPP1* locus, located on chromosome 3, in context with *H. arabidopsidis* pathogenicity, I perform genetic analyses and identify possible loci for resistance on chromosome 1 and 4. Lastly, I investigate an *A. thaliana* population lacking the *RPP1* locus and show that RPP1-deficient plants do not seem to perform worse in terms of *H. arabidopsidis* resistance compared to *RPP1*-containing plants. My results contribute to our understanding of the complexity of this pathosystem and shed new light on the species-wide diversity in the highly variable *RPP1* locus of *A. thaliana*.

Zusammenfassung

Die Fähigkeit, sich schnell an abiotische und biotische Veränderungen anzupassen, ist für Pflanzen und ihr Mikrobiom aufgrund ihrer sessilen Natur unerlässlich. Pflanzen beherbergen zwar viele verschiedene Bakterienstämme, tragen aber auch viele andere Organismen in sich, wie z. B. Pilze, Viren und Oomyceten. Einige von ihnen können für ihren Wirt schädlich sein, wie Oomyceten (Kamoun et al., 2014). Es wurde berichtet, dass sie drastische Ausbrüche bei Kulturpflanzen verursachen, z. B. bei dem Oomyceten *Phytophthora infestans*, der für die verheerende Kraut- und Knollenfäule von Tomaten und Kartoffeln verantwortlich ist (Dong & Zhou 2022). Um solche drastischen Ausbrüche zu verhindern, ist zunächst das Verstehen der engen Beziehung zwischen Erreger und Wirt erforderlich. Ein gutes Modellsystem, um diese Wechselwirkungen zu untersuchen, sind *Hyaloperonospora arabidopsidis* – *Arabidopsidis thaliana*. Der Oomycete *H. arabidopsidis* ist ein obligater biotroph, der hochspezifisch für *A. thaliana* und ist nicht in der Lage ist, andere Wirte zu besiedeln (Coates & Beynon 2010).

Wie andere Krankheitserreger sekretieren *H. arabidopsidis* sogenannte Effektoren in die Pflanze, Proteine, die das pflanzliche Immunnetzwerk manipulieren können. Die Pflanze hat wiederum Mechanismen entwickelt, um intrazelluläre Rezeptoren einzusetzen, um invasiven Effektoren zuerkennen und die Immunantwort zu aktivieren. Diese Interaktion zwischen Erregereffektoren und Wirtsrezeptoren ist entscheidend für die Koevolution zwischen beiden Organismen. Die Sequenzen sowohl der Rezeptoren als auch der Effektoren können zwischen verschiedenen *A. thaliana*-Pflanzen und *H. arabidopsidis* Isolaten erheblich variieren, da die Interaktion zwischen diesen Proteinen oft von einzelnen Aminosäuresubstitutionen abhängt, die auch die Resistenz des Wirts beeinflussen können. Diese Sequenzen unterliegen einem starken Selektionsdruck, was zu einer hohen Diversität zwischen den Genomen führt.

Ein prominentes Beispiel für ein hochvariables Effektor-Rezeptor-Paar im Pathosystem von *H. arabidopsidis* - *A. thaliana* ist der Effektor ARABIDOPSIS THALIANA RECOGNIZED 1 (ATR1) und der Rezeptor RESISTANT TO PERONOSPORA PARASITICA 1 (RPP1). Bei der Bindung von ATR1 bildet RPP1 ein Tetramer, das als Resistosom bekannt ist, eine Struktur, die erst im Jahr 2020 durch Kryo-EM aufgelöst wurde (Ma et al., 2020). Die Bedeutung der ATR1/RPP1-

Interaktion wurde durch die Induktion der Resistenz von *A. thaliana* gegen *H. arabidopsidis* durch stabile Transformation eines RPP1-Allels demonstriert, das das entsprechende ATR1-Allel detektiert (Rehmany et al., 2005). Diese Interaktion ist stark allel-spezifisch. Obwohl die ATR1/RPP1-Interaktion seit mehr als 20 Jahren untersucht wird, sind die öffentlich zugänglichen genetischen Ressourcen auf vier *A. thaliana* Linien und vier *H. arabidopsidis*-Isolate beschränkt und reichen nach wie vor nicht aus, um den Einfluss zu verstehen, den die Diversität sowohl auf dem Effektor als auch auf den Rezeptor auf die gemeinsamen Evolutionsprozesse zwischen beiden Organismen hat.

Diese Arbeit befasst sich mit der ATR1/RPP1-Koevolution durch systematische Annotation von ATR1 und RPP1 in groß angelegten Sammlungen von über 100 europaweit gesammelten *H. arabidopsidis* und über 200 global LONG-READ sequenzierten *A. thaliana*-Genomen. Ich habe die Genlokus Ähnlichkeiten und Unterschiede in *RPP1* hervorgehoben, sowie auf funktionaler Ebene ATR1-interagierende RPP1-Rezeptoren vorhergesagt und entsprechend Repräsentanten getestet, durch Ko-Exprimierungen in Tabak. Um die biologische Relevanz des hochdiversifizierten *RPP1*-Lokus im Zusammenhang mit der Pathogenität von *H. arabidopsidis* zu verstehen, führte ich genetische Analysen durch und identifizierte mögliche alternative Genregionen zu *RPP1*, die für Resistenz zu *H. arabidopsidis* eine große Rolle spielen können, diese befinden sich auf Chromosom 1 und 4.

Zudem untersuchte ich eine *A. thaliana*-Population, in der *RPP1* Lokus fehlte, und zeigte, dass *RPP1*-fehlende Pflanzen höhere Resistenzen gegen *H. arabidopsidis* aufweisen können. Diese Ergebnisse machen einen bedeutenden Fortschritt in unserem Verständnis der Komplexität dieses Pathosystems aus und werfen ein neues Licht auf einen hochvariablen Lokus *RPP1*.

Acknowledgements

I would like to thank first and foremost my supervisor Detlef Weigel, he has been great and very motivating especially when I started my PhD during the difficult time of the Pandemic. During my PhD he gave me lots of guidance, support and scientific freedom which I highly appreciated. Many thanks to Rebecca Schwab from whom I received lots of guidance and advice, she was the go-to person for sudden science questions and was just amazing in helping to solve every challenge no matter from what level, she also helped me with sampling. A special thanks goes also to all the people who made the life and lab during the pandemic more joyful and were very helpful during my PhD: Adrián Contreras, Lei Li, Derek Lundberg, Sophia Schwarz, Natalie Betz, Alejandra Duque, Lukas Maischak, Erica Dinatale, Haim Ashkenazy, Ilja Bezrukov, Andrea Sajuthi., Max Collenberg, Thanvi Srikant, Pablo Carbonell, Sebastian Vorbrugg, Oliver Deusch and Anja Barth. Thanks also to Fiona Paul and Diep Tran for their beautiful documentation of their work and availability for discussions.

Throughout my PhD, Haim Ashkenazy was always very open for discussion and gave me lots of scientific advice and code. Together with Luisa Teasdale we had many sessions just discussing RPP1 sequences. Katrin Fritschi and Fernando Rabanal I am thanking for re-sequencing IP-Moa-0.

Thanks to my super helpful Hiwis, especially Alexa-Maria Wangler who thought me sometimes more than I wanted to teach her, Lea Wöllner and Christian Hartmann, for their technical help. Rui Wu for her training during my undergrad. Lei Li for his Chinese protocols.

I would like to thank all the people involved in the Pathodopsis sampling trip and sequencing of all these pathogens in 2018, Bridgit Waithaka-Vasiljević and Sergio Latorre have been great sampling partners. Throughout the years I had several people sitting right next to me and with whom I shared the day-to-day life – Lukas Burkhardt, Wanyan Xi, Edward Kiegle, Patience Chatukuta, Daniela Ramirez. Thanks to you all for making frustrating times wonderful. Of course, also those at the benches around me: Shanshan Wang, Helena Pfingst, Wagner Fagundes, Natalie Betz and Sheila Roitman. Shanshan Wang for being so great scientifically, socially and leaving me in the lab was a nice butt-kick to finally write my thesis, many kisses also to Shanshanshan. Sheila Roitman and her amazing family for giving me at least once a week a proper dinner. Andrea Movilli thanks a lot for all the scientific discussions and

pranks. Many thanks go also to Gal Ofir for constantly asking about my manuscript and giving valuable scientific input. Same goes for Zhigui Bao, who always told me that I have enough data to write this thesis.
Farid El-Kasmi and his lab deserve big thanks for providing all the plants and being a great TAC member. Together with him, Heike Brötz-Oesterhelt, Martin Bayer and Detlef Weigel, we had very fruitful discussions.
I would like to thank all the people during my thesis writing phase for input Alejandra Duque, Edward Kiegle, Shanshan Wang, Sheila Roitman, Helena Pfingst, Patrick Boppert, Eirik Lågeide and Rebecca Schwab!
Thanks to more people outside the laboratory, I need to thank: Kee Hoon Sohn for providing me with plasmids for the pEDV experiments, Henriette Lässle from Jane Parker's lab for teaching me co-infection experiments – vortexing. Mohamed El-Walid from Ed Buckler's lab who taught me the basics of protein analysis, of course thanks to Ed Buckler who allowed me to stay in his lab for 2 months.
From meetings at conferences and symposiums, special thanks go to Eunyoung Chae for pushing me to look into IP-Moa-0 accession, Ksenia Krasileva for lots of new ideas and perspectives.

Big thanks to my family for their support, friends from home, and my partner.

Table of Contents

1. Background

1.1 Plant defenses against pathogens

1.1.1 Extra- and intracellular mechanisms for pathogen defense

Plants have evolved a variety of defense mechanisms to counteract pathogen invasion, including mechanical barriers, hormonal signaling, and molecular recognition systems. The first line of defense typically involves physical barriers, such as the epidermal cuticle and cell wall, which form a structural shield against the entry of the invader. However, many microorganisms pathogens - such as bacteria, fungi and oomycetes, can breach these barriers by entering through natural openings like stomata and colonizing the apoplastic space, a region that hosts not only microbial invaders but also a complex milieu of signaling molecules, hormones, and metabolites (Hacquard et al., 2017; Jones & Dangl, 2006; Pieterse et al., 2012; Yu et al., 2024).

Embedded within the plasma membrane are pattern recognition receptors (PRRs) that detect microbial-associated molecular patterns (MAMPs) that are usually shared across many taxa, such as bacterial flagellin peptides and peptidoglycans and fungal chitin fragments. Upon recognition, these receptors initiate a basal immune response known as pattern-triggered immunity (PTI) (Couto & Zipfel, 2016; Jones & Dangl, 2006; Macho & Zipfel, 2014), which activates downstream defense signaling cascades, often mediated by mitogen-activated protein kinases (MAPKs) and calcium signaling pathways and reactive oxygen burst (ROS) (Sang & Macho, 2017). While PTI offers broad-spectrum protection against many pathogens, adapted pathogens have evolved virulence strategies to evade or suppress this immune layer. For instance, bacteria use the type III secretion system (T3SS) to deliver proteins directly into plant cells. These molecules, known as effectors, often function to suppress immune responses and facilitate the colonization process (Jiménez-Guerrero et al., 2015; Pieterse et al., 2014).

To detect intracellularly delivered effectors, plants have evolved additional immune surveillance mechanisms. Specifically, plants use intracellular immune receptors called nucleotide-binding leucine-rich repeat proteins (NLRs), which directly or indirectly recognize the presence of effectors and lead to effector-triggered

immunity (ETI). While qualitatively similar to PTI, ETI represents a more robust immune response and is often associated with localized programmed cell death, termed the hypersensitive response (HR). (Förderer & Kourelis, 2023; Jones & Dangl, 2006; Y. Liu et al., 2023). This response helps to limit pathogen spread by sacrificing infected or cells next to the infection site. ETI is considered a hallmark of plant immunity and often provides strong, race-specific resistance against pathogens.

Although PTI and ETI were initially viewed as two distinct and largely independent layers of plant immunity, increasing evidence suggests extensive crosstalk and mutual reinforcement between these pathways. PRRs and NLRs are interconnected through multiple signaling systems. Moreover, PRR and NLR signaling can act synergistically through the simultaneous detection of extracellular and intracellular pathogen signals (Ngou et al., 2021, 2022). PTI and ETI are known to share signaling components, further blurring the distinction between them. For example, BAK1 and SOBIR1, membrane-bound co-receptors involved in PTI, can activate the PHYTOALEXIN-DEFICIENT 4/ ENHANCED DISEASE SUSCEPTIBILITY 1 / ACTIVATED DISEASE RESISTANCE 1 (PAD4/EDS1/ADR1) module, a signaling node previously thought to be exclusive to NLR-mediated ETI (Pruitt et al., 2021).

In addition to localized immune responses, plants can initiate systemic immunity, which prepares distal tissues for potential pathogen attack. This systemic response is often primed by ETI, particularly through the activation of TIR-NLRs, which promote the accumulation of SA and enhance basal defense responses (Bhandari et al., 2019; Lapin et al., 2020).

1.1.2 Different Types of NLRs and Their Regulation

Nucleotide-binding leucine-rich repeat receptors (NLRs) are key components of plant immunity (Busche & Laflamme, 2024; Ercolano et al., 2022; F. Jacob et al., 2013).

In plants, NLRs vary widely in structure and function; some act as sensor NLRs, directly or indirectly recognizing pathogenic effectors, while others function as helper NLRs, transducing signals from sensor NLRs to initiate downstream immune responses. Both classes share three conserved domains: a central nucleotide-binding (NB) domain, an apoptotic protease activating factor 1 (APAF-1)/Resistance (R)/Cell Death Protein 4 (CED-4) (ARC) domain, and a C terminal leucine-rich repeat (LRR) domain. At their N termini, many NLRs contain either a Toll/interleukin-1 receptor (TIR)

domain or a coiled-coil (CC) domain. A distinct clade of NLRs has variant CC domains of the RPW8 type, called CC_R domains (Castel et al., 2019).

Upon activation, typically through pathogen effector recognition, NLRs trigger a complex immune signaling cascade involving transcriptomic reprogramming, reactive oxygen species (ROS) production, salicylic acid (SA) accumulation, and hypersensitive cell death (HR) at the site of infection, leading to resistance (Caillaud et al., 2013).

TIR-NLRs

TIR domains are known for NAD^+ hydrolysis and are found throughout all domains of life (Nimma et al., 2021; Essuman et al., 2022; Maekawa et al., 2011). For instance, in animals, TIR domains function as non-enzymatic adaptors through TIR–TIR interactions, activating intracellular signaling complexes and mediating inflammatory responses or cell death (Nimma et al., 2021). In humans, one well-known TIR domain protein is SARM1, which regulates neurodegeneration and functions as a NAD^+-hydrolyzing enzyme (Essuman et al., 2017). In bacteria, TIR enzymatic modules serve in immune responses against bacteriophage infection (Wein & Sorek, 2022).

Recently, the 'Thoeris' anti-phage resistance mechanism was discovered in numerous microbial genomes (Tamulaitiene et al., 2024; Ofir et al., 2021). It involves dimerization of TIR domains, including a sensor TIR-containing protein that hydrolyzes NAD^+. In *Bacillus subtilis*, the TIR dimer ThsB hydrolyzes NAD^+ and produces a cADPR derivative that activates ThsA, triggering a cell death response (Tamulaitiene et al., 2024; Wein and Sorek, 2022).

Plants share close homologs of TIR-NLRs across algae, bryophytes, lycophytes, monilophytes, gymnosperms, and dicots (Maruta et al., 2022; Chia & Carella, 2023; Chia, Kourelis et al., 2024). In *Arabidopsis thaliana*, around 70 TIR-NLRs have been identified (Van de Weyer et al., 2019). Structurally and mechanistically well-characterized examples include RPP1 in *A. thaliana* and ROQ1 (RECOGNITION OF XOPQ1) in *Nicotiana benthamiana* (Harant et al., 2022a; Ma et al., 2020; Martin et al., 2020; Schultink et al., 2017). A unique feature of TIR-NLRs is the C terminal jelly roll/Ig-like domain (C-JID), which contributes to effector binding and protein stability (Ma et al., 2020).

RPP1 is activated through effector binding at the LRR domain, which triggers a conformational change that allows tetramerization via asymmetric TIR homodimers forming a BB-loop (Ma et al., 2020). The resulting P-loop, alongside the α2 and β2 loops from the right protomer with nucleotide-binding (NBD) and winged helix domains (WHD), creates two active NAD^+-cleaving sites (Song et al., 2024; Ma et al., 2020). Their enzymatic activity generates signaling molecules such as phosphoribosyl adenosine mono/diphosphate (pRib-AMP/ADP) and di-ADPR or ADP-ribosylated ATP (ADPr-ATP), which activate downstream receptor complexes (Jia et al., 2022).

TIR-only proteins, which lack effector-sensing domains, share identical downstream signaling components with complete NLRs (Song et al., 2024). For example, RBA1, consisting only of a TIR domain, triggers cell death upon recognizing HopBA1 (Nishimura et al., 2017). Another example is TN2, a TIR-NB protein that guards EXO70B1, a component of the plant exocyst complex (N. Liu et al., 2017). Insights into NLR biology have also come from the study of polymorphisms. Natural mutations in the TIR and NB-ARC domains of flax (*Linum usitatissimum*) immune receptors L6 and L7 were demonstrated to alter recognition of the AvrL567 effector from rust fungi (Bernoux et al., 2011, 2016; Williams et al., 2014). These studies laid the groundwork for identifying autoactive minimal TIR domains in other cases, including *A. thaliana* RPP1 (Schreiber et al., 2016a).

Pathogens such as *Pseudomonas* have evolved effectors (e.g., HopAM1, HopBY) that interfere with NAD^+-dependent signaling by generating cyclic ADPR variants, thereby suppressing TIR-NLR–mediated immunity (Eastman et al., 2022; Hulin et al., 2023; Manik et al., 2022).

Not all TIR-NLRs function as homomers; many act in sensor–executor pairs. For example, the RPS4/RRS1 TIR-NLR pair recognizes effectors such as AvrRps4 from *Pseudomonas syringae* and PopP2 from *Ralstonia solanacearum* (Birker et al., 2009; Deslandes et al., 2003; Gassmann et al., 1999; Narusaka et al., 2009). CHILLING SENSITIVE 3–CONSTITUTIVE SHADE AVOIDANCE 1 (CHS3–CSA1) is another TIR-NLR pair forming a heterodimer through the AE interface and BB-loop via head-to-head interaction (Yang et al., 2022).

CC-NLRs

Unlike TIR-NLRs, CC-NLRs do not always require helper NLRs to induce cell death (Chang et al., 2022). In *A. thaliana*, up to 20 CC-NLRs have been reported (Van de

Weyer et al., 2019), including HOPZ-ACTIVATED RESISTANCE 1 (ZAR1), a well-studied CC-NLR that functions as both a sensor and executor of immune signaling.

The structure of ZAR1 has been resolved using cryo-electron microscopy (cryo-EM) (Bi et al., 2021; Adachi et al., 2020; Laflamme et al., 2020; Lewis et al., 2010; Schultink et al., 2019; Seto et al., 2017; Wang et al., 2015; Wang et al., 2019; Hu et al., 2020). Upon effector recognition, ZAR1 forms a pentameric resistosome complex with RESISTANCE-RELATED KINASE 1 (RKS1) and the uridylated decoy PBL2, a modification mediated by the effector AvrAC (Wang et al., 2019; Hu et al., 2020). This complex localizes to the plasma membrane and acts as a calcium-permeable channel, triggering a cell death response (Bi et al., 2021). A similar mechanism has also been found in wheat through the Sr35 resistosome (Förderer et al., 2022).

In the *Solanaceae* family, NRCs (NLR required for cell death) play a critical role in CC-NLR-mediated immunity (van Wersch et al., 2019). Members like NRC1, NRC2, NRC3, NRC4, and NRCX confer resistance to a broad spectrum of pathogens (Wu et al., 2016; Wu et al., 2017).

The MADA motif, conserved in ~25% (Adachi et al., 2019) of flowering plant NLRs, is crucial for pore-forming activity. Mutations in this motif can alter NLR function and specificity (Ahn et al., 2023; Contreras et al., 2023; Förderer et al., 2022; Harant et al., 2022).

Helper NLRs

N required gene 1 (NRG1) was the first described helper NLR, identified in *Nicotiana benthamiana* via virus-induced gene silencing (VIGS) screen as essential for the function of the TIR-NB-LRR protein N, which mediates resistance to tobacco mosaic virus (TMV) (Peart et al., 2005). Helper NLRs share homology to fungal and animal membrane pore-forming proteins and feature a N terminal CC_{HeLo} domain (named after HET-S and LOP-B) (Daskalov et al., 2016), which shares sequence and structural similarity with the four-helix bundle (4HB) of the mammalian cell death executor MLKL and the CC domains of plant helper NLRs, including the RPW8-like coiled-coil domain. Helper NLRs can be divided into two subgroups: NRG1 and activated disease resistance 1 (ADR1) (Jubic et al., 2019).

In *Arabidopsis*, Resistance to Powdery Mildew 8 (RPW8) amino acid residues in the CC_{HeLo} domain have been shown to target the host membrane, leading to localization and execution of cell death (Wang et al., 2013). Similarly, in *Nicotiana*

benthamiana, a MADA motif, consisting of the first 29 amino acids at the N-terminus, is required for helper function within the NRC4 network (Wang et al., 2019; Adachi et al., 2019).

Helper NLRs can oligomerize into funnel-like structures that mediate cell death independently of EDS1 signaling, particularly in autoactive mutants (P. Jacob et al., 2021; F. Liu et al., 2024; Xiao et al., 2025). As mentioned earlier, sensors like RPP1 and other TIR-NLRs require downstream helper NLRs for execution of the cell death response (Gantner et al., 2019).

EDS1 forms a heterodimer with either PAD4 or SAG101 to mediate immune responses (Cui et al., 2017; Feys et al., 2005; Gantner et al., 2019; Neubauer et al., 2020; Wagner et al., 2013). EDS1 uses the same interface to interact with both partners, mediated by a hydrophobic LLIF α-helix, while an additional EP domain stabilizes the interaction (Rietz et al., 2011; Wagner et al., 2013).

Signal molecules such as pRib-AMP/ADP promote formation of the EDS1–PAD4 complex, while di-ADPR or ADPr-ATP signal through the EDS1–SAG101 complex to activate NRG1 (Huang et al., 2022; Jia et al., 2022).

Generally, EDS1, PAD4, and ADR1 co-occur in seed plants (Liu et al., 2023; Chia et al., 2024), whereas SAG101 and NRG1 orthologs are absent from several gymnosperm and angiosperm lineages (Chia & Carella, 2023; Chia et al., 2024). These signaling modules were shown to function independently, as evidenced by *A. thaliana* triple mutants in the PAD4 pathway (*adr1*, *adr1-L1*, *adr1-L2*) (Dong et al., 2016; Lapin et al., 2019; Wu et al., 2019), and through sag101 mutants in the nrg1 family of *A. thaliana* and *N. benthamiana*, which exhibited TIR-NLR-primed cell death defects (Castel et al., 2019; Lapin et al., 2019; Wu et al., 2019).

Furthermore, PAD4 and ADR1 are relevant to basal immunity and are generally utilized by both TIR-NLR and CC-NLR receptor classes to induce salicylic acid accumulation and other defense pathways (Wang et al., 2011). In contrast, SAG101 and NRG1 contribute little or not at all to cell death triggered by CC-NLRs (Wiemer et al., 2005).

Importantly, the EDS1 pathway can be initiated not only through intracellular sensor NLRs but also by cell surface receptors. For example, RLP23, a LRR-type receptor, triggers PTI and, through the RLCK SOBIR1, activates EDS1–PAD4–ADR1 signaling, which subsequently induces a cell death response (Pruitt et al., 2021; Tian et al., 2021; Chang et al., 2022).

Hybrid incompatibility

Within the *RPP1* locus lie the encoding *DANGEROUS-MIX 2 (DM2)* genes, NLRs which are known for their involvement in hybrid incompatibility (Bomblies et al., 2007; Chae et al., 2014; Lei & Weigel 2021). Hybrid incompatibility was initially discovered through crosses between two *A. thaliana* accessions, where their progeny exhibited reduced fitness and necrosis phenotypes, caused by incompatibilities between genetically unlinked genes *DM1* from one parent with *DM2* from the other (Bomblies et al., 2007). Additional hybrid incompatibility loci (*DM3-DM9*) were subsequently identified through further genetic crosses (Chae et al., 2014). The DM2/RPP1 resistosome can be activated via multiple mechanisms. These include direct recognition of the *H. arabidopsidis* effector ATR1 (Krasileva et al., 2010; Rehmany et al.2005), pairing with the TIR-NLR DM1/SS14 (Bomblies et al., 2007; Chae et al., 2014; Tran et al., 2017), or interaction with DM3, a prolyl aminopeptidase, which regulates prolines homeostasis (Ghifari et al., 2020) and capable of inducing DM2h condensate formation (Chae et al., 2014; Wan et al., 2025).

Furthermore, *DM2/RPP1* activity appears to be modulated by additional host components involved in cellular homeostasis (Lei & Weigel 2021). These include allelic variants of the receptor kinase *STRUBBELIG-RECEPTOR FAMILY 3 (SRF3)* (Alcazar et al., 2010; 2014), variants of OASTL-A1 an acetylserine (thiol) lyase (Tahir et al., 2013), and synthetic EDS 1 fusion proteins (Stuttmann et al., 2016). These diverse modes of regulation underscore the complex genetic architecture and regulatory plasticity of the *RPP1* locus, with implications for both pathogen recognition and autoimmune responses. These mechanisms are not limited for *A. thaliana* and similar observations were made in other plant species (Lei & Weigel 2021).

1.2 The *H. arabidopsidis-A. thaliana* pathosystem

Hyaloperonospora arabidopsidis is an obligate biotrophic oomycete that infects only *A. thaliana*, making this specialized system perfect for studying co-evolution (Thines & Choi, 2016, McDowell 2013). Oomycetes have morphological similarities to fungi but are phylogenetically more closely related to algae (Coates & Beynon, 2010; Thines & Choi, 2016). The homothallic, *H. arabidopsidis*, can reproduce sexually through conidiospores and asexually through oospores (Koch and Slusarenko 1990). The

asexual reproduction occurs on the host through the growth of conidiophore and the produced conidiospores, which release conidia. Upon germination these can re-initiate the infection. Oospores are formed simultaneously with asexual spores and are the result of fused differentiated hyphal tips, antheridia and oogonia. These spores consist of an additional cell-wall, which allows the survival within soil (Lucas et al., 1995). The lifecycle is initiated on the surface of *A.thaliana* before penetration of the hypha into the cell wall an appressorium is being formed at the tip of the germ tube (Soylu & Soylu 2003). Following entry, the pathogen develops a specialized intracellular structure known as haustorium (Figure 1.1). This structure enables *H. arabidopsidis* to manipulate host cellular processes by secreting effector proteins that suppress immune responses, promote susceptibility, and alter plant physiology to its advantage, which may include targeting plant developmental processes to avoid any stress responses or to increase nutrient uptake (Fabro, Steinbrenner, Coates, Ishaque, & Baxter, 2011). The formation of haustoria is a common infection strategy among filamentous pathogens such as rusts and powdery mildews, which are responsible for substantial crop losses globally (Haverkort et al., 2009; Singh et al., 2017). However, the obligate biotrophic lifestyle and the complexity of culturing these organisms *in vitro* result in significant limitations for applying molecular genetic techniques.

The host, *A. thaliana* a self-pollinator*,* is native to Europe and Asia (Hoffmann 2002), within and across different local groups of *A. thaliana*, shows quite some heterogeneity (Platt et al., 2010; Bomblies et al., 2010). Its convenient maintenance allowed the understanding of fundamental biological processes (Woodward and Bartel 2018).

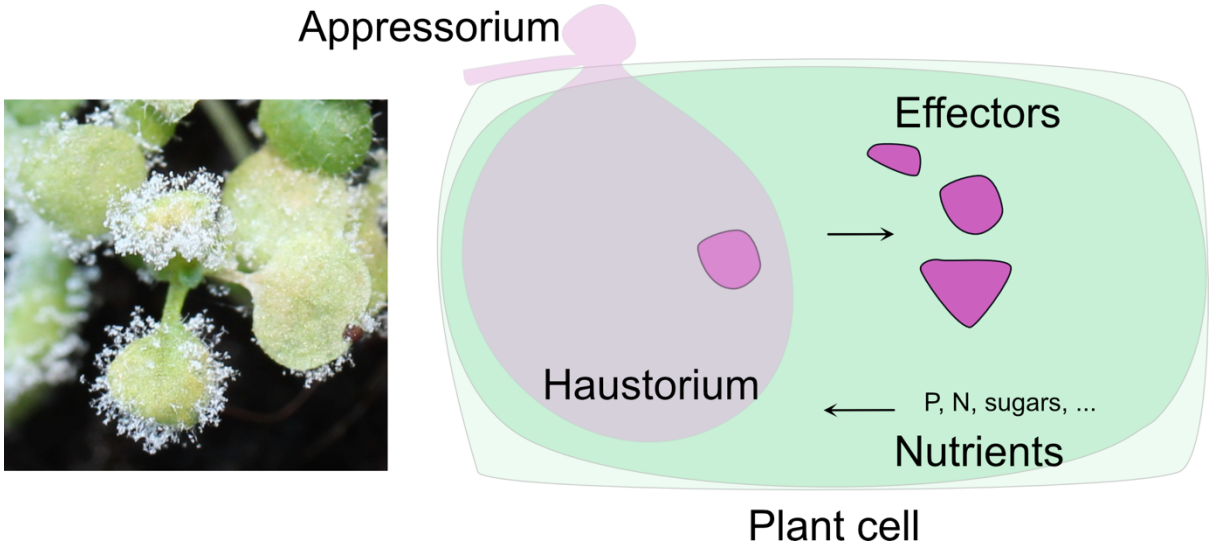

Figure 1.1: Scheme of *A. thaliana* and *H. arabidopsidis* infection. Left, *A. thaliana* infected with *H. arabidopsidis*, sporulation observed after 10 days of infection. Right, Appressorium relevant for haustoria formation is indicated in bright pink. Secreted effectors into the plant cell are shown in pink and nutrient uptake (P: phosphorus, N: nitrogen) of the pathogen is illustrated on the bottom.

Genetic analysis of *A. thaliana* populations that had been infected with diverse *H. arabidopsidis* isolates led to the discovery of multiple RPP (RECOGNITION OF PERONOSPORA PARASITICA) loci. Concurrent genome sequencing of *H. arabidopsidis* enabled identification of numerous RxLR and LFLAK effector motifs, which were swiftly associated with ARABIDOPSIS THALIANA RECOGNIZED (ATR) effectors (Koch & Slusarenko, 1990). To date, six well-characterized RPP–ATR pairs have been identified: ATR1/RPP1, ATR2/RPP2, ATR4/RPP4, ATR5/RPP5, ATR13/RPP13, and ATR39/RPP39 (Allen et al., 2004; Bailey et al., 2011; Bittner-Eddy & Beynon, 2001; Kee et al., 2007; Schreiber et al., 2016; Sohn et al., 2007).

These effector–receptor interactions have provided a rich framework for investigating allelic diversity and coevolutionary dynamics, revealing how specific mutations in either the host or pathogen can enhance recognition or promote evasion (Chou et al., 2011; Krasileva et al., 2011; Prigozhin & Krasileva, 2021). These ATR effectors represent a robust model system for dissecting molecular mechanisms of host-pathogen interaction.

Additionally, ongoing research has begun to explore a broader set of effectors beyond the ATRs defined from genetics. Advances in sequencing technologies have facilitated the identification of a wide array of putative *Hyaloperonospora arabidopsidis*

effectors, many of which are characterized by distinct amino acid motifs, including the RxLR and LFLAK motifs (Bailey et al., 2011; Coates & Beynon, 2010; Fabro, Steinbrenner, Coates, Ishaque, Baxter, et al., 2011). In a comprehensive transcriptional time-course analysis of the *H. arabidopsidis* lifecycle, over 300 putative effector genes were identified (Asai et al., 2014). Subsequent functional studies have elucidated parts of molecular targets and roles of these effectors, many of which interfere with key regulatory pathways in the host.

For example, HaRxL106 alters the activity of RADICAL-INDUCED CELL DEATH1 (RCD1), a transcriptional co-regulator that suppresses salicylic acid (SA)-mediated defense signaling (Wirthmueller et al., 2018). Similarly, HaRxLL470 targets ELONGATED HYPOCOTYL 5 (HY5), a transcription factor central to photomorphogenesis (Chen et al., 2021). HaRxL21 interacts with TOPLESS (TPL), a transcriptional co-repressor involved in plant development (Harvey et al., 2020), while HaRxL45 targets TCP14, a transcription factor shown to connect to in plant immunity (L. Yang et al., 2017). Moreover, HaRxL10 promotes the proteasomal degradation of JAZ3, a transcriptional repressor of the jasmonic acid (JA) signaling pathway, thus modulating hormone-mediated defense responses (Anderson et al., 2019). HaRxL44-MED19 is a nuclear-localized effector that interacts with Mediator subunit 19a (MED19a), a positive regulator of immunity against *H.arabidopsidis* (Caillaud et al., 2013), while HaRxL62 can enhance growth of the bacterial pathogen *Pst* DC3000 on *A. thaliana* by an unknown mechanism (Fabro, et al., 2011).

1.3 Pan-genomes of *A. thaliana* help unravel allelic diversity

The *Hyaloperonospora arabidopsidis–Arabidopsis thaliana* interaction has long served as a powerful model for the discovery and functional characterization of numerous NLRs through extensive genetic analyses. Allelic diversity and the presence of multiple NLR copies within a locus have been recognized for some time.

RPP1 is one of 20 *RPP* loci initially identified through genetic crosses and segregation analysis of progeny challenged with various *H. arabidopsidis* isolates (Botella et al., 1997; Holub et al., 1994). It was later revealed, using high-capacity cloning vectors such as fosmids, that the *RPP1* locus contains multiple gene copies (Botella et al., 1998; Gordon, 2002; Goritschnig et al., 2016). Nearly two decades later, ATR1 and

RPP1 were co-expressed in *Nicotiana tabacum*, allowing to test allele-specific interactions (Krasileva et al., 2010). However, only a limited number of RPP1 and ATR1 variants have been functionally analyzed, and the roles of most remain unknown (Goritschnig et al., 2016). Further studies showed that the interaction between ATR1 and RPP1 is highly dependent on specific point mutations (Ma et al., 2020).

Beyond *RPP1*, many studies have highlighted the complexity of NLR loci, which are shaped by gene rearrangements, duplications, and transposon insertions, factors that complicate the identification of allelic diversity (McDowell et al., 1998; Baumgarten et al., 2003; Meyers et al., 2003; Leister, 2004). These loci, ranging from a few kilobases to several megabases, are dynamic regions that promote the evolution of novel resistance specificities, often through partial or complete domain swapping between homologous genes (Jiao & Schneeberger, 2020; Meyers et al., 2003; Michelmore & Meyers, 1998a; Tamborski & Krasileva, 2020; Wicker et al., 2007).

While diversity at NLR loci supports adaptability, excessive variation can be detrimental. Mismatched NLR proteins may trigger autoimmunity or hybrid incompatibility, limiting the combination of beneficial alleles (Chae et al., 2014; Barragan et al., 2019; Todesco et al., 2014; Alcázar et al., 2009; Bomblies et al., 2007).

To further understand these complex loci, more genomes have been sequenced in recent years as technological and financial constraints have eased. The most common sequencing approach involves mapping short reads to a single reference genome to assess genomic variation. However, many reads often fail to map to the reference (Barragan & Weigel, 2020; Cao et al., 2011; Long et al., 2013). To capture these unmapped reads, many of which may represent NLR sequences, hybridization-based enrichment methods are employed before short- or long-read sequencing (Jupe et al., 2013; Van de Weyer et al., 2019; Witek et al., 2016).

While effective, hybridization-based enrichment has limitations, particularly the requirement for sufficiently long flanking sequences to match the reference genome (Van de Weyer et al., 2019). To overcome these limitations, many groups have recently turned to long-read sequencing and *de novo* genome assemblies (Consortium et al., 2024; Kang et al., 2023; Lian et al., 2024; Teasdale et al., 2024; Wlodzimierz et al., 2023).

Another ongoing challenge is annotation. For example, *RPP13* was initially described as a single, highly polymorphic gene (Bittner-Eddy et al., 2000). However, Lee and Chae (2020) found that most *A. thaliana* accessions carry an average of three

RPP13 copies, based on the Van de Weyer dataset (Van de Weyer et al., 2019). As discussed by Lee and Chae, NLR annotation is challenging, as it often relies on the best-matching homologs, leading to potential errors (Lee & Chae, 2020). Automated annotations, though widely used, may misrepresent gene numbers and structures (Meyers et al., 2003; Van de Weyer et al., 2019). To improve accuracy, researchers have supplemented automated annotations with RNA-seq data and extensive manual curation (Lai & Eulgem, 2018; Steuernagel et al., 2020). More recently, long-read RNA sequencing and epigenetic profiling have enabled the annotation of entire NLR loci, including their genomic neighborhoods (Teasdale Murray et al., 2024).

1.4 Aim of this study

This thesis aims to shed light on the complex *A. thaliana RPP1* locus and to describe its interaction with the corresponding and co-evolving ATR1 effector in *H. arabidopsidis* by studying natural variants of both genes in large datasets.

The first chapter focuses on a population sample of the pathogen *H. arabidopsidis* and highlights the trajectories of overall effector variation in a European-wide collection, with ATR1 being particularly diverse. Experiments with different ATR1 variants on various host plants demonstrate that recognition of specific ATR1 variants is relatively rare. In both genetic and local population analyses, I found that the *RPP1* locus is apparently only rarely the key player in *H. arabidopsidis* recognition.

In the second chapter, I explore the *A. thaliana RPP1* locus on a global scale. Through an in-depth analysis of this locus, I demonstrate that, although complex at first glance, the *RPP1* locus exhibits less variation than expected and more similarities among plant populations worldwide. I demonstrate that *RPP1* exhibits identical sequences across accessions at both nucleotide and amino acid levels, extending to intergenic sequences. Whereas, identical sequences found within the accession are relatively rare in this set. Many loci contain multiple *RPP1* truncations and unknown roles. I conclude from this chapter that NLR sequence analysis cannot reveal much information on the NLR function, and instead, the entire locus needs to be analyzed in order to determine functionality.

Overall, this thesis presents a multiscale approach to studying the natural variation of both *ATR1* and *RPP1* loci. It sheds new light on the evolutionary history of the complex *RPP1* locus and opens up new avenues for understanding NLR functionality in the context of natural variation.

2. The role of *ATR1* and *RPP1* in the *A. thaliana* - *H. arabidopsidis* pathosystem

2.1 Newly-collected *H. arabidopsidis* isolates

Several studies have explored allelic diversity to understand the co-evolution of host-pathogen interactions and to identify functional sequence variants, as nicely reviewed by Win and colleagues (Win et al., 2012). Most of these investigations have been limited to *H. arabidopsidis* isolates from the UK (Bittner-Eddy & Beynon, 2001). In the meantime, there may be significantly more genetic diversity among isolates elsewhere, which could result in different gene-by-gene interactions between the host and pathogen.

Even within the limited collections, *ATR1* and *ATR13* stood out because of their allelic diversity. For *ATR13* alone, 15 alleles have been described in 16 UK isolates (Hall et al., 2009). For the corresponding receptor *RPP13* high polymorphism, 19 different alleles in 24 *A. thaliana* accessions, was observed and reported together with its effector to be subject to balancing selection (Allen et al., 2004). In contrast, *ATR1* is characterized by presence/absence (P/A) variation (Rehmany et al., 2005). Similarly, its corresponding plant immune receptor, *RPP1*, ranges from absent to 17 copies in *A. thaliana* and *RPP13* has up to five copies (Lee & Chae, 2020). Although there is presence/absence variation in both the host and pathogen, specific RPP1 variants in the plant have been described to recognize specific ATR1 variants and trigger resistance to *H. arabidopsidis*. (Chou et al., 2011; Goritschnig et al., 2016; Rehmany et al., 2005).

To broaden this perspective, we expanded the set of *H. arabidopsidis* with isolates from across Europe (Figure 2.2 A). 289 *A. thaliana* populations were sampled in 18 countries ranging from Spain to Azerbaijan and from Italy to Sweden. These plants were processed for metagenomics and *H. arabidopsidis* isolation (Karasov et al., 2024; PATHODOPSIS unpublished data). We isolated 129 *H. arabidopsidis*, sequenced them using illumina short-read technology and generated a new reference genome called 495-1 (Figure 2.1 A) by long-read PacBio. Short-reads were mapped back to the new reference genome (Figure 2.1 B-E).

A

Isolate	Provenance	Contigs	Total (Mb)	lengthMax. (Mb)	lengthN50 (Mb)	N90 (Mb)	BUSCO complete (%)
Emoy2 reference	England	3,108	78.38	1.23	0.33	0.02	96.7
495-1	Germany	98	76.14	4.08	1.40	0.52	96.3

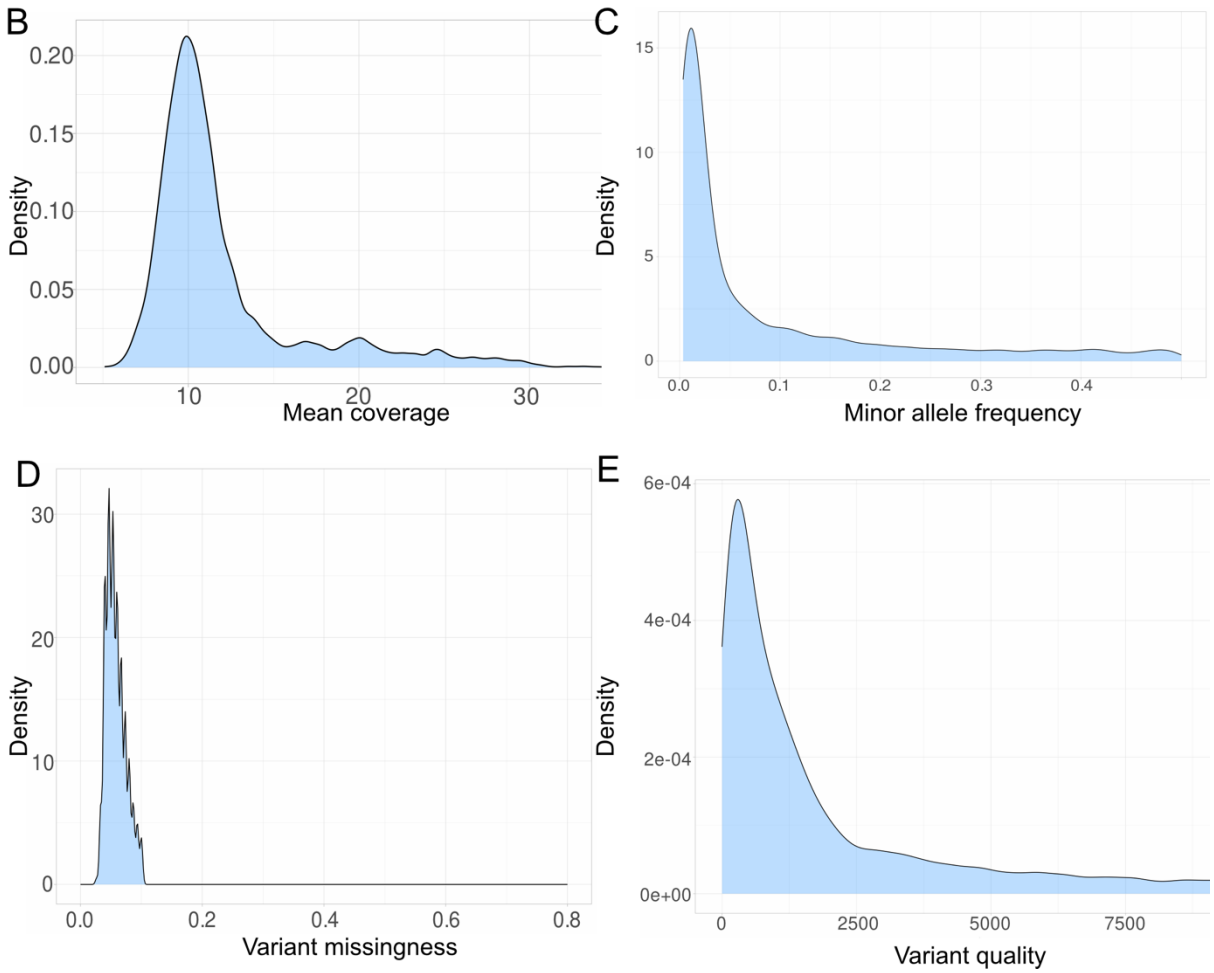

Figure 2.1: **Quality control of sequenced *H. arabidopsidis* genomes.** A) 495-1, a long-read sequenced isolate, was used as a new reference genome, and its assembly was compared to the previous reference Emoy2. 495-1 has only 98 contigs, with the maximum contig size (lengthMax.) 4.08 Mb, 50 % of the genome is in contigs ≥ 1.4 Mb N50 (lengthN50), 90 % of the genome is in contigs ≥ 0.52 Mb (N90). Completeness of the *H. arabidopsidis* genome assembly evaluated using BUSCO v5.1.3 (Benchmarking Universal Single-Copy Orthologs; Simão et al., 2015) resulting in 96.3% of orthologs found. B-E) Short-read sequenced isolates were mapped to 495-1 and called for variants with GATK. After filtering, the quality of these genomes was visualized by B) mean coverage, C) minor allele frequency, D) missing data, and E) variant quality.

2.2 *Hyaloperonospora arabidopsidis* effector diversity in the new isolate collection

To assess the diversity of the newly isolated *H. arabidopsidis* I first analyzed their genetic relatedness based on SNP calls against the reference genome 495-1 (R. Schwab, G. Shirsekar and O. Deusch, pers. communication), and calculated genome-wide genetic distances. I included isolates from North America as potential outgroups (Karasov et al., 2024; Shirsekar et al., 2021). The dataset yielded a genotyping rate of 0.92 and identified the number of SNPs as 1,852,153 (before filtering) and 213,616 (after filtering) (Methods, Figure 2.2 B). Different genetic clusters were observed, with one cluster primarily consisting of isolates from Germany, and a few outliers from Italy and Ireland. The largest and most distinct cluster contained only isolates from Italy, while a third central cluster comprised isolates from the UK, Ireland, and the Netherlands. Notably, isolates from the same country could display substantial genetic differentiation (Figure 2.2 B).

To further explore functional variation, I focused on effectors - genomic areas known to be likely to show high diversity due to the co-evolutionary arms race between pathogens and hosts (Win et al. 2012; Chisholm et al., 2006). I searched all 339 known *H. arabidopsidis* effectors and effector candidates from the Asai collection (Asai et al., 2014) in the 129 isolates. On average, 207 effectors per genome had above 5 x coverage, indicating the presence of an allele closely related to the reference.

For each effector locus, I calculated the number of polymorphic SNPs and normalized it to the length of the corresponding effector and overall nucleotide diversity (π) (Figure 2.2 C, Supplementary Table 2.2). The most variable effectors included both well-characterized effectors such as *ATR1* (mean π: 0.26; polymorphic SNPs normalized to effector length: 163), *ATR5* (0.15; 78), *ATR13* (0.44; 15), *HaRxL62* (0.25; 56), and *HaRxLR106* (0.21; 105), as well as lesser-studied effectors such as *HaRxL128* (0.25; 186), and *HaRxLL119c* (0.14; 161). Some effectors exhibited high mean nucleotide diversity despite having zero polymorphic SNPs. This apparent discrepancy likely results from sequence gaps or missing data at specific genomic sites, rather than true underlying genetic variation. Nucleotide diversity is calculated across all available sites, and in regions with low coverage or inconsistent read mapping, uncertain or ambiguous base calls can artificially inflate diversity estimates. Meanwhile, variant callers typically require a certain level of read support and base

quality to confidently identify SNPs, so if coverage is insufficient, no variants are called, even if diversity metrics still register variability.

For example, *ATR13* frequently had missing data at multiple positions across most genomes, leading to low and uneven coverage and inflated nucleotide diversity due to ambiguous base representation (Figure 2.3 A). In contrast, *ATR1* also showed low overall coverage; however, the available reads aligned consistently to similar positions across all genomes (Figure 2.3 B). As a result, both the low SNP count and lower nucleotide diversity in *ATR1* are likely accurate reflections of true sequence conservation, whereas the high diversity reported for *ATR13* is likely an artifact of incomplete or poor-quality data.

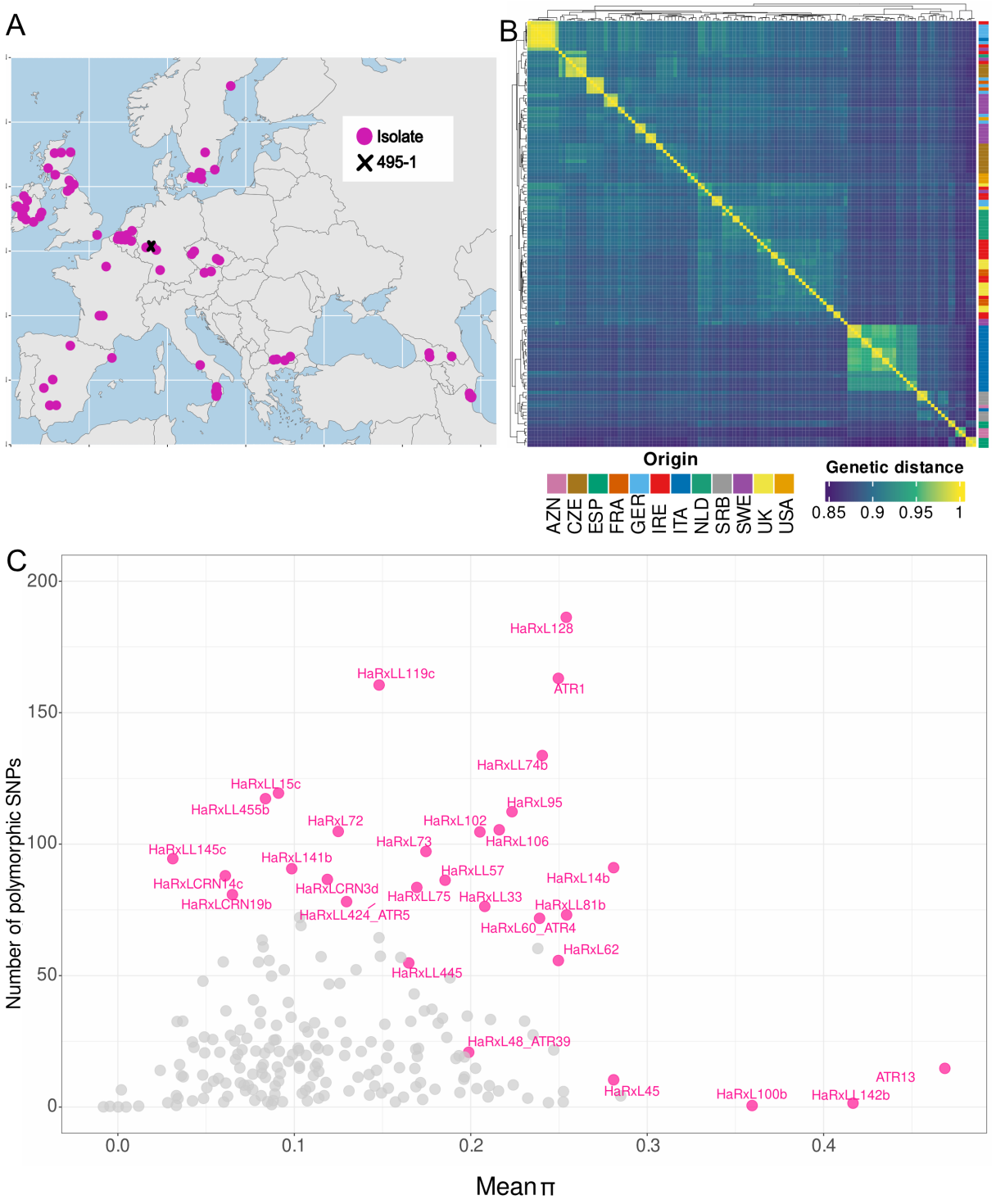

Figure 2.2: **Genetic and effector diversity of the European-wide collection of *H. arabidopsidis* isolates.** A) Geographic origin of all sampled isolates. Isolate 495-1 was used to generate a new reference genome. B) Whole-genome relatedness of *H. arabidopsidis* isolates based on average nucleotide identity. C) Relationship between the number of polymorphic SNPs and the overall nucleotide diversity in *H. arabidopsidis* isolates for each effector normalized by length. Each dot represents an effector, highlighted in pink are ATR

effectors with published functions along with those effectors that had the highest values for nucleotide diversity and number of SNPs.

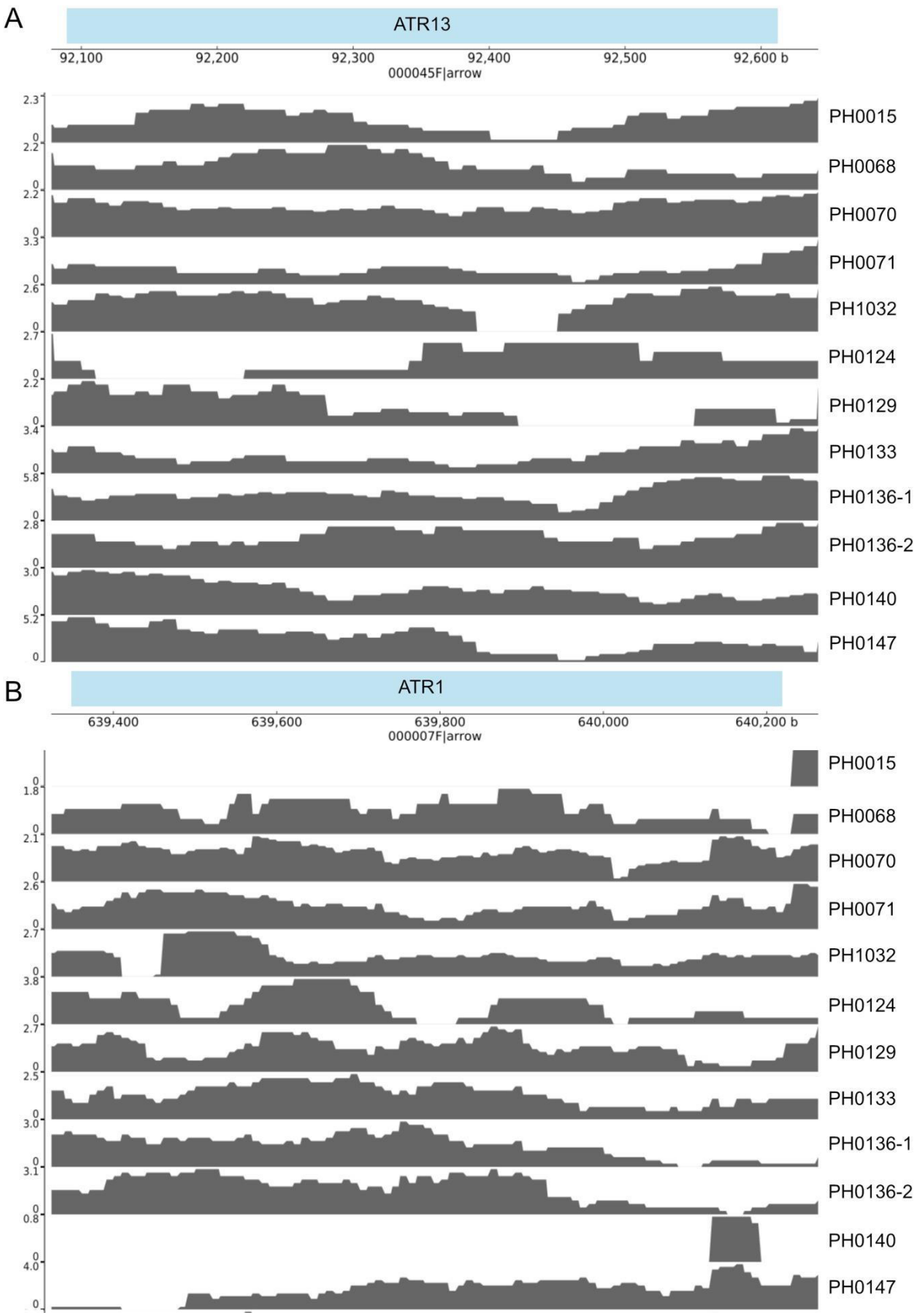

Figure 2.3: **Examples of genome coverage in effector regions.** A) ATR13 and B) ATR1 for several isolates.

Since *ATR1* is a well-characterized effector (Chou et al., 2011) and was also among the most variable effectors in our isolates, I focused on this effector and re-sequenced it using either Sanger sequencing of blunt-end cloned PCR products, targeting conserved flanking regions, or by pooling the cloned PCR products together and sequence high-coverage (50 x) Illumina data, allowing *de novo* assembly of the plasmid. I successfully obtained PCR-amplified sequences from 60 isolates. Among these, only 27 showed nonsynonymous variation (Figure 2.4). Most differences occurred in the sequences encoding the C terminal domain. The N terminal domain exhibited only minor variation, but there were nonsynonymous changes in codons reported to be critical for RPP1 recognition (Chou et al., 2011). Notably, seven variants were identical to ATR1^{Emoy2} variant, suggesting that this variant may be the most prevalent across diverse *H. arabidopsidis* isolates, regardless of geographic origin.

To assess the functional relevance of allelic variation in pathogenicity, I selected a subset of six ATR1 variants from different phylogenetic clades (Figure 2.4, highlighted in pink) for further analysis. These variants carried nonsynonymous substitutions in both the C terminal and N terminal domains, potentially affecting receptor recognition.

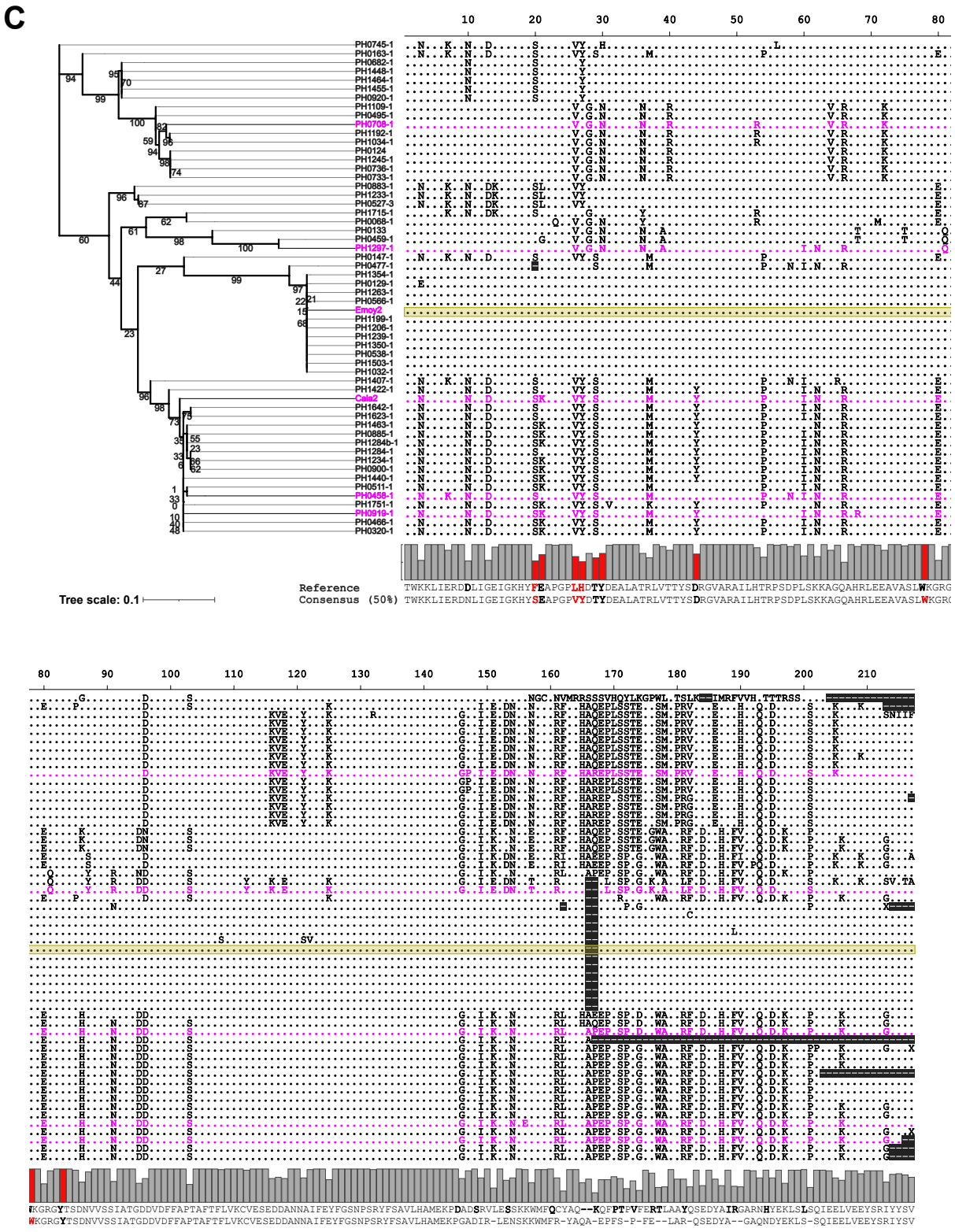

Figure 2.4: **Alignments of predicted proteins encoded by ATR1 variants.** Phylogenetic tree of ATR1 sequences (amino acids- based maximum likelihood tree was inferred with LG substitution model and gamma distribution plus invariant for among sites rate variation; used bootstrap 1,000), was generated together with the known ATR1^{Emoy2} (yellow) and ATR1^{Cala2}

variants. Sequence conservation of the ATR1^{Emoy2} variants is indicated with ".", differences to ATR1^{Emoy2} are indicated by letters. Gaps are indicated in black. Red bars at the bottom point out residues important for receptor recognition. Pink-highlighted alleles were used for functional experiments.

2.3 Role of ATR1 variation in *H. arabidopsidis* virulence and pathogenicity

To assess the impact of different ATR1 variants on host responses, I employed multiple expression platforms, including *Pseudomonas*-mediated delivery into *A. thaliana* and *Agrobacterium*-mediated transient expression in *Nicotiana* species. The first system allows testing whether an effector can confer virulence when delivered by a non-pathogenic soil bacterium, *Pseudomonas fluorescens* Pf0-1, which has been engineered with a functional type III secretion system (T3SS) to translocate effectors into plant cells (Thomas et al., 2009). Similar to other secretion systems, the T3SS enables direct delivery of effector proteins into the host cell cytoplasm (Lucke et al., 2020). *Pseudomonas syringae* (*Pst*), for instance, uses T3SS to deliver effectors that typically contain an N terminal signal peptide (Jin et al., 2003). This feature is also seen in oomycete effectors such as ATR1 and ATR13, which carry both a signal peptide and an RxLR motif, the latter being crucial for host translocation (Allen et al., 2004; Rehmany et al., 2005). However, the commonly used *Pst* DC3000 contains a large repertoire of endogenous type III effectors, which can interfere with or mask the activity of heterologously expressed oomycete effectors (Sohn et al., 2007). To overcome this limitation, alternative delivery systems such as Pf0-1 have been adopted (Thomas et al., 2009). Unlike *Pst* DC3000, Pf0-1 lacks endogenous virulence factors, does not support bacterial growth *in planta*, and was reported to cause no disease symptoms in 88 *A. thaliana* accessions (Thomas et al., 2009; Goritschnig et al., 2016).

The effectors were expressed from the AvrRps4 promoter and fused at the N terminus to a signal peptide for T3SS delivery and a C terminal HA-tag to track translocalization of the effector into the cell cytoplasm (Supplementary Figure 2.1; Sohn et al., 2007; Thomas et al., 2009). I used this approach with two *A. thaliana* accessions Gel-1 and DraIII-1. Gel-1 was previously reported in our laboratory to be one of the more susceptible accessions to *H. arabidopsisis*, while DraIII-1 was among the more resistant accessions. I also tested Pf0-1 on IP-Moa-0 but it triggered a PTI response which was not useful to detect ATR1-induced ETI response.

I syringe-infiltrated Gel-1 and DraIII-1 with five different Pf0-1 derivatives, each expressing one ATR1 variant. Included were the ATR1 variants from the well-studied *H. arabidopsidis* isolates Emoy2 and Cala2 as controls. DraIII-1 strongly recognized

the AvrRps4N-ATR1$^{PH1297-1}$-HA effector and exhibited a strong leaf wilting phenotype 3 days after infiltration. Weaker responses were observed for the other effector variants (Figure 2.5 A, B). Gel-1 showed the strongest leaf wilting phenotype when treated with Pf0-1 carrying AvrRps4N-ATR1$^{PH191-1}$-HA, some response to the other effectors and not response at all to AvrRps4N-ATR1^{Cala2}-HA.

I also wanted to test whether these effectors could induce virulence in a model pathogen, so I introduced the ATR1 variants into *Pseudomonas syringae* pv. tomato DC3000 (*Pst* DC3000). None of the ATR1 variants substantially increased bacterial growth within the leaf (Figure 2.5 C). There were some weak trends, such as *Pst* DC3000 AvrRps4N-ATR1^{Cala2}-HA showing a higher load of bacterial growth on Gel-1 and AvrRps4N-ATR1$^{PH1297-1}$-HA showing a reduced bacterial growth for Gel-1 and IP-Moa-0. These findings echoed the results of Pf0-1 in Gel-1, as Gel-1 reacted the least to Pf0-1 expressing AvrRps4N-ATR1^{Cala2}-HA. Results were not significant and therefore excluded for further analysis.

I complemented these results with infection of the *A. thaliana* accessions Gel-1, DraIII-1 and IP-Moa-0 with *H. arabidopsidis* isolates carrying different *ATR1* alleles. Gel-1 and DraIII-1 were infected with 59 isolates while IP-Moa-0 was infected with 38 isolates. Among those isolates three do not carry an *ATR1* copy (Figure 2.5 D, Supplementary Table 2.3). For all accessions I spot-inoculated 7-day old seedlings. 1 day post infection the humidity decreased from 70 % to 30 % and increased again 6 days post infection. Disease symptoms in the form of pathogen sporulation were scored 10 days post infection. DraIII-1 showed the least disease symptoms, including *H. arabidopsidis* isolates lacking *ATR1*. In contrast, the *A. thaliana* accessions Gel-1 and IP-Moa-0 were more susceptible, Gel-1 was resistant to less than a quarter of the tested isolates and IP-Moa-0 was resistant to only two isolates (Figure 2.5 D, Supplementary Table 2.3).

By combining results from both the Pf0-1 delivery system and *H. arabidopsidis* infection assays, several patterns of recognition and resistance emerged. The accession DraIII-1 was resistant to *H. arabidopsidis* isolate PH1297-1 and showed strong recognition of its corresponding ATR1 variant. Additional ATR1 variants, ATR1^{Cala-2}, ATR1^{Emoy2}, ATR1$^{PH708-1}$, and ATR1$^{PH919-1}$, were also recognized by DraIII-1 to varying degrees when delivered via Pf0-1. Correspondingly, DraIII-1 exhibited high resistance to the associated *H. arabidopsidis* isolates, with the exception of Cala-2, to which it showed only weak resistance. The accession Gel-1 strongly recognized

ATR1$^{PH919-1}$, yet remained susceptible to *H. arabidopsidis* PH919-1, suggesting a lack of effective resistance despite recognition. In both Pf0-1 and *H. arabidopsidis* assays, Gel-1 failed to recognize ATR1^{Cala-2}, which was consistent with its susceptibility to *H. arabidopsidis* Cala-2. Such alignment between effector recognition and resistance was also observed for ATR1$^{PH708-1}$ and its corresponding isolate in Gel-1. However, for the other ATR1 variants and isolates, no clear correlation was observed between recognition patterns and resistance responses in this accession. These results indicate pathogen recognition is independent of *ATR1.*

To identify potential effector candidates contributing to distinct pathogen phenotypes, I examined which effectors are present in isolates that elicit similar host responses (Table 2.1, Figure 2.5 D). Gel-1 was resistant to *H. arabidopsidis* PH458-1 and partially resistant to PH708-1; notably, these two isolates share 15 effectors that are absent in the other four isolates. Similarly, DraIII-1 showed reduced resistance only to Cala-2, which uniquely contains six effectors not found in any of the other five isolates (Table 2.1, Figure 2.5 D).

In summary, I showed that recognition of a specific ATR1 variant by an *Arabidopsis thaliana* accession does not always correlate with resistance to the corresponding *Hyaloperonospora arabidopsidis* isolate carrying that allele. Nevertheless, I could identify candidate effectors in *H. arabidopsidis* PH458-1 and PH708-1 that may act as additional targets of host immune recognition (Table 2.1). It is likely that overall pathogenicity is determined by the combined action of multiple secreted effectors and their specific interactions with the NLR repertoire of the host plant.

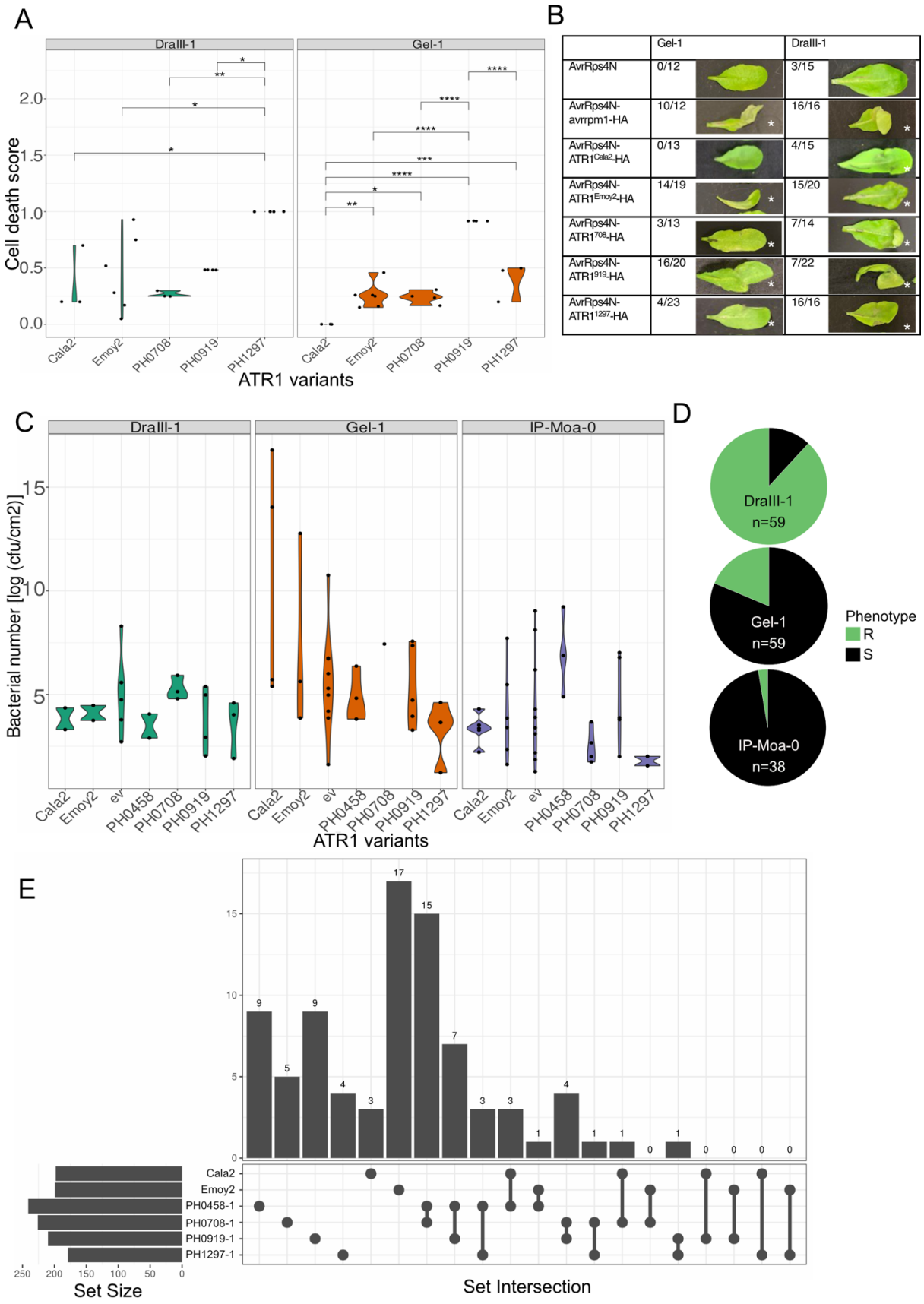

Figure 2.5: Response of three *A. thaliana* accessions to ATR1 variants and *H. arabidopsidis* strains carrying different *ATR1* variants. A) Response of *A. thaliana* accessions DraIII-1 and Gel-1 to ATR1 variants delivered through the Pf0-1 pEDV system.

Cell death responses were scored 3 dpi and normalized to the empty vector (EV) control, with at least 3 replicates. “1” indicates strong cell death and “0” no response, extension of the Y-axis is due to the visualization of the statistics. Two-way ANOVA: **** corresponds to $p \leq 0.0001$, *** $p \leq 0.001$, ** $p \leq 0.01$, * $p \leq 0.05$. B) Phenotypes observed with *A. thaliana* accessions Gel-1 and DraIII-1 2 dpi after syringe infiltration of Pf0-1 expressing different effectors and controls (AvrRps4-N and AvrRps4-N-AvrRpm1). Leaf wilting or cell death response, highlighted with asterisks. C) Growth of *Pst* DC3000 expressing different ATR1 variants on accessions DraIII-1, Gel-1 and IP-Moa-0. *Pst* DC3000 carried different ATR1 variants. Statistical test was performed on pairwise comparison of the means (Tukey HSD), with significance determined relative to the empty vector (ev), no significance was observed for all treatments. D) 14-day old *A. thaliana* accessions DraIII-1, Gel-1 and IP-Moa-0 infected with *H. arabidopsidis* isolates. Successful infection indicated as S and plant resistance as R. E) Comparison of six *Hyaloperonospora arabidopsidis* isolates and all annotated effectors identified in their genomes. The set size (left barplot) indicates the total number of effectors annotated in each isolate. The set intersection is visualized with dots representing individual isolates and connected lines indicating shared effectors across them. The top barplot shows the number of effectors shared among specific combinations of isolates. Single dots without connecting lines represent effectors unique to that isolate.

Table 2.1: Effector content of different *H. arabidopsidis* isolates. The table presents the unique effector repertoire of each isolate, as well as the set of effectors conserved across all six isolates.

H. arabidopsidis isolate	Effector
PH458	HaRxLL107c, HaRxLL47, HaRxLL18, HaRxL136c, HaRxL89, HaRxL87i, HaRxL62, HaRxL57, HaRxL6
PH708	HaRxLL455c, HaRxLL113, HaRxL120b, HaRxL43b, HaRxL8
PH919	HaRxLL455d, HaRxLL445, HaRxLL48b, HaRxL159, HaRxL151, HaRxL87h, HaRxL67b, HaRxL65, HaRxL17
PH1297	HaRxLL427, HaRxLL142c, HaRxLL65, HaRxL163
Cala2	HaRxL80, HaRxL94, HaRxLL434, HaRxLCRN19b, HaRxLL133d, HaRxLL125d
Emoy2	HaRxL46, HaRxL63, HaRxL80b, HaRxL81, HaRxL133c, HaRxLL15c, HaRxLL75,

	HaRxLL80b, HaRxLL160, HaRxLL173, HaRxLL181, HaRxLL188b, HaRxLL447, HaRxLL465, HaRxLL491, HaRxLCRN22
Shared in all six isolates	HaRxLCRN9b, HaRxLL500, HaRxLL433, HaRxLL429, HaRxLL145c, HaRxLL133c, HaRxLL125b, HaRxLL89, HaRxLL75e, HaRxLL45, HaRxLL40, HaRxLL38b, HaRxLL15b, HaRxLL6, HaRxL107, HaRxL83, HaRxL55, HaRxL35, HaRxL22, HaRxL21, ATR1

2.4 Analysis of functional RPP1 variants in the context of ATR1 recognition

After determining the ATR1 recognition and pathogen resistance/susceptibility patterns in the accessions DraIII-1, Gel-1, and IP-Moa-0, I next investigated the *RPP1* content in these hosts and explored potential protein interactions between different ATR1 and RPP1 variants.

Gel-1–the most susceptible accession, harbored the highest number of *RPP1* copies, with 10 annotated *RPP1* genes, making this locus also the largest one among the three accessions (Figure 2.6 A,B). DraIII-1 contained five *RPP1* copies, while IP-Moa-0 possessed only two altered *RPP1* alleles. Several of these *RPP1* genes appeared to encode truncated proteins, and some copies were found in an inverted orientation within the genome (Figure 2.6 B). For clarity, I refer to the *RPP1* from Gel-1 as *RPP1*$^{GelA–J}$ and those from DraIII-1 as *RPP1*$^{DraA–E}$.

To further characterize these genes, I conducted *in silico* analysis using AlphaFold (Abramson et al., 2024) and compared the protein sequences to RPP1^{WsB} (PDB Identifier: 7CRC). Given that co-modeling ATR1 and RPP1 variants using AlphaFold2 did not provide sufficient resolution to reliably predict protein–protein interactions (data not shown), I instead focused on modeling the tetrameric structure of RPP1 using AlphaFold3. To assess whether AlphaFold3 model confidence scores could serve as indicators of potential ATR1-binding functionality, I analyzed several RPP1 variants previously demonstrated to trigger macroscopic cell death upon co-expression with specific ATR1 alleles. These included RPP1^{NdA}, RPP1^{EstA}, and RPP1^{ZdrA} (Goritschnig et al., 2016). I also examined RPP1^{WsC}, which was reported to confer resistance to *Hyaloperonospora arabidopsidis*, although it had not been tested in direct co-expression assays with ATR1 (Botella et al., 1998). Based on these data, I hypothesized that functional RPP1 variants would yield high-confidence

AlphaFold3 structural predictions and high sequence alignment scores, while truncated variants, such as RPP1^{ZdrC}, RPP1^{ZdrD}, and RPP1^{WsA} (Goritschnig et al., 2016), would be associated with lower confidence scores and low sequence alignment scores. Additional variants included in the analysis were RPP1^{ZdrE} and RPP1^{ZdrB}, full-length proteins. but not previously linked to cell death responses (Goritschnig et al., 2016). AlphaFold3 was unable to generate tetrameric models for RPP1^{EstA} and RPP1^{ZdrA}. RPP1^{WsA}, RPP1^{ZdrB}, and RPP1^{ZdrD}, along with the truncated variants from

IP-Moa-0, displayed both low structural confidence scores and poor sequence alignment to the reference structure 7CRC. These observations are consistent with earlier findings suggesting that RPP1^{ZdrB}, RPP1^{ZdrD}, RPP1^{WsA}, and the IP-Moa-0 variants are truncated forms (Figure 2.6 C). By contrast, RPP1^{DraA}, RPP1^{GelA}, RPP1^{GelB}, and RPP1^{GelC}, together with RPP1^{WsC}, RPP1^{ZdrE}, RPP1^{NdA}, and RPP1^{ZdrC}, exhibited the highest AlphaFold3 model confidence and sequence alignment scores, indicating a higher likelihood of structural integrity and potential tetramerization. As expected for RPP1^{NdA}, since it has been reported to interact with certain ATR1 variants. Interestingly, RPP1^{WsB,} the experimentally resolved structure represented by PDB: 7CRC, displayed high, but not the highest, AlphaFold3 confidence scores. This observation indicates that confidence scores alone may not be sufficient to predict tetramerization potential. However, when considered alongside other parameters, such as sequence alignment to a reference structure, AlphaFold3 output can provide valuable additional insight into protein functionality. RPP1^{DraE} and RPP1^{GelE} showed high ipTM scores but low sequence alignment score which could be due the truncated domains of TIR and LRR in RPP1^{DraE} and shorter LRR domain in RPP1^{GelE} (Figure 2.6 C). Due to consistently low model confidence and alignment scores, the RPP1 variants identified in IP-Moa-0 were excluded from further analyses.

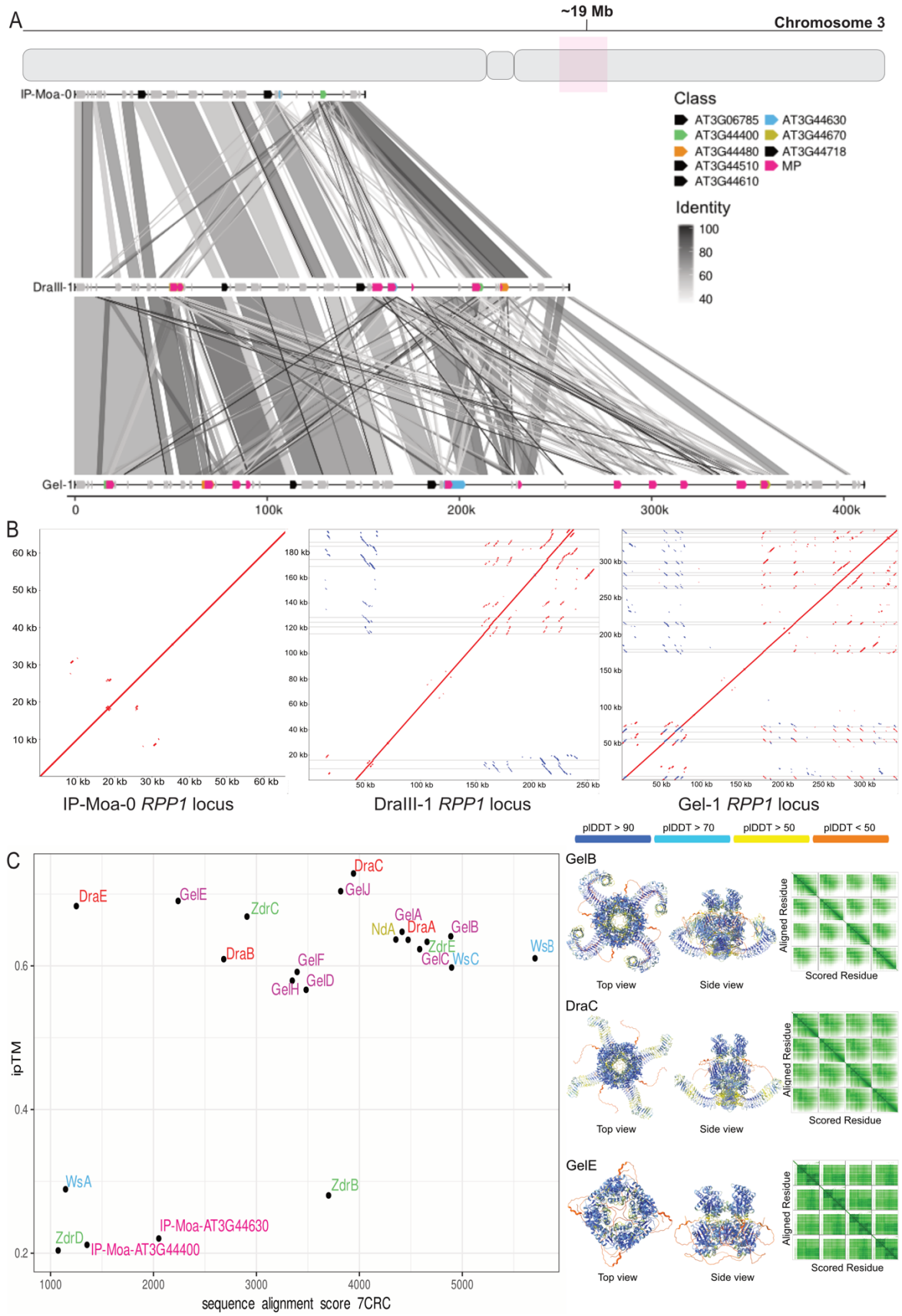

Figure 2.6: *RPP1* annotation and prediction of functionality. A) Synteny plot of the *RPP1* locus in *A. thaliana* accessions IP-Moa-0, Gel-1 and DraIII-1. Colors indicate flanking genes

in black, *RPP1* copies as annotated by miniprot in pink, and TAIR10 homologs annotated with liftoff highlighted in orange, green, olive and blue. Syntenic links indicate sequence similarity with >40% identity. B) Sequence alignment of *RPP1* locus against itself represented as dotplot. The red line indicates identical sequence and blue lines highlight gene inversions within the locus. The *RPP1* locus from left to right was visualized for IP-Moa-0, DraIII-1 and Gel-1. C) RPP1 proteins with respective AlphaFold3 modelled confidence values for the interface predicted modelling score (ipTM) and sequence alignment scores to 7CRC (PDB ID for $RPP1^{WsB}$) were visualized in two dimensions. Examples of some of these AlphaFold3 predicted models were visualized on the right. Colors indicate the predicted local distance difference test (pLDDT) ranging from below 50 (orange) to above 90 (dark blue). The green matrix next to it, is the array of all residues (Aligned Residue) and the predicted error for each position (Residue Score).

Furthermore, I examined the multiple sequence alignment (MSA) focusing on sites known to be important for RPP1 activity (Figure 2.7 A). $RPP1^{GelF}$, RPP^{GelI}, $RPP1^{GelC}$, $RPP1^{GelH}$, $RPP1^{GelG}$ and $RPP1^{DraC}$ showed N terminal gaps, whereas $RPP1^{DraA}$ has an N terminal extension (Figure 2.7 B). High conservation was observed in the BB-loop I121M in $RPP1^{DraA}$ (Figure 2.7 C). The serine (S) histidine (H) motif for TIR homodimer formation was also conserved (Figure 2.7 D) and $RPP1^{DraE}$ lacked the TIR domain entirely (Figure 2.7 C-E), for TIR with NBD interaction mutations were observed across the MSA (Figure 2.7 E). In the P-loop region (β2-α2-loop), there are many different mutations that could interfere with NADase activity (Figure 2.7 F). The ATR1-interacting interface displayed various mutations relative to the reference $RPP1^{WsB}$, also in residues that have been reported to be essential for ATR1 recognition (Fig 3.7 G). The number of LRR motifs range in $RPP1^{GelA}$(15), $RPP1^{GelB}$(16), $RPP1^{GelC}$(19), $RPP1^{GelD}$(17), $RPP1^{GelE}$(12), $RPP1^{GelF}$(11), $RPP1^{GelG}$(17), $RPP1^{GelH}$(17), $RPP1^{GelI}$(15), $RPP1^{GelJ}$(15), $RPP1^{DraA}$(23), $RPP1^{DraB}$(20), $RPP1^{DraC}$(19), $RPP1^{DraD}$(16), $RPP1^{DraE}$(18). The C-JID domain was present in all sequences (Supplementary Figure 2.3).

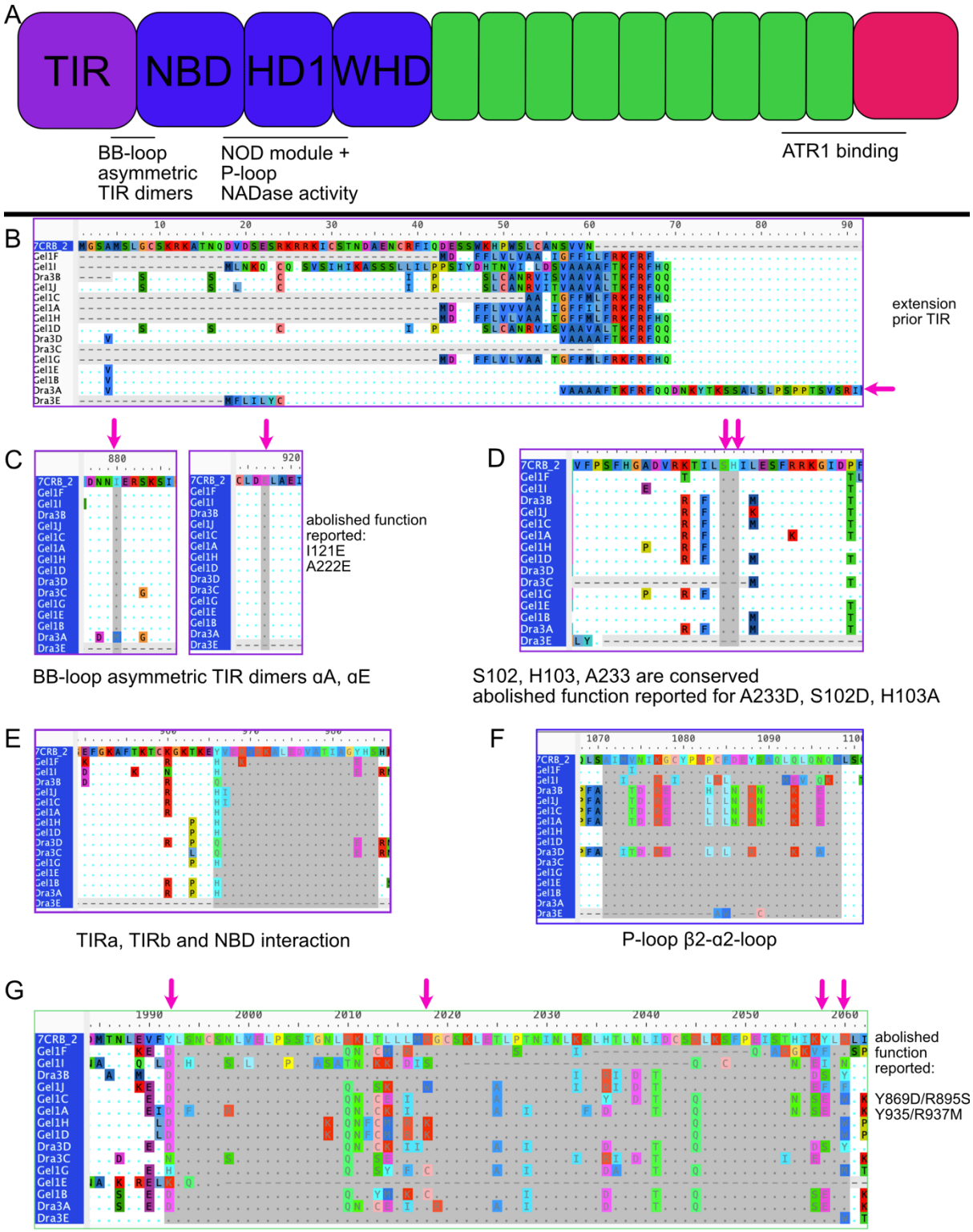

Figure 2.7: **Sequence alignment of DraIII-1 and Gel-1 RPP1 variants on known sites.** A) Schematic representation of RPP1 domain architecture, followed by selected segments from a multiple sequence alignment of RPP1 variants identified in Gel-1 and DraIII-1. The

highlighted regions correspond to known functional interfaces implicated in tetramerization, NADase activity, and ATR1 recognition. Mutations in these sites have been shown to abolish RPP1 functionality. Arrows indicate amino acid residues where specific substitutions are known to disrupt function (C-G). B) Alignment of the N terminal region, highlighting an N terminal extension unique to $RPP1^{DraA}$. C) BB-loop, with critical residues marked; $RPP1^{DraA}$ carries aI121M substitution. $RPP1^{DraE}$ lacks most of the TIR domain C-F. D) Highlighted SH motif is conserved but for $RPP1^{DraC}$ and $RPP1^{DraE}$, which have gaps. E) Alignment of the TIR/NB-ARC interaction interface. F) P-loop region with many amino acid substitutions for $RPP1^{GelF}$, RPP^{GelI}, $RPP1^{DraB}$, $RPP1^{GelJ}$, $RPP1^{GelC}$, $RPP1^{GelA}$, $RPP1^{DraD}$ and $RPP1^{DraE}$. G) ATR1-binding interface, aligned across all variants.

Finally, I synthesized all 15 genomic full-length *RPP1* alleles and cloned these together with a constitutive promoter 35S (Fraley et al., 1983) and added a C terminal MYC-tag in order to test protein stability and expression (Supplementary Figure 2.2 A). 16 *ATR1* alleles were PCR-amplified and cloned into the respective vector with a 35S promoter and C terminal HA-tag. All 240 combinations of ATR1 and RPP1 variants were co-expressed in *N. benthamiana* and since the first experiments were conducted in *N. tabacum* I also tested some of these combinations in *N. tabacum* in order to verify cell-death responses and to test if I might have missed some of the no eliciting cell-death responses. In expression tests, most Gel-1 RPP1 variants were successfully expressed in *N. benthamiana*, except for $RPP1^{GelI}$ (Supplementary Figure 2.2 B). In contrast, expression of RPP1 variants from DraIII-1 was generally weaker. $RPP1^{DraE}$ showed the expected truncation (Supplementary Figure 2.2 B).

Notably, $RPP1^{DraD}$ and $RPP1^{GelG}$ exhibited auto-activity in both *N. benthamiana* and *N. tabacum* when over-expressed alone (Supplementary Figure 2.2C), however not when expressed under the native promoter of DM2 this phenotype was abolished (data not shown). Since I did not further investigate the autoactivity as possible result through interaction with other proteins in *Nicotiana sp.* I therefore excluded these two variants from further experiments. For $RPP1^{GelG}$, I detected a range of cell death responses when co-expressed with different ATR variants including a slight suppression of the cell death when being co-expressed with $ATR1^{Cala2}$ and $ATR1^{PH883}$, however these observations were inconsistent (Supplementary Figure 2.3). However, I did not properly track the development of the cell death as well as the protein expression during the 2-day period for cell death response, as the variation on the cell

death response was too high (Supplementary Figure 2.3). Also, when assessing further the RPP1 sequence of the autoactive DraIII-1 and Gel-1 variants, especially in the range of 98 - 230 amino acids, where autoactivity in TIR only domains from WsB and NdA was described (Bernoux et al., 2011; Zhang et al., 2017), I did not detect any amino acid changes restricted to these two variants, $RPP1^{DraD}$ and $RPP1^{Gel}$, which could explain autoactivity (Supplementary Figure 2.4). I excluded $RPP1^{DraD}$ and $RPP1^{GelG}$ for further analysis.

After co-expressing as many combinations of ATR1 and RPP1 variants as possible, I normalized the observed cell death responses and averaged the results across biological replicates to obtain a cell death score for each interaction pair (Figure 2.8). For the purpose of interpretation, cell death scores ranging from 0.25 to 0.5 are classified as '*weak'*, scores between 0.5 and 0.6 as '*intermediate'*, and scores above 0.6 as '*strong'* cell death responses. The positive control, co-expression of $RPP1^{WsB}$ with $ATR1^{Emoy2}$, induced a strong cell death response (Figure 2.8). Some of my ATR1 variants were recognized by multiple RPP1 variants ($RPP1^{WsB}$, $RPP1^{GelA}$, $RPP1^{GelC}$, $RPP1^{GelD}$, $RPP1^{GelH}$), as predicted with the alignment sequencing scores and ipTM values. The majority of ATR1 variants differed in the C terminal portion (α4–α13 of the structure), which mainly interacts with the anti-β-sheet -C-JID, from the $ATR1^{Emoy2}$ reference, therefore most of these variants were not expected to induce cell death when being expressed with $RPP1^{WsB}$. Strong cell death response was obtained when $RPP1^{WsB}$ was co-expressed with $ATR1^{PH129}$, the only effector which differs in only a single amino acid K99E from the reference $ATR1^{Emoy2}$, this aligns the already known information that the N terminal domain is not relevant for interaction with RPP1.

When comparing the different RPP1 and ATR1 variants, which elicited cell death responses, it is unclear from the effector sequences which residues contribute to RPP1 interaction. For instance, $RPP1^{GelH}$ cause strong cell death when being co-expressed with $ATR1^{PH495}$, $ATR1^{PH1034}$, and $ATR1^{PH1245}$; these sequences share residues which are known to contribute to binding and differ from the $ATR1^{Emoy2}$ variant. However, these residue differences are also shared across other effector variants. A probable explanation is that the variable C terminus may contribute to protein folding and complex stability, which means the different effector variants needed to be investigated more fully by amino acid substitutions, which I have not done in this study.

Among the RPP1 variants of DraIII-1, RPP1^{DraA} was the only variant that elicited not only weak but also intermediate cell death responses when co-expressed with ATR1 variants. One hypothesis is that the extended LRR domain in RPP1^{DraA} provides a broader or more flexible interface for ATR1 recognition, resulting in generally higher responsiveness. Alternatively, the presence of a W388S substitution near the P-loop, uniquely observed in this variant, may impact the conformational changes required for full activation, thus accounting for the mixture of weak and intermediate responses.

As expected, RPP1^{DraE}, which lacks most of the TIR domain, did not trigger a cell death response when co-expressed with any ATR1 variant. RPP1^{DraB} elicited weak responses only in combination with ATR1^{Emoy2} and ATR1^{PH1464}. Notably, RPP1^{DraB} had one of the lowest sequence alignment scores to the RPP1WsB reference structure (PDB: 7CRC), ranking just above RPP1^{DraE} and RPP1^{GelE}. RPP1^{DraC} e induced weak cell death responses when co-expressed with four ATR1 variants. Despite having high AlphaFold3 confidence scores for tetramer formation, it is possible that a compatible ATR1 variant was missing from the panel tested, an explanation that could also apply to other RPP1 variants that failed to trigger a response. RPP1^{GelJ} and RPP1^{GelI} failed to induce cell death with most ATR1 variants. In the case of RPP1^{GelI}, this may be attributed to protein instability, as no detectable protein band was observed, suggesting poor or absent expression. RPP1^{GelE} and RPP1^{GelF}, which have the lowest number of LRR motifs among the Gel-1 variants, only triggered weak responses with a few ATR1 variants. This may indicate that a minimum number of LRR repeats is necessary for stable effector recognition and signal initiation.

The variation in outcomes observed in the *Nicotiana* system suggests that the different RPP1 variants vary in their ability to recognize ATR1 variants during natural infections of *Arabidopsis thaliana* by diverse *Hyaloperonospora arabidopsidis* strains. To further investigate these results and reconcile them with prior experimental discrepancies, future research should explore the regulatory mechanisms governing the RPP1 pathway in these accessions, since some of these NLRs could be potentially regulated like previous described DM2/RPP1variants (Lei & Weigel 2021; Chae et al., 2014; Wan et al., 2025; Stuttmann et al., 2016; Tahir et al., 2013)

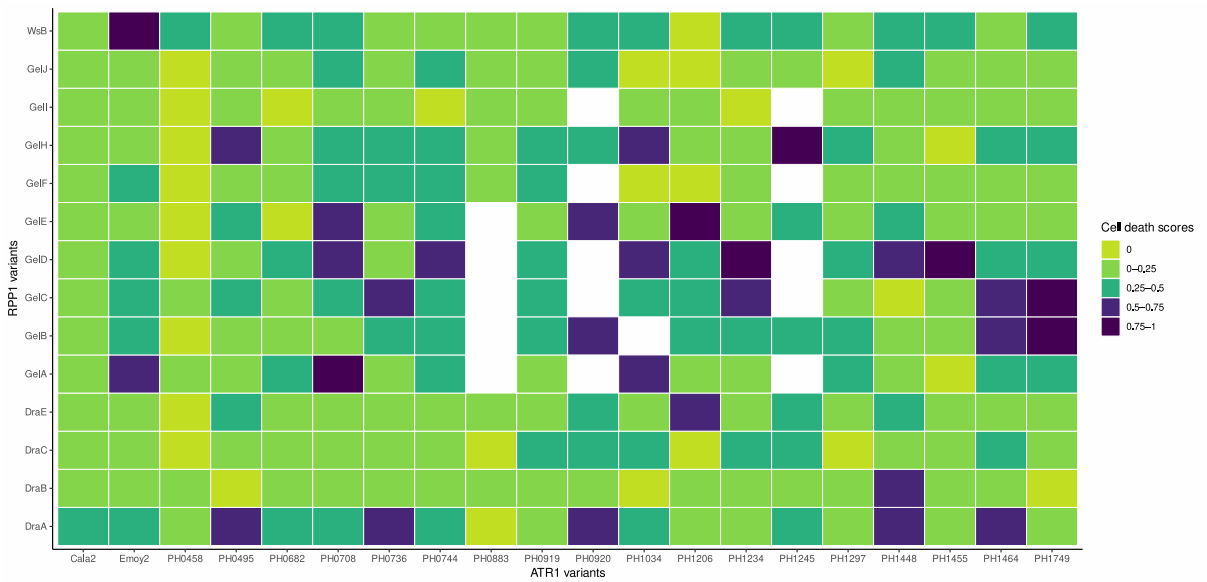

Figure 2.8: **Co-expression matrix of all tested RPP1 and ATR1 variants in *Nicotina spp*.** Included were controls: $RPP1^{WsB}$ with $ATR1^{Emoy2}$ as positive control and $RPP1^{WsB}$ with $ATR1^{Cala2}$ as negative response. Cell death score represents the normalized number of leaves showing cell death response, combined across each experiment which consisted of at least six infiltrated leaves, as technical replicates, and at least 3 biological replicates. Strong cell death is indicated as 1 and no cell death response as 0. White boxes indicate missing values, or an insufficient number of replicates.

2.5 Chromosome 3 is not relevant for resistance to *H. arabidopsidis*

Based on the heterologous expression assays in *Nicotiana* species, I observed stronger cell death responses from several RPP1 variants derived from Gel-1, whereas only a single RPP1 variant from DraIII-1 ($RPP1^{DraA}$) exhibited an intermediate response. Notably, $RPP1^{GelA}$ appeared capable of recognizing multiple ATR1 variants in the *Nicotiana* system. However, Gel-1 displays limited resistance to various *H. arabidopsidis* isolates, including those encoding ATR1 variants that were recognized by $RPP1^{GelA}$ in the heterologous assay.

To assess the contribution of the *RPP1* locus to disease resistance in an unbiased manner, I wanted to identify genomic regions associated with *H. arabidopsidis* resistance. I therefore performed genetic mapping using bulk segregant analysis (BSA) (Mansfeld and Grumet 2018; Takagi et al., 2013; Magwene and Kelly 2011). I generated F_2 populations from crosses between Gel-1, DraIII-1, and IP-Moa-0, and infected approximately 150 plants per F_2 population with *H. arabidopsidis* isolates that showed contrasting resistance or susceptibility in the parental lines. I collected both resistant and susceptible plants of roughly 100 plants, ending up with resistant and susceptible pools of 25-125 individuals per F_2 population (Table 2.2). Eight *H. arabidopsidis* isolates were selected based on their ability to elicit clear resistance or susceptibility phenotypes in the parental *Arabidopsis* accessions. Nine F_2 populations were analyzed, each displaying segregation ratios consistent with a 3:1 distribution, indicative of monogenic inheritance (Table 2.2). For each F_2 population, plants exhibiting susceptible phenotypes were pooled separately from those showing resistance. Genomic DNA was then extracted from each of the pooled groups and sequenced for further analysis.

The DraIII-1 × Gel-1 populations infected with *H. arabidopsidis* isolates Emoy2, PH0527-3, PH0919-1, PH1234-1, and PH1239-1 as well as from DraIII-1 × IP-Moa-0 populations infected with PH0458-1, PH0527-3, and PH0708-1, revealed both shared and population-specific quantitative trait loci (QTL). Quantitative trait locus (QTL) analysis revealed distinct peaks on chromosome 1 (in four populations), chromosome 4 (in three populations), and chromosome 5 (in one population) (Figure 2.9). Notably, no significant QTL peaks were detected on chromosome 3, where the *RPP1* locus is located. These findings suggest that the *RPP1* locus does not play a major role in

resistance to *H. arabidopsidis* in the F_2 populations tested. Instead, resistance is likely governed by loci on chromosomes 1, 4, and 5, which may encode key determinants of immunity in this *H. arabidopsidis* - *A. thaliana* pathosystem.

Table 2.2: Overview of QTL mapping of *H. arabidopsidis* resistance in *A. thaliana* F_2 populations. Tricube-smoothed *G'* values are shown for each F_2 population. Red lines indicate significance thresholds established from Magwene et al. (2011). F_2 populations consisted of resistant (R) and susceptible (S) plants.

Cross	*H. arabidopsidis* isolate	F_2 segregation ratio	QTL maps
DraIII-1 X Gel-1	Cala2	75 R / 25 S	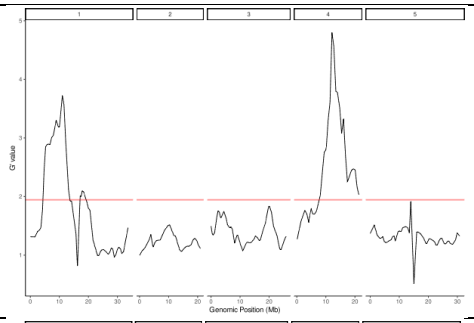
DraIII-1 X Gel-1	Emoy2	75 R / 25 S	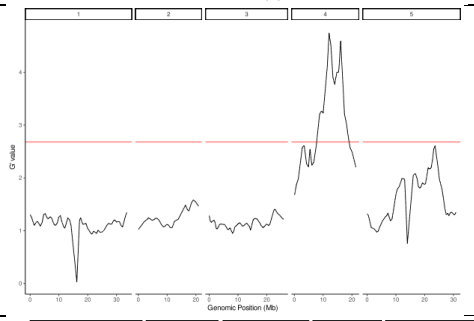
DraIII-1 X IP-Moa-0	PH0458	93 R / 31 S	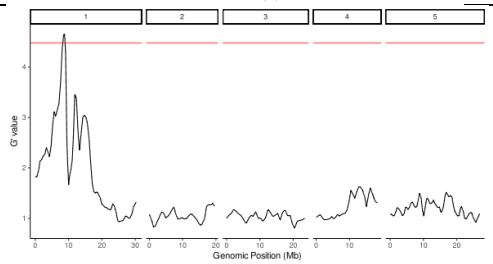
DraIII-1 x Gel-1	PH0527	125 R / 52 S	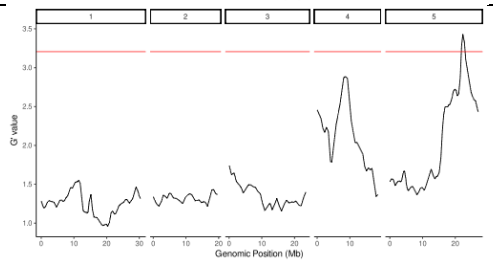
DraIII-1 x IP-Moa-0	PH0527	75 R / 25 S	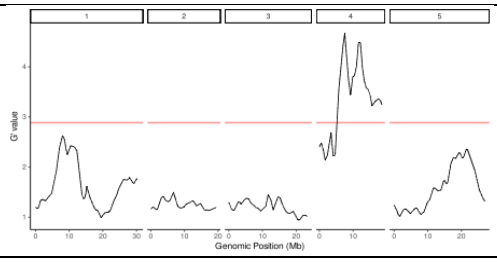

DraIII-1 x IP-Moa-0	PH0708	75 R / 25 S	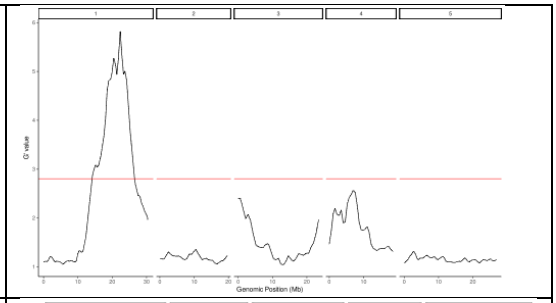
DraIII-1 x Gel-1	PH0919	93 R / 31 S	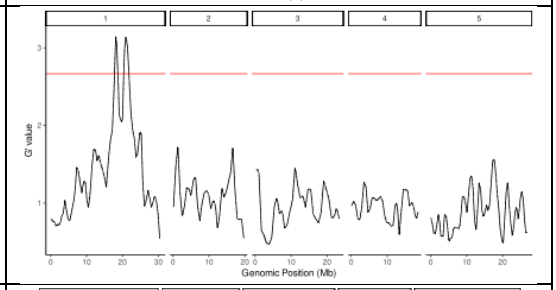
DraIII-1 x Gel-1	PH1234	78 R / 25 S	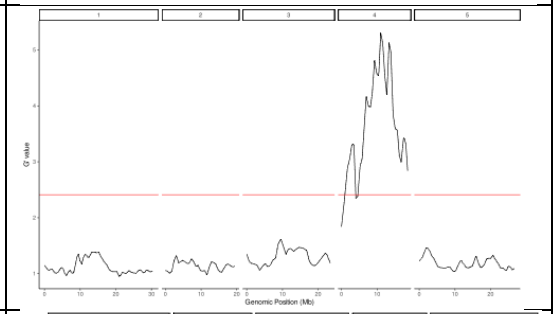
DraIII-1 x Gel-1	PH1239	84 R / 28 S	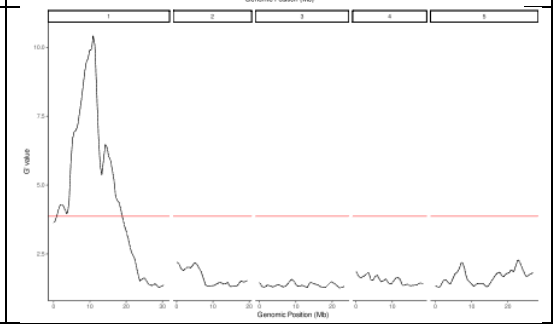

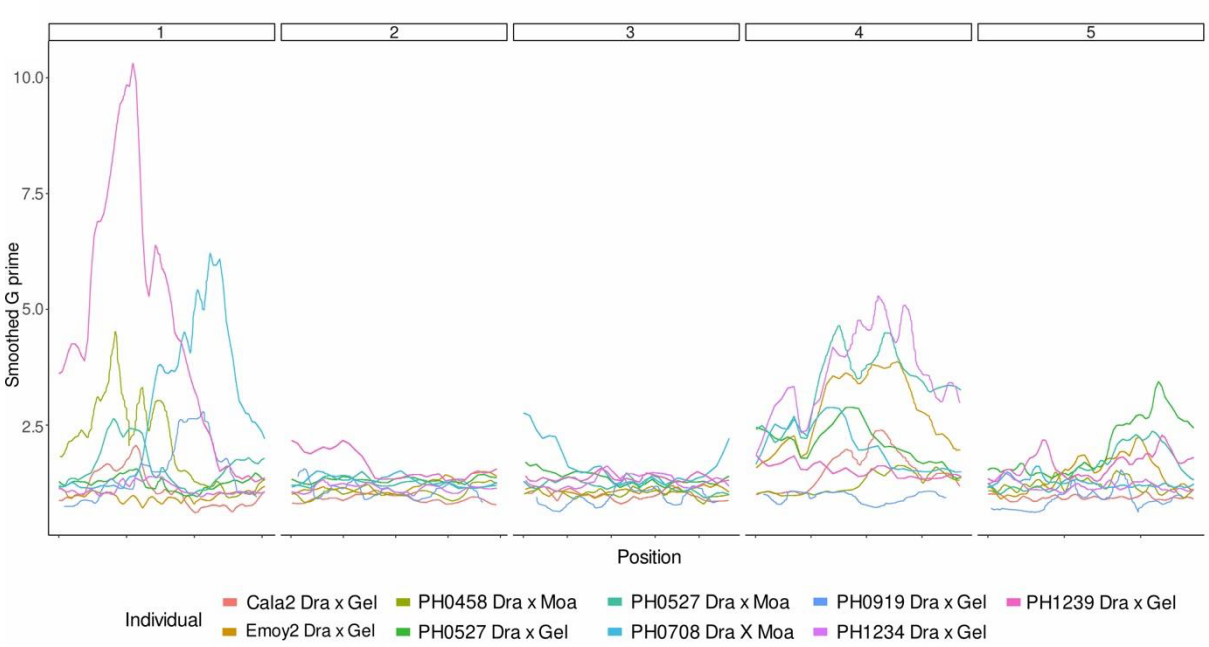

Figure 2.9: **Summary of QTL.** Tricube-smoothed *G'* values are shown for each F_2 population. Each lines represents one F_2 populations from crosses between IP-Moa-0, Gel-1 and DraIII-1 accessions, which had been infected with *H. arabidopsidis* Cala2, Emoy2, PH0458, PH0527, PH0708, PH0919, PH1234 and PH1239. Genome position is indicated chromosomes 1 -5.

2.6 Patterns of *RPP1* presence and absence in a local population

In my analysis of variation at the *RPP1* locus, the accession IP-Moa-0 stood out due to its apparent lack of the entire locus. To determine whether this absence was the result of a rare mutation or represented a broader pattern, I returned to the original IP-Moa-0 collection site in Montanuy, Spain (Alonso-Blanco et al., 2016). In the spring of 2024, I collected 117 *Arabidopsis thaliana* plants and three *Hyaloperonospora arabidopsidis* isolates within a radius of 4.38 km and 2.73 km, respectively (Supplementary Figures 2.7, 2.8). At the exact reported IP-Moa-0 site, 32 individual plants were sampled (Supplementary Table 2.3, Figure 2.10 A).

To place these samples in a broader geographic context, I also included seven accessions from the 1001 Genomes Project (Alonso-Blanco et al., 2016), 9827, 9525, 9567, 9588, 9899, 9950, and 9844, located up to 50 km from the original IP-Moa-0 site, as potential outliers. Whole-genome sequencing (at 10× coverage) was performed on the progeny of the collected plants, and sequencing reads were mapped to the long-read Gel-1 genome (Teasdale et al., 2024) to assess *RPP1* locus presence (Supplementary Figure 2.5). In addition, I sequenced the genomes of the three *H. arabidopsidis* isolates and confirmed that all carry an *ATR1* allele (Supplementary Figure 2.6).

Read mapping revealed that only 73 out of 117 *A. thaliana* plants (62%) carried *RPP1* sequences, consistent with the absence observed in IP-Moa-0 (Figure 2.10 A,B). To assess functional consequences, I infected the progeny of 112 of the 117 plants, along with the seven 1001 Genomes accessions, with the three local *H. arabidopsidis* isolates: *H. arabidopsidis*^{PH5421}, *H. arabidopsidis*^{PH5422}, and *H. arabidopsidis*^{PH5442}. Resistance to these isolates was rare: only ~2% of plants showed resistance to *H. arabidopsidis*^{PH5421} or *H. arabidopsidis*^{PH5442}. There was no apparent correlation between *H. arabidopsidis* resistance and the presence of *RPP1* sequences in the host plants: Of the plants that were resistant to at least one *H. arabidopsidis* isolate, 11 lacked any detectable *RPP1* sequences, while 18 carried at least one *RPP1* copy. Only one plant, 9827, was resistant to all three isolates and also harbored *RPP1* sequences (Figure 2.10 B).

To explore the population structure in my *A. thaliana* collected, I calculated SNP-based genetic distances between all individuals (Figure 2.10 B). This analysis

revealed two major genetic clusters and one smaller outlier group containing mostly but not only the geographically more isolated plants. The largest, most distinct genetic cluster had only plants with at least one *RPP1* copy. Most of these plants were susceptible to the three local *H. arabidopsidis* isolates. The second, more diffuse cluster included both plants with and without *RPP1* sequences in their genomes.

Together, our results demonstrate that the complete absence of *RPP1* sequences is not rare in the Montanuy population. Furthermore, infection assays with local *H. arabidopsidis* isolates hint that *RPP1* is unlikely to act as a dominant resistance factor under the tested conditions.

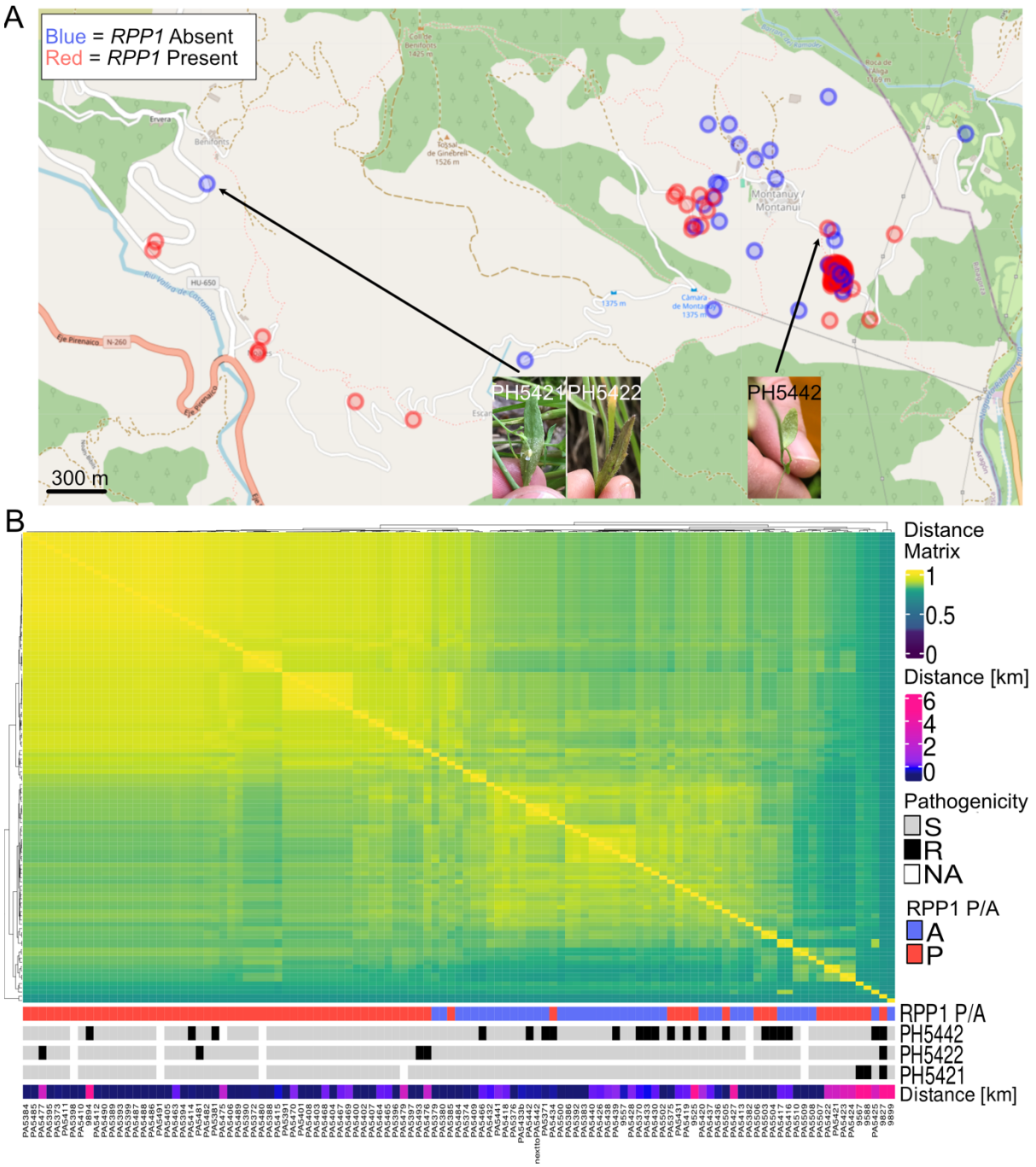

Figure 2.10: **Overview of the IP-Moa-0 population.** A) In total, 117 *A. thaliana* plants and three *H. arabidopsidis* isolates were collected in and around Montanuy (Spain). Field-collected plants with visible signs of *H. arabidopsidis* infection and the corresponding *H. arabidopsidis* isolate names are provided in the three photographs. After propagation in the lab, progeny plants were short-read sequenced and the presence/absence of *RPP1* in this collection was determined. B) Genome-wide genetic distance based on all SNPs across all plants. For each plant, the presence/absence of *RPP1* reads is indicated (blue: absence, red: presence), followed by its resistance (R, black) or susceptibility (S, grey) to the three local *H. arabidopsidis* isolates PH5421, PH5422 and PH5442. Relative geographic distance was relative to the focal IP-Moa-0 site.

2.7 Discussion

In this chapter, I investigated the natural diversity of *H. arabidopsidis* effectors. In addition to the identification of overall effector diversity in 129 isolates, I focused on different ATR1 variants and their contribution to pathogenicity. While some ATR1 variants are recognized *in planta*, they are not the sole contributors to pathogenicity or host effector recognition. By selecting three *Arabidopsis thaliana* accessions differing in both the number and allelic diversity of *RPP1* genes, I demonstrated that the accession Gel-1 harboring the largest set of *RPP1* alleles exhibited greater susceptibility to *H. arabidopsidis* than DraIII-1**,** which contains approximately half as many *RPP1* alleles. In contrast with these findings of high susceptibility Gel-1 induced strong cell death response in four RPP1 variants when co-expressed with different ATR1 variants, these results suggest potential negative regulations among *RPP1* copies within the plant.

To address which other effectors besides ATR1 could have potential roles in pathogenicity, I systematically characterized the effector repertoires of multiple *H. arabidopsidis* isolates and compared them with the phenotypic data from the aforementioned experiments, and provided new candidate effectors.

On the plant side to validate that *RPP1* is not the key-player in this pathosystem I generated new F^2 populations across the three accessions Gel-1, DraIII-1 and IP-Moa-0. The majority of the Quantitative Trait Locus pointed to chromosomes 1 and 4 and not chromosome 3 where *RPP1* is located.

In the ecological context of how *RPP1* is shaped within a population I went back to the origin: Montanuy (Spain), where IP-Moa-0, the *RPP1* absent accession, was collected. 37 % of all sampled plants showed absence of *RPP1* and higher resistance to the local isolates from *H. arabidopsidis*, after testing these infections under laboratory conditions.

Seeds from these collections were bulked for the community, and short-read sequencing data were generated for future genomic analyses.

2.7.1 European-wide effector diversity

It has been reported that *Hyaloperonospora arabidopsidis* secretes approximately 339 effector proteins during its lifecycle (Asai et al., 2014). In this study, I identified 330 of these effectors across 129 isolates, capturing the vast majority of known effectors. The

remaining nine effectors were likely not detected due to reference bias associated with the isolate 495-1, which lacks these genes. Effector research in *H. arabidopsidis* has so far been relatively focused on few effectors, leaving much to be explored within its repertoire of over 300 effectors. Here, I provide an overview of the most variable effectors, prime candidates for further functional studies, as effectors with high sequence variability are often involved in pathogenicity and may co-evolve with highly polymorphic plant immune receptors (Eves-van den Akker et al., 2016; Sutherland et al., 2023). When comparing effector profiles between isolates based on host plant phenotypes, I observed only a small subset of effectors that differed among them. Of 49 effectors specific to six isolates, only four could be linked to known functionality: HaRxL89 (Badel et al., 2013), HaRxL57 (Fabro et al., 2011), HaRxL17 (Caillaud et al., 2013), and HaRxLL447 (Asai et al., 2018a). The remaining 45 effectors represent promising candidates for functional screens, such as assessing their impact on bacterial growth (Fabro et al., 2011) or probing effector-receptor interactions via protoplast assays (Arndell et al., 2024).

2.7.2 Possible scenarios suppressing ATR1/RPP1-mediated immune response

In the entire short-read sequenced data of collected *H. arabidopsidis*, *ATR1* with 163 polymorphic SNPs appeared as the second highest candidate for effector diversity, right after HaRXL128 with 186 polymorphic SNPs. In 60 isolates the *ATR1* sequence was re-sequenced to validate their sequences. I identified 27 distinct alleles, substantially expanding the eight previously described ATR1 alleles originating from isolates collected in the UK (Botella et al., 1998; Holub et al., 1995; Tor et al., 1994). These alleles mainly differ by single amino acid substitutions in the C terminal α4–α8 helices, which are known to be implicated in receptor binding (Chou et al., 2011; Ma et al., 2020; Steinbrenner et al., 2015). Greater variation was observed in the upstream α9–α13 region. From these 27 alleles, I selected six representative variants for functional analysis across *Arabidopsis thaliana* accessions with varying *RPP1* content. Heterologous expression of systematically selected ATR1 variants in Gel-1 and Dra III-1, did not align with the observed phenotypes *H. arabidopsidis* pathogenicity profiles. Echoing observations made for ATR13^{Emco5}, where effector recognition did not guarantee immunity (Kee et al., 2007). It has been reported that ATR1 is expressed during infection (Asai et al., 2014), and its recognition by the compatible RPP1 variants

can reduce susceptibility (Rehmany et al., 2005). Even though I did not test for *ATR1* expression in isolates infecting Gel-1 and DraIII-1, the different *RPP1* alleles in these two accessions were described to be expressed in both accessions (Teasdale, Murray et al., 2024). Interestingly, Gel-1, despite its higher susceptibility, harbored RPP1 variants that strongly recognized certain ATR1 alleles, suggesting suppression of NLR activity within the plant and potential targets of the effector which might induce suppressive regulations. In contrast, RPP1 variants from DraIII-1, the more *H. arabidopsids* resistant accession, showed overall weaker cell death responses after being co-expressed with different ATR1 variants.

These findings suggest that Gel-1's overall susceptibility may result from the presence of core effectors in most isolates rather than from the absence of recognition. For example, Gel-1 was resistant to *H. arabidopsidis*^{PH708} but did not recognize ATR1^{PH708}, pointing toward unidentified effectors driving resistance. The concept of "core effectors" driving major phenotypes is well-established across diverse plant-pathogen systems (Baltrus et al., 2011; Habich et al., 2022; Laflamme et al., 2020; Lindeberg et al., 2005; Peeters et al., 2013). My experimental design, by focusing on two extreme phenotypes, may have missed intermediate phenotypes necessary to pinpoint such core effectors.

2.7.3 RPP1 variants for ATR1 recognition and autoactivity

To further dissect effector-receptor interactions, I utilized AlphaFold2 (Jumper et al., 2021) and the AlphaFold3 (Abramson et al., 2024) webserver to model and co-model various RPP1 and ATR1 variants. While co-modeling remains challenging, especially for point mutation-dependent interactions (Pak et al., 2023), structural predictions helped identify potential RPP1 tetramerization interfaces. Visual inspection and comparison with reference structures provided clues on which RPP1 variants were more likely to interact with specific ATR1 alleles. Recent studies, including unbiased structural comparisons that reveal global topology differences across variants (Abramson et al., 2024), have shown how AlphaFold predictions are re-shaping NLR research (Qiao et al., 2024; Seong & Krasileva, 2023; Toghani et al., 2024). I tested the function of various RPP1 variants by assessing cell death induction upon co-expression with ATR1 alleles. The RPP1 variants (e.g., RPP1^{GelB}, RPP1^{GelJ}, RPP1^{DraC}, RPP1^{GelF}) with high confidence modelling score and high alignment sequencing

scores to WsB did not trigger visible cell death, possibly due to the absence of incompatible ATR1 alleles. Notably, RPP1^{DraA} consistently induced intermediate cell death responses, potentially due to E385D and W388S substitutions near the MHD motif, which may impair activation. Intermediate responses were particularly interesting, as subtle conformational changes can modulate interaction strength (Steinbrenner et al., 2015). To further explore this, I repeated some "negative" interactions in *N. tabacum*, where cell death responses sometimes differed from those in *N. benthamiana*. Remarkably, ATR1^{PH883} and ATR1^{Cala2} partially suppressed autoactivity of RPP1^{GelG}, suggesting effector-mediated NLR suppression, a mechanism not previously described for RPP1 (Contreras et al., 2023). Minimal RPP1 variants (e.g., RPP1^{DraE} and RPP1^{GelE}) lacked key domains necessary for activity. RPP1^{DraE}, which showed truncations and gaps in the TIR, NB-ARC, and LRR regions, showed no cell death, as expected. RPP1^{GelE} lacked known residues associated with autoactive minimal TIR function (Schreiber et al., 2016). Autoactivity of RPP1^{DraD} and RPP1^{GelG}, however, could not be explained by currently known motifs.

Linking the recognition of the RPP1 variants, within the same accession, to different ATR1 variants has been tested before in the accessions Estland and Zdarec (Goritschnig et al., 2016). The novelty of my approach lies in identifying an accession (Gel-1) that is highly susceptible to *H. arabidopsidis*, yet it encodes multiple RPP1 variants with strong ATR1 recognition. Including one autoactive variant per accession, RPP1^{GelG}and RPP1^{DraD}. However, I did not reveal the target of these ATR1 variants, potentially ATR1 or other effectors could target host proteins which in turn can suppress *in planta* regulatory mechanisms. Which could involve the suppression of these ATR1-recognizing RPP1 variants. For the other RPP1 variants I did not investigate further if they can be regulated through other proteins as described before in the context with DM2/RPP1 (Lei & Weigel 2021; Chae et al., 2014; Tahir et al., 2013; Wan et al., 2025). Future work could focus on assessing *RPP1* alleles individually in Gel-1 by sequential knock-out lines to determine whether the absence of specific alleles contributes to resistance against *H. arabidopsidis*.

2.7.4 Chromosome 1 and 4 as potential key regulators for resistance

While several RPP1 variants induced molecular-level responses (e.g., cell death upon co-expression with ATR1), these responses were not always reflected at the whole-

plant level. To explore this discrepancy, I performed quantitative trait locus (QTL) analysis using multiple F_2 mapping populations. This analysis revealed chromosomal regions associated with resistance on chromosomes 1 and 4, four F_2 populations mapped to chromosome 1, three to chromosome 4, one to chromosome 5, and one to both chromosomes 1 and 4. The latter could potentially represent a cross-contamination event involving different isolates. These results partially overlap with findings from Nemri et al. (2010), which also identified resistance loci on chromosomes 1 and 4. Notably, these regions harbor several well-characterized NLR genes: RPP2, RPP4/5, RPP7, and RPP39. All have been studied in relation to *H. arabidopsidis* and their corresponding effectors, with the exception of RPP7, for which the matching effector, ATR7, has yet to be discovered. To identify potential ATR7 candidates, co-modelling RPP7 with the set of highly polymorphic effectors may offer valuable leads.

The RPP4–ATR4 interaction, long considered canonical, has been complicated by findings that ATR4 can evade RPP4 recognition through altered expression and subcellular localization (Asai et al., 2018; Botella et al., 1998). Given this, it would be worthwhile to fine-map the F_2 populations showing peaks on chromosome 4 and functionally test high-diversity effectors found in isolates PH1234, PH0527, and Emoy2. In contrast, RPP2 and RPP39 have already been reliably linked to their cognate effectors ATR2 and ATR39, respectively (Goritschnig et al., 2012; Kim et al., 2024). These well-established relationships serve as useful models for dissecting the genetics of isolate-specific resistance.

2.7.5 Presence/Absence Polymorphisms and Balancing Selection in Natural Populations

The presence and absence (P/A) of immune receptor loci such as RPP1 represent a striking example of natural variation maintained across *A. thaliana* populations. Studies have shown that such allelic polymorphisms, whether in the form of functional/non-functional, resistant/susceptible, or P/A variants, are often maintained through balancing selection, particularly in spatially structured metapopulations (Bakker et al., 2006; Caicedo et al., 1999; Gos et al., 2012; Koenig et al., 2019; Mauricio et al., 2003; Rose et al., 2012; Stahl et al., 1999; Tian et al., 2002). These dynamics are driven by co-evolution with multiple pathogens, whose prevalence and diversity fluctuate over space and time (Koenig et al., 2019), constrained by the

inherent limits on immune gene diversity within plant genomes (Bakker et al., 2006; Karasov et al., 2017; Michelmore & Meyers, 1998b). In addition to *RPP1*, P/A polymorphisms have also been observed in other resistance genes such as *RPS5* (Henk et al., 1999) and *RPS2*, the latter displaying presence/absence as well as resistant/susceptible allelic variation (Platt et al., 2010). Given that *RPP1* copy number variation was previously reported to average around six per accession (Lee & Chae, 2020), I revisited the only reported accession lacking a single *RPP1* copy to determine whether this absence was stable within the local population. Remarkably, I observed an almost balanced P/A pattern of *RPP1* within naturally collected individuals from that site, coupled with higher levels of resistance to *H. arabidopsidis* in plants lacking RPP1. This suggests that the *RPP1*-absent genotype may confer a selective advantage in the current pathogen landscape, reflecting theoretical models of immune gene evolution under fluctuating selective pressure (Brown & Tellier, 2011). I identified two distinct populations, but it remains unresolved whether the *RPP1*-absent group is a recent invader into the *RPP1*-present population. The long-term stability and fitness of this variant could be evaluated by repeated sampling over time, which would help determine whether this resistance-associated absence becomes fixed or continues to be balanced by other selective forces.

2.8 Supplementary

Supplementary Table 2.1: List of *H. arabidopsidis* collected isolates.

ID	Latitude	Longitude
PH0015-1	38.05736	-4.19318
PH0068-1	39.39484	-5.78286
PH0070-1	39.39484	-5.78286
PH0071-1	39.39484	-5.78286
PH0124-1	38.76024	16.23519
PH0129-1	38.76024	16.23519
PH0133-1	38.96973	16.3407
PH0136-1	38.96973	16.3407
PH0136-2	38.96973	16.3407
PH0140-1	38.96973	16.3407
PH0147-1	39.12925	16.16778
PH0156-1	39.26974	16.27086
PH0157-2	39.26974	16.27086
PH0157-3	39.26974	16.27086
PH0162-1	39.48333	16.2784
PH0162-2	39.48333	16.2784
PH0162-3	39.48333	16.2784
PH0163-1	39.48333	16.2784
PH0164-1	39.48333	16.2784
PH0166-1	39.48333	16.2784
PH0166-2	39.48333	16.2784
PH0166-3	39.48333	16.2784
PH0166-4	39.48333	16.2784
PH0168-1	39.48333	16.2784
PH0211-1	41.72872	2.9077
PH0257-1	41.17051	14.17522
PH0320-1	44.99942	1.30068
PH0325-1	45.00064	1.74917
PH0458-1	48.52938	9.05863
PH0459-1	48.52938	9.05863
PH0459-2	48.52938	9.05863
PH0466-1	50.29125	7.26436
PH0471-1	50.38839	8.06598
PH0477-1	50.0905	8.56435
PH0494-1	50.29125	7.26436
PH0495-1	50.38839	8.06598
PH0511-1	38.97427	48.55284
PH0517-1	38.7354	48.84103
PH0527-3	38.74044	48.61248
PH0538-1	38.65625	48.80046
PH0564-1	41.82686	46.28318
PH0566-1	41.79564	43.46844
PH0660-1	48.80611	2.16515
PH0661-1	48.80611	2.16515
PH0681-1	48.52938	9.05863
PH0682-1	48.52938	9.05863
PH0695-1	48.32721	14.71513
PH0708-1	41.82786	25.68699
PH0711-1	41.82786	25.68699
PH0724a-1	41.53786	24.97745
PH0733-1	41.61943	23.93737
PH0736-1	41.61943	23.93737
PH0736-2	41.61943	23.93737
PH0744-1	41.58686	23.5561
PH0745-1	41.58686	23.5561
PH0877-1	48.33204	14.71572
PH0878-1	48.33204	14.71572
PH0883-1	48.33204	14.71572
PH0884-1	48.33204	14.71572
PH0885-1	48.42641	15.56995
PH0891-1	49.27734	16.63
PH0892-1	49.27734	16.63
PH0900-1	49.40779	16.27657
PH0919-1	49.9842	13.41717
PH0920-1	49.9842	13.41717
PH0944-1	51.5744	5.46741

PH1032-1	51.25483	1.02029
PH1034-1	51.25483	1.02029
PH1094-1	50.89959	4.12158
PH1105-1	50.7892	5.37844
PH1109-1	50.7892	5.37844
PH1123-1	52.99227	-6.07541
PH1124-1	52.99227	-6.07541
PH1192-1	55.16567	-1.9606
PH1199-1	54.66228	-2.75662
PH1206-1	55.4767	-2.55439
PH1207-1	55.4767	-2.55439
PH1233-1	51.2502	4.81116
PH1234-1	51.2502	4.81116
PH1239-1	51.16745	4.2268
PH1245-1	51.16784	3.76163
PH1251-1	50.93634	3.62578
PH1252-1	50.93634	3.62578
PH1263-1	50.88866	4.60247
PH1270-1	52.67437	-6.29735
PH1272-1	52.67437	-6.29735
PH1284-1	52.26638	-7.10075
PH1284-1b	52.26638	-7.10075
PH1297-1	52.44792	-8.06358
PH1312-1	52.66856	-8.55832
PH1317-1	52.81228	-8.45633
PH1323-1	52.89413	-8.5529
PH1324-1	52.89413	-8.5529
PH1350-1	53.47957	-9.13189
PH1353-1	53.34742	-8.9437
PH1354-1	53.34742	-8.9437
PH1373-1	53.43545	-9.30709
PH1407-1	54.26488	-8.33463
PH1422-1	55.75142	13.04138
PH1424-1	55.75142	13.04138
PH1440-1	55.67777	13.42023
PH1448-1	55.69422	14.16774
PH1455-1	55.57917	14.33291
PH1456-1	55.57917	14.33291
PH1457-1	55.57917	14.33291
PH1463-1	56.12458	-3.94606
PH1464-1	56.05585	14.30316
PH1469-1	56.08969	14.04852
PH1470-1	56.31554	14.04852
PH1471-1	56.31554	14.04852
PH1477-1	56.31554	16.03761
PH1492-1	56.31554	16.03761
PH1503-1	57.65104	14.80439
PH1504-1	57.65104	14.80439
PH1505-1	57.65104	14.80439
PH1623-1	57.66273	-2.3748
PH1625-1	57.66273	-2.3748
PH1629-1	57.63403	-3.56683
PH1642-1	57.59487	-4.42132
PH1645-1	57.59487	-4.42132
PH1713-1	56.42869	-5.23618
PH1715-1	56.42869	-5.23618
PH1719-1	55.91952	-4.3345
PH1736a-1	56.04442	-4.37275
PH1749-1	42.67566	-2.40631
PH1751-1	42.67566	-2.40631
PH1837-1	53.32991	-8.22293
PH1962-1	62.80042	18.075546
PH2002-1	48.564461	9.156005

Supplementary Table 2.2: Detected effectors and their calculated mean nucleotide diversity across the sequence and their SNP polymorphism.

Effector	Mean Nucleotide diversity	Count
ATR13	0.449402	15
HaRxLL142b	0.406735	1

HaRxL100b	0.349893	1
HaRxL45	0.300692	10
HaRxL14b	0.2701459	91
HaRxLL188b	0.2675863	4
ATR1	0.2655532	163
HaRxLL170	0.2632967	2
HaRxL62	0.2588923	56
HaRxLL24	0.2574613	2
HaRxL23	0.2544859	6
HaRxL128	0.2496033	186
HaRxLL447	0.2492473	27
HaRxLL81b	0.2470891	73
HaRxL57b	0.241272	60
HaRxLL5	0.2375874	22
HaRxL129	0.2371545	33
HaRxLL6b	0.2344444	3
HaRxLL74b	0.2329546	134
HaRxL87i	0.2274624	33
HaRxL95	0.2269604	112
HaRxL60_ATR4	0.2233281	72
HaRxL48_ATR39	0.2180473	21
HaRxLL33	0.2176792	76
HaRxLL121	0.2175623	6
HaRxL106	0.2170461	105
HaRxLL42	0.2137677	8
HaRxLL488	0.2081212	8
HaRxL63	0.2019652	15
HaRxLL50b	0.2007742	26
HaRxL102	0.200481	105
HaRxLL79b	0.1968206	49
HaRxLL109b	0.1934448	11
HaRxLL57	0.1917343	86
HaRxLL444	0.1913023	4
HaRxLL59	0.1896455	6
HaRxLL431	0.1895939	7
HaRxL25	0.1884879	34
HaRxLL423	0.1884328	37
HaRxLL75	0.1880505	84
HaRxLL159	0.1873018	11
HaRxL162	0.1862043	19
HaRxLL160	0.1861148	20
HaRxLL445	0.1846175	55
HaRxLL57b	0.1845519	7
HaRxL61	0.1830407	32
HaRxL112	0.1815856	35
HaRxLL430	0.1788553	18
HaRxLL498	0.1750381	3
HaRxLL437b	0.1737818	37
HaRxLL58	0.173556	33
HaRxL73	0.1716386	97
HaRxL105	0.1715023	22
HaRxLL78	0.1671982	23
HaRxLL489	0.166613	4
HaRxLL6	0.1664764	43
HaRxLL15b	0.1650658	9
HaRxLL22d	0.1617343	7
HaRxLL52	0.1616547	22
HaRxL110b	0.1597133	19
HaRxLCRN22j	0.15942	2
HaRxLL84	0.1591926	8
HaRxLL65	0.1564	15
HaRxLL80	0.1550719	57
HaRxLL132	0.1513064	19
HaRxLL119c	0.1482297	161
HaRxL127b	0.1476838	15
HaRxLL424_ATR5	0.1470195	78
HaRxLL496	0.1463024	8
HaRxLL166	0.14561	5
HaRxLCRN3	0.1426414	12
HaRxL115	0.142072	21
HaRxLCRN19c	0.1408163	57

HaRxLL35	0.1392756	47
HaRxLL153	0.1374865	14
HaRxL131b	0.1361469	25
HaRxLL133d	0.1359568	32
HaRxLL459b	0.1327925	11
HaRxL72	0.1326145	105
HaRxLL439	0.1322843	22
HaRxLCRN12b	0.1312982	57
HaRxLL105	0.1296082	4
HaRxL10	0.1294194	64
HaRxLL61	0.124865	20
HaRxLL18	0.124842	6
HaRxLL429	0.1241825	47
HaRxLL188b	0.1228991	5
HaRxLL126d	0.1216877	8
HaRxLL128b	0.1202573	25
HaRxLL102	0.1195844	12
HaRxL87b	0.1193001	6
HaRxLL165	0.1191439	2
HaRxLL119b	0.1182357	28
HaRxLL73	0.1165779	52
HaRxLL174	0.1157817	40
HaRxLCRN22j	0.1155064	32
HaRxL88	0.115245	5
HaRxLCRN3d	0.1150234	87
HaRxLL140	0.1137057	9
HaRxLL157	0.1109407	17
HaRxL141b	0.110651	91
HaRxLCRN3c	0.1105637	69
HaRxLL432b	0.1100502	2
HaRxLL15b	0.1081457	3
HaRxLL120	0.1066359	5
HaRxLL16b	0.1063398	23
HaRxLL134	0.1056985	72
HaRxLCRN22h	0.1045481	29
HaRxLL163c	0.1044939	15
HaRxL152	0.1032384	10
HaRxLCRN22	0.1031626	2348
HaRxLL147	0.1026407	30
HaRxL80b	0.102276	21
HaRxLL183b	0.1021067	22
HaRxLL163b	0.1017716	23
HaRxLL455c	0.1011962	32
HaRxL70	0.1007991	20
HaRxLL463	0.0996772	4
HaRxLL446	0.0987013	14
HaRxLL82	0.0980229	21
HaRxL3	0.0966683	31
HaRxL98	0.0947718	41
HaRxLL123	0.094573	34
HaRxL103	0.0942091	21
HaRxLL99	0.0941893	22
HaRxLL441	0.0941276	22
HaRxLL133c	0.09338	64
HaRxL155	0.0932058	15
HaRxL119	0.0928491	20
HaRxLL455d	0.0913979	26
HaRxLL88	0.0910546	13
HaRxL32b	0.0900241	32
HaRxLCRN14b	0.0889449	55
HaRxLL468b	0.0885169	25
HaRxLL167	0.0883298	17
HaRxL153	0.0872472	15
HaRxL87f	0.0871645	36
HaRxL161	0.0869065	29
HaRxLL22c	0.084552	52
HaRxLL146b	0.0845093	20
HaRxLL94	0.0844967	15
HaRxLL188b	0.0840898	1
HaRxL120b	0.0833377	8
HaRxLCRN19c	0.0811622	50

HaRxL112	0.0791701	56
HaRxLL186b	0.0783035	2
HaRxLL427	0.0762983	15
HaRxLL465	0.0746583	15
HaRxLL15c	0.074417	119
HaRxLCRN14c	0.0741016	88
HaRxLL126e	0.0738381	27
HaRxLL22d	0.073701	25
HaRxL15	0.0736084	3
HaRxLCRN14	0.0735082	61
HaRxLL94	0.0733916	2
HaRxLL455b	0.0730868	117
HaRxLL474b	0.0723547	11
HaRxLL22	0.0720856	13
HaRxLL1	0.0720525	55
HaRxLCRN19b	0.0708239	81
HaRxLL111	0.0702611	8
HaRxL107	0.0686956	16
HaRxL154	0.0681476	2
HaRxL44	0.0668289	7
HaRxLL141	0.0666316	9
HaRxL108	0.0654974	18
HaRxLL125	0.0651811	3
HaRxLL452	0.0651132	6
HaRxLL38b	0.0640672	48
HaRxL2	0.062847	10
HaRxL24b	0.0621424	13
HaRxLL45	0.0620388	27
HaRxL27	0.0613346	7
HaRxLL455	0.0612489	37
HaRxLL110	0.0594239	26
HaRxLL497	0.0591277	26
HaRxLL137b	0.058923	4
HaRxLL43b	0.0587484	8
HaRxLL9	0.0580452	25
HaRxLL41	0.0561348	21
HaRxLL188c	0.0538956	12
HaRxLL428	0.0533924	12
HaRxLL150	0.05323	22
HaRxLL484	0.052919	23
HaRxL6	0.0529014	9
HaRxLL145c	0.0486918	94
HaRxLL12	0.0466536	21
HaRxLL148	0.0455267	2
HaRxLL188b	0.0444347	33
HaRxLL180	0.0390236	14
HaRxLCRN9b	0.0378613	11
HaRxL58	0.0356688	12
HaRxL111	0.0311243	33
HaRxLL44	0.0311226	2
HaRxL130	0.0259733	3
HaRxLL145b	0.0256912	16
HaRxLL182	0.0189314	7
HaRxLL106	0.0157945	4
HaRxL19	0.0154435	1
HaRxLL180	0	0
HaRxLL101	0	0
HaRxLL438	0	0
HaRxLL438	0	0
HaRxLL107c	0	0
HaRxLL188b	0	0
HaRxLL138	0	0
HaRxLCRN3	0	0

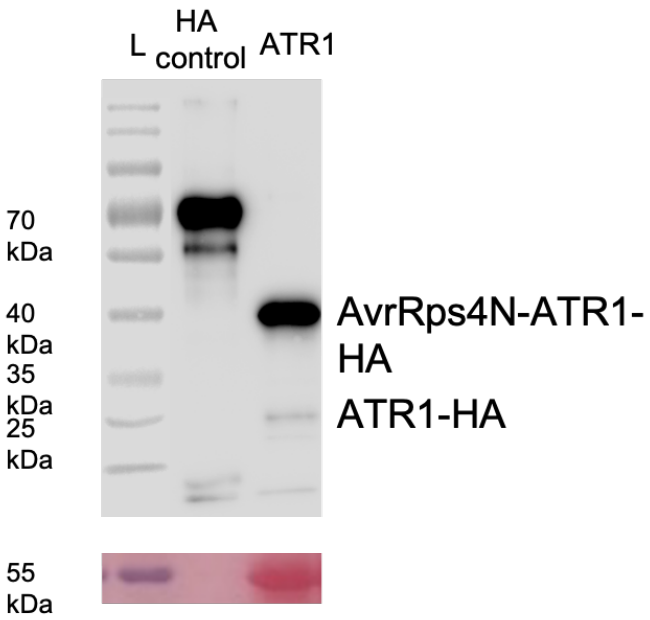

Supplementary Figure 2.1 Translocation of AvrRps4N-ATR1^{Emoy2}-HA in *A. thaliana:* Protein ladder (L), control protein with HA-tag, and AvrRps4N-ATR1^{Emoy2}-HA. Two bands are detected, the top band is the full length protein and the bottom band is after cleavage at the signal peptide. Ponceau staining of rubisco as loading control (bottom).

Supplementary Table 2.2 Infection pattern of *H. arabidopsidis* isolates on *A. thaliana* accessions Gel-1, DraIII-1, IP-Moa-0. Infections were repeated at least 3 times with 5 - 20 seedlings. Plants were susceptibility (S) or resistance (R) to the different isolates, NA indicates missing data.

***H. arabidopsidis* isolate**	**Gel-1**	**DraIII-1**	**IP-Moa-0**
Cala2	S	R	S
Emoy2	S	R	S
PH0068-1	S	R	S
PH0124-1	S	R	S
PH0129-1	S	R	S
PH0133-1	S	R	NA
PH0147-1	S	R	S
PH0163-1	S	R	S
PH0320-1	S	R	S
PH0458-1	R	R	S
PH0459-1	S	R	NA
PH0466-1	S	R	S
PH0477-1	S	S	NA
PH0495-1	S	R	NA
PH0511-1	S	R	S
PH0527-3	S	R	S
PH0538	R	R	NA
PH0566-1	S	S	S
PH0682-1	S	R	R
PH0708-1	weak S	R	S
PH0733-1	R	S	NA
PH0736	R	R	NA
PH0745-1	R	R	NA
PH0883-1	S	R	S
PH0885-1	S	R	NA
PH0900-1	S	S	S
PH0919-1	S	R	S
PH0920-1	S	R	S

PH1032	R	R	NA
PH1034	S	R	NA
PH1109-1	S	R	S
PH1192	R	R	NA
PH1199	S	R	S
PH1206-1	S	R	NA
PH1233-1	S	R	S
PH1234-1	S	R	S
PH1239-1	R	R	S
PH1245-1	R	R	S
PH1263-1	S	R	NA
PH1284-1	S	R	S
PH1284b-1	S	R	NA
PH1297-1	S	R	S
PH1350-1	S	R	NA
PH1354-1	S	R	NA
PH1407-1	S	R	S
PH1422-1	S	R	S
PH1440-1	R	R	NA
PH1448-1	S	S	S
PH1455-1	S	R	S
PH1463-1	S	R	S
PH1464-1	S	R	NA
PH1503-1	S	R	S
PH1623-1	S	R	S
PH1642-1	S	R	S
PH1715-1	S	S	NA
PH1751-1	S	R	S
PH5421	S	R	S
PH5422	R	S	R
PH5442	S	R	S


Consensus
Gel1G
Dra3D
7CRB_2
Gel1F
Gel1I
Dra3B
Gel1J
Gel1C
Gel1A
Gel1H
Gel1D
Dra3C
Gel1E
Gel1B
Dra3A
Dra3E


Consensus
Gel1G
Dra3D
7CRB_2
Gel1F
Gel1I
Dra3B
Gel1J
Gel1C
Gel1A
Gel1H
Gel1D
Dra3C
Gel1E
Gel1B
Dra3A
Dra3E

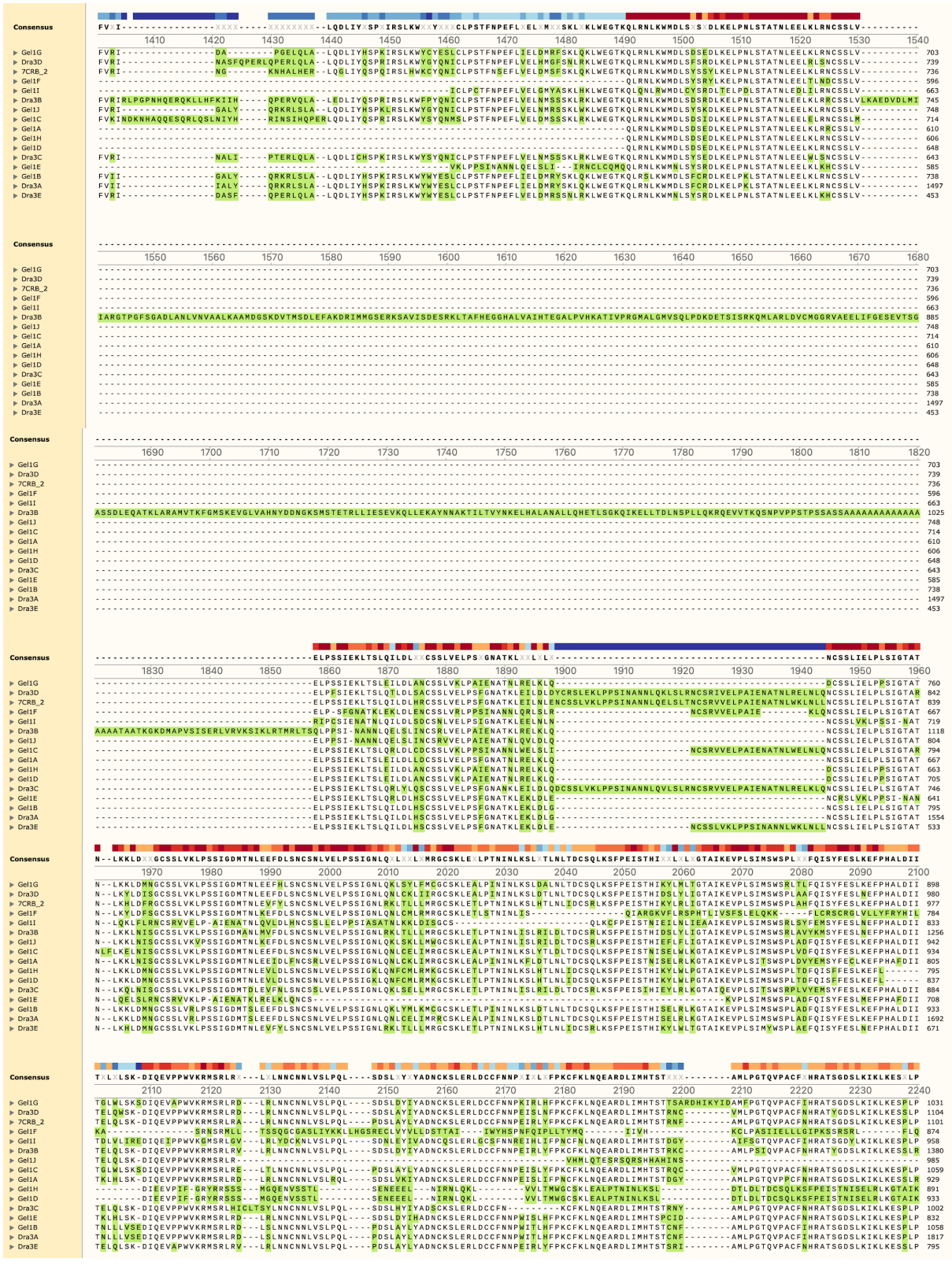
Consensus
Gel1G
Dra3D
7CRB_2
Gel1F
Gel1I
Dra3B
Gel1J
Gel1C
Gel1A
Gel1H
Gel1D
Dra3C
Gel1E
Gel1B
Dra3A
Dra3E

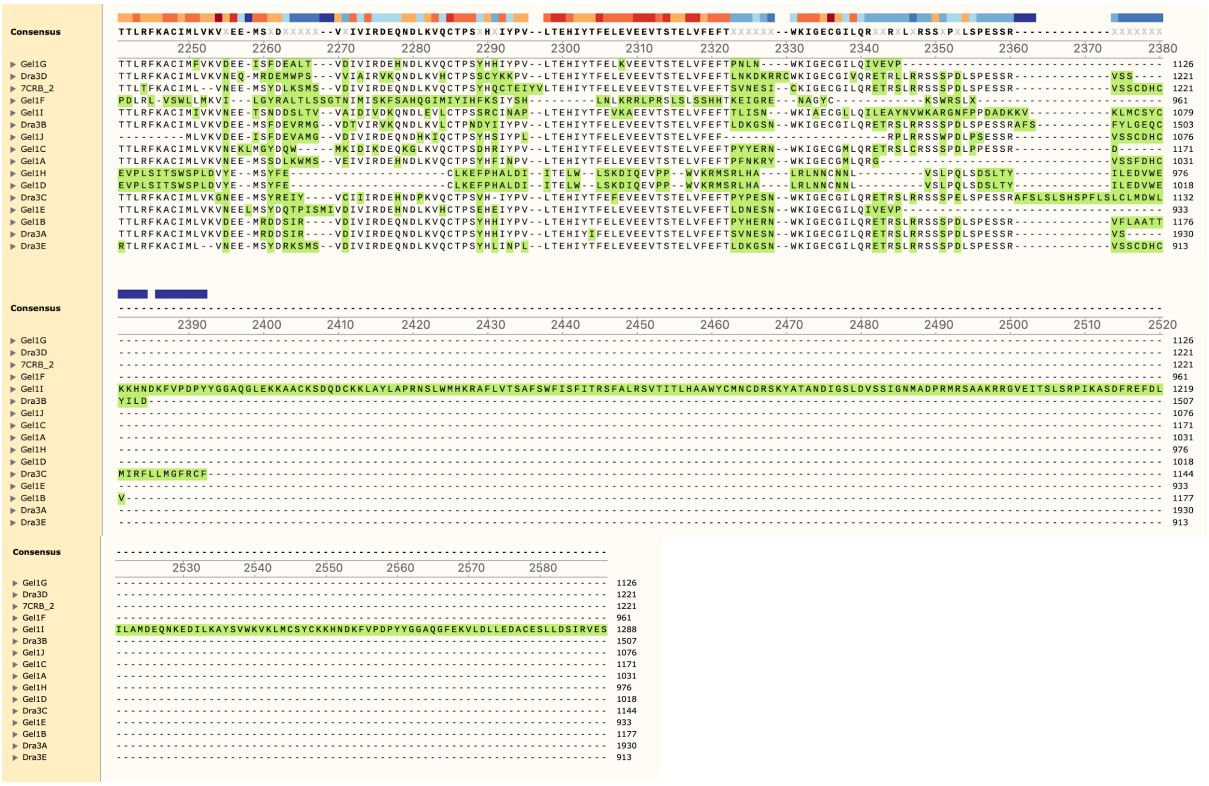

Supplementary Figure 2.2: Multiple sequence alignment of predicted RPP1 proteins from DraIII-1 and Gel-1 and the reference RPP1-WsB (indicated as 7CRB). Gaps are indicated as dots and amino acid differences are highlighted in green.

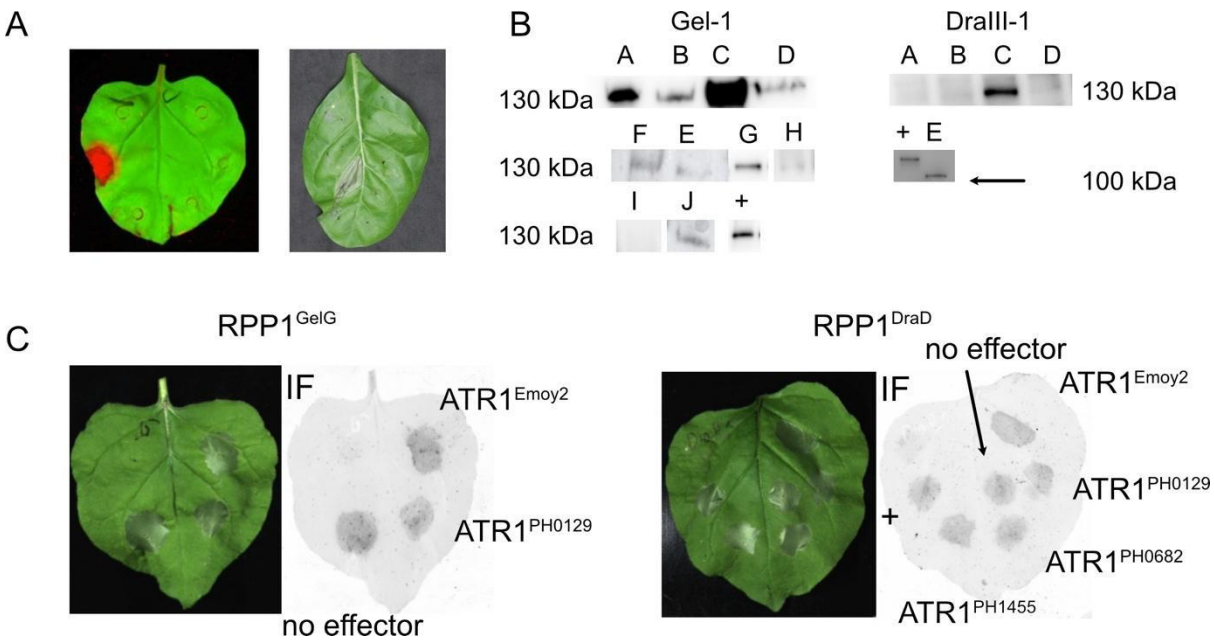

Supplementary Figure 2.3: A) Example of visualized cell-death three days post infection (dpi) of ATR1^{Emoy2} and RPP1^{WsB} in *N. benthamiana* marked in red and picture taken under UV light (left) and cell death of ATR1^{Emoy2} and RPP1^{WsB} shown in grey in *N. tabacum* (right). B) Immunoprecipitation of RPP1 constructs in *N. benthamiana* twp dpi. All RPP1 variants from Gel-1 showed expression except 35S-RPP1^{GelI}. All DraIII-1 RPP1 variants showed

expression, although 35S-RPP1^{DraE}-Myc seems truncated. C) Auto-activity was observed for 35S-RPP1^{GelG}-Myc and 35S-RPP1^{DraD}-Myc when being co-expressed with different ATR1 variants.

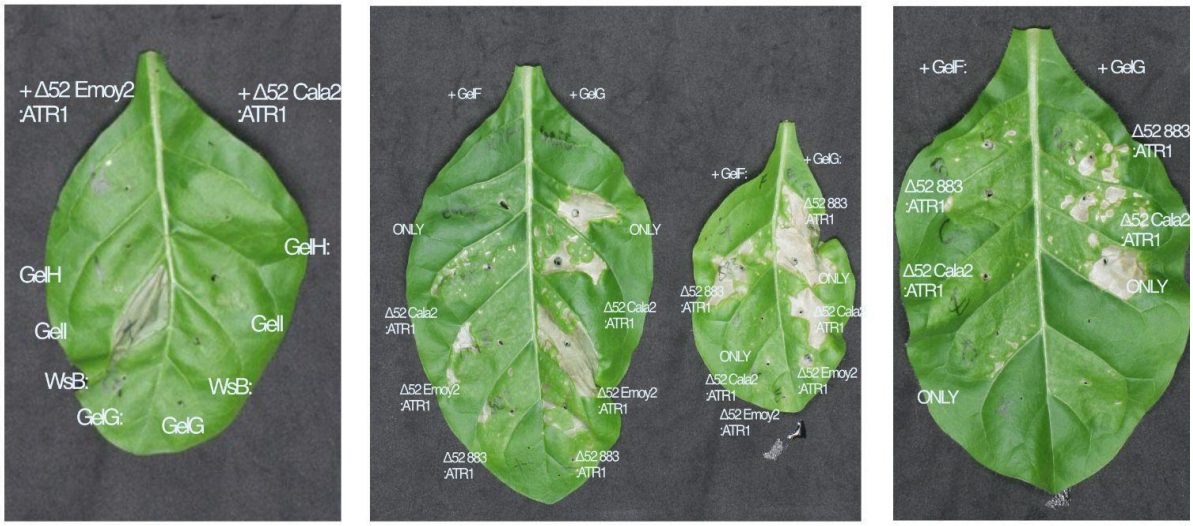

Supplementary Figure 2.4: Co-expression of different RPP1 and ATR variants in *N. tabacum*. Highlighted are the autoactive 35S-RPP1^{GelG}-Myc, this autoactivity was slightly suppressed when being co-expressed with 35S-ATR1^{Cala2}-HA and 35S-ATR1^{PH883}-HA variants, however these observations were not consistent. This is in contrast to the other autoactive variant 35S-RPP1^{DraD}-Myc (not shown here). These observations only appeared in *N. tabacum* infiltrated leaves.

Supplementary Table 2.3: List of collected plants from Montanuy, Spain, the origin of IP-Moa-0.

ID	Latitude	Longitude
PA5370	42.46638	0.69443
PA5371	42.46135	0.69871
PA5372	42.46147	0.69846
PA5373	42.46157	0.69833
PA5374	42.46159	0.69833
PA5375	42.46161	0.6983
PA5376	42.46185	0.69805
PA5377	42.46184	0.69804
PA5378	42.46189	0.69801
PA5379	42.46189	0.698
PA5380	42.4619	0.69801
PA5381	42.46191	0.69801
PA5382	42.46191	0.698
PA5383	42.46191	0.69798

PA5384	42.46192	0.69798
PA5385	42.46192	0.698
PA5386	42.46191	0.69798
PA5387	42.46191	0.69797
PA5388	42.46194	0.69798
PA5389	42.46195	0.69798
PA5390	42.46195	0.69797
PA5391	42.46194	0.69796
PA5392	42.46195	0.69799
PA5393	42.46196	0.69798
PA5394	42.46198	0.69797
PA5395	42.46196	0.69796
PA5396	42.46199	0.69796
PA5397	42.46201	0.69796
PA5398	42.46201	0.69796
PA5399	42.46202	0.69794
PA5400	42.46202	0.69794
PA5401	42.46203	0.69793
PA5402	42.46204	0.69794
PA5403	42.46204	0.69793
PA5405	42.46207	0.69793
PA5406	42.4621	0.69791
PA5407	42.46209	0.69792
PA5408	42.4621	0.6979
PA5409	42.46212	0.6979
PA5410	42.46216	0.69789
PA5411	42.46219	0.69789
PA5412	42.46224	0.69787
PA5413	42.46162	0.6983
PA5414	42.46161	0.69835
PA5415	42.46384	0.70174
PA5416	42.46611	0.69103
PA5417	42.46627	0.69094
PA5418	42.46539	0.68978
PA5419	42.46444	0.68948
PA5420	42.45825	0.67904
PA5421	42.45889	0.66296
PA5422	42.45888	0.66295
PA5423	42.4635	0.65642
PA5424	42.46348	0.65627
PA5425	42.46566	0.65967
PA5426	42.46779	0.69404

PA5427	42.47189	0.64727
PA5428	42.47004	0.69722
PA5429	42.46984	0.69727
PA5430	42.46568	0.6908
PA5431	42.46512	0.69049
PA5432	42.46393	0.69106
PA5433	42.46314	0.69281
PA5433b	42.46025	0.69598
PA5434	42.46037	0.6972
PA5435	42.46058	0.69715
PA5436	42.46361	0.69758
PA5437	42.46724	0.69285
PA5438	42.46825	0.6913
PA5439	42.46861	0.69027
PA5440	42.46735	0.69196
PA5441	42.46782	0.70544
PA5442	42.46361	0.69758
nexttoPA5442	42.46361	0.69758
PA5463	42.46486	0.68974
PA5464	42.46518	0.68979
PA5465	42.46399	0.6895
PA5466	42.46386	0.68957
PA5467	42.46445	0.68902
PA5468	42.46506	0.68884
PA5469	42.46569	0.6883
PA5470	42.46571	0.68816
PA5471	42.45922	0.68295
PA5472	42.45921	0.68294
PA5473	42.45686	0.67204
PA5474	42.45692	0.67161
PA5475	42.45551	0.67174
PA5476	42.45656	0.66824
PA5477	42.4589	0.66287
PA5478	42.45886	0.6629
PA5479	42.45026	0.66644
PA5480	42.462	0.698
PA5481	42.462	0.698
PA5482	42.462	0.698
PA5483	42.462	0.698
PA5484	42.462	0.698
PA5485	42.462	0.698
PA5486	42.462	0.698

PA5487	42.462	0.698
PA5488	42.462	0.698
PA5489	42.462	0.698
PA5490	42.462	0.698
PA5491	42.462	0.698
PA5492	42.462	0.698
PA5493	42.462	0.698
PA5494	42.462	0.698
PA5495	42.462	0.698
PA5496	42.462	0.698
PA5497	42.462	0.698
PA5498	42.462	0.698
PA5499	42.462	0.698
PA5500	42.462	0.698
PA5501	42.462	0.698
PA5502	42.462	0.698
PA5503	42.462	0.698
PA5504	42.462	0.698
PA5505	42.462	0.698
PA5506	42.462	0.698
PA5507	42.462	0.698
PA5508	42.462	0.698
PA5509	42.462	0.698
PA5510	42.462	0.698
PA5511	42.462	0.698
9525	42.49	0.54
9557	42.46	0.7
9567	42.34	1.3
9588	42.11	0.6
9827	42.78	0.69
9899	42.27	0.19
9894	42.59	0.76
PA5378	42.46189	0.69801
PA5404	42.46205	0.69794
9950	42.54	0.84
9844	42.63	0.76

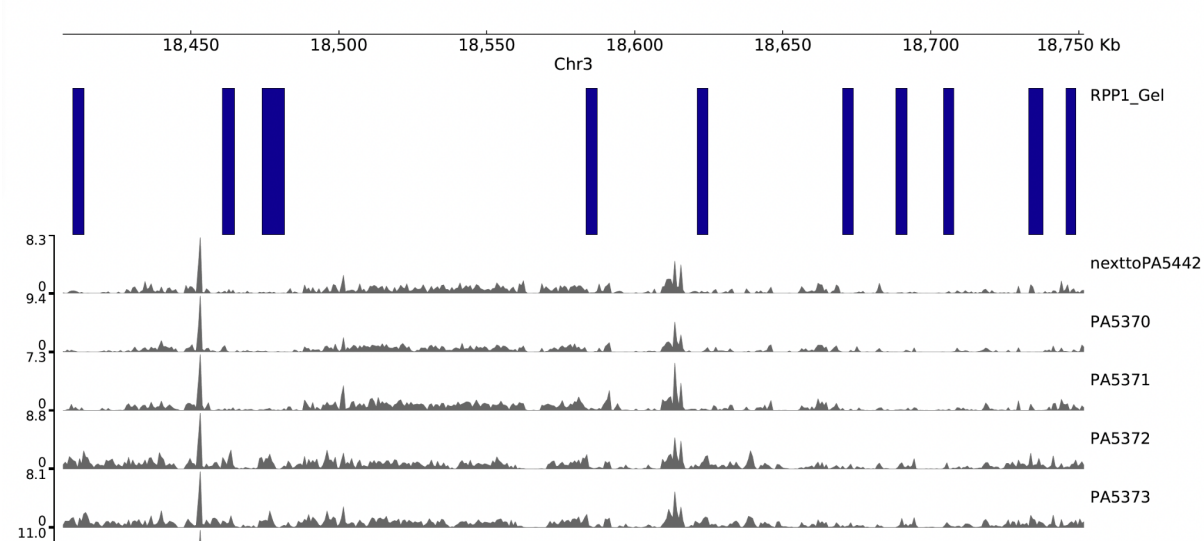

Supplementary Figure 2.5: *RPP1* locus and its short read coverage for five out of 129 *H. arabidopsidis* isolates.

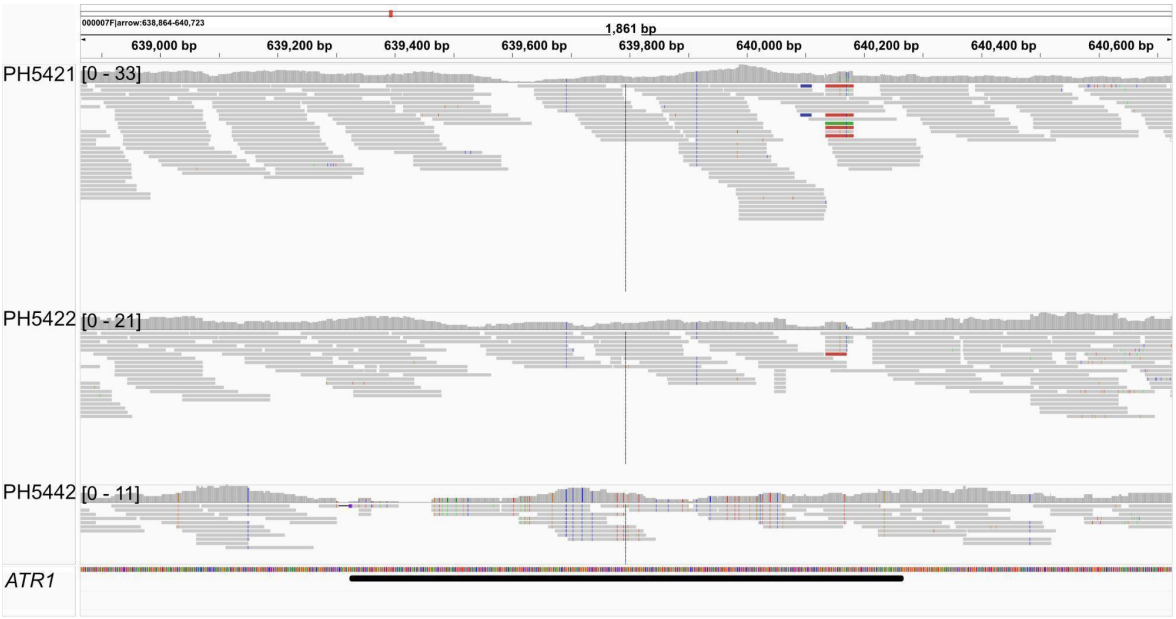

Supplementary Figure 2.6: IGV visualization of short reads from *H. arabidopsidis* genomes PH5421, PH5422, and PH5442 mapped against the PacBio sequenced PH0495-1 genome. The *ATR1* region is highlighted in black, and grey bars indicate individual reads mapped to this region.

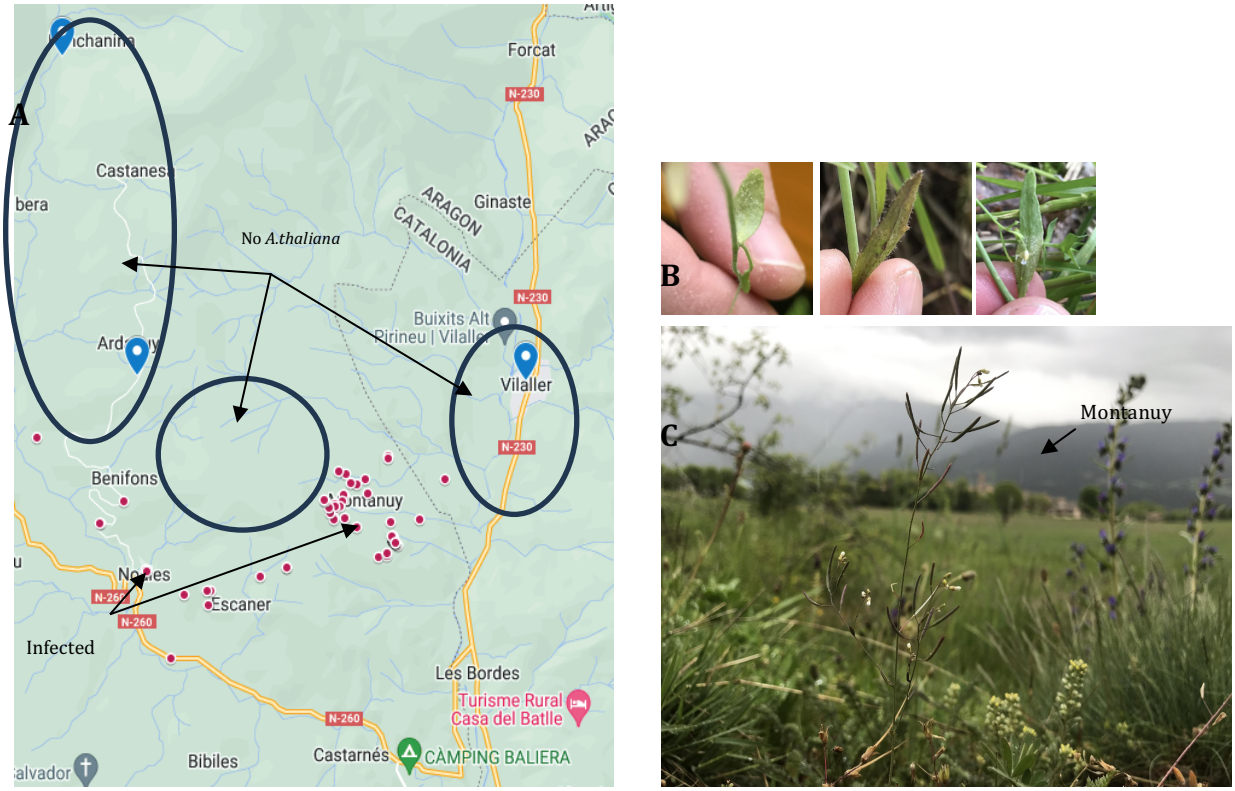

Supplementary Figure 2.7: Collected *A. thaliana* plants around Montanuy (Spain). A) Sampled locations where plants could be found represented by red dots, areas we visited but did not find *A. thaliana* plants indicated by black circles. Arrows indicate *H. arabidopsidis*-infected plants. B and C) Representative pictures of *A. thaliana* plants at the time of sampling in May 2024.

Supplementary Figure 2.8: Example of a very dry and small *A. thaliana* plant near Montanuy (Spain).

2.9 Methods and Materials

Oomycete infection and DNA extraction:

To bulk *Hyaloperonospora arabidopsidis* isolates, 10-day-old *Arabidopsis thaliana* eds1-1 seedlings (ABRC Stock ID: CS67134) were inoculated by spraying with spore suspensions prepared in sterile water. Following inoculation, plants were maintained under high humidity conditions. From 2 to 6 days post-inoculation (dpi), humidity was temporarily reduced to limit excessive tissue collapse, after which high humidity was reintroduced to promote sporulation. Spores were harvested by vortexing infected leaves in sterile water, and the resulting spore suspension was filtered through a Miracloth (Sigma, Cat. No. 475885), for further propagation.

CTAB DNA extraction *H. arabidopsidis*:

Prior to DNA extraction, spores were washed from infected plant tissue using sterile water and collected by vortexing. The spore suspension was then filtered through Miracloth into a 5 mL reaction tube. Spores were pelleted by centrifugation for 2 minutes at 3,000 rpm, allowing removal of excess water and residual plant debris. Spore disruption was performed using one of several methods depending on sample throughput: mechanical grinding with 0.01 mm acid-washed glass beads (Sigma, Cat. No. G8772-10G) in a Qiagen TissueLyser, vortexing for 5 minutes, manual grinding with a plastic pestle. Spore lysis efficiency was confirmed by light microscopy to ensure disruption prior to DNA extraction. To each sample, 300 µL of pre-warmed CTAB extraction buffer (1.4 M NaCl, 100 mM Tris-HCl pH 8.0, 20 mM EDTA, 2% CTAB, 1% polyvinylpyrrolidone) was added. Samples were incubated at 65 °C for 1 hour, then allowed to cool at room temperature for ~5 minutes. An equal volume (300 µL) of chloroform:isoamyl alcohol (24:1) was added, and the mixture was gently inverted ~20 times to mix thoroughly. Samples were centrifuged at 12,000 rpm for 15 minutes. The upper aqueous phase was carefully transferred to a new 1.5 mL reaction tube, and 200 µL of ice-cold isopropanol was added. Samples were incubated at –20 °C for at least 30 minutes to precipitate DNA. DNA was pelleted by centrifugation at high speed (≥12,000 rpm) for 15 minutes. The supernatant was discarded, and the pellet was washed with 80% ethanol by gentle inversion. A final centrifugation at high speed for 10 minutes was performed, after which the ethanol was removed, and the pellet was air-dried.

The DNA pellet was resuspended in 50 µL of nuclease-free water containing RNase A (10 mg/mL; Qiagen, Cat. No. 19101) for RNA removal.

CTAB DNA extraction *A. thaliana*:

Frozen *Arabidopsis thaliana* tissue (~0.01 g) was homogenized using metal beads in a Qiagen TissueLyser. DNA extraction was then carried out following the same CTAB-based protocol described above.

***ATR1* PCR amplification for sequencing:**

Flanking primers G-47540 and G-47541 were designed to amplify the target region by PCR from a total of 129 *H. arabidopsidis* isolates (DNA was provided by R. Schwab). Successful amplification was achieved in 60 isolates. PCR products were blunt-end cloned into a SmaI (Thermo Fisher, Cat. No. ER0662) pBluescript II SK (-) vector, which had been pre-digested overnight at 30 °C. Ligation was carried out overnight at 16 °C using T4 DNA Ligase (Thermo Fisher, Cat. No. EL0011). The ligation products were transformed into *E. coli* DH5α via heat-shock transformation and plated on Luria-Broth (LB) agar containing 100 ug/mL Ampicillin and X-gal for blue/white screening. White (positive) colonies were selected, and plasmids were extracted using the GeneJET Plasmid Miniprep Kit (Thermo Fisher, Cat. No. K0503). These plasmids were subsequently used for in-house Nextera-based library preparation and sequenced on the Illumina platform. Sequencing reads were *de novo* assembled using Unicycler (Wick et al., 2017).

***RPP1* annotation:**

The long-read assembled genomes of *Arabidopsis thaliana* accessions DraIII-1, Gel-1, and IP-Moa-0 (Teasdale et al., 2024; The 1001 Genomes Plus Consortium, 2024) were annotated using Liftoff v2.0 (Shumate & Salzberg, 2021), which transfers gene models from the Araport11 reference annotation. The *RPP1* locus was specifically annotated using Miniprot v0.12 (Li, 2023), employing previously annotated RPP1 protein sequences (Teasdale et al., 2024), including pseudogenized variants, as input. The best *RPP1* candidate in each accession was manually selected based on sequence integrity. Genomic alignments across accessions were performed using Minimap2 (Li, 2021), and visualized with GGGenomes (Hackl et al., 2021).

Library preparation

After quantification using a Qubit fluorometer, DNA samples were normalized to equivalent concentrations. Prior to library preparation, Tn5 transposase (provided by the laboratory) was pre-coupled to Hydrophilic Streptavidin Magnetic Beads (NEB, S1421). Typically, 2.5 µL of beads per sample was used, and Tn5 was added based on the concentration (typically something like this: 0.5 µL/ 250 µL beads). The desired volume of necessary beads needed to be calculated at first, since this is the volume used to wash the beads. Beads were washed with 4× the desired total volume in streptavidin binding buffer (0.6 M NaCl, 10 mM Tris-HCl pH 8, 0.5 mM EDTA, 0.1% Triton X-100), followed by a second wash with 6× volume. The required amount of Tn5 was added to the beads and gently rotated at 10 rpm for 30 minutes at room temperature (RT). After removing the buffer, beads were washed with 6× volume of dialysis buffer (50 mM HEPES-KOH, pH 7.2; 0.2 M NaCl; 0.2 mM EDTA; 2 mM DTT; 0.2% Triton X-100; 20% glycerol) and rotated again at 10 rpm for 5 minutes at RT. This was followed by a final wash in 2× volume of wash buffer (10 mM Tris-HCl, pH 8; 30 mM NaCl; 0.1% Triton X-100) before immediate use. For tagmentation, 3 µL of DNA was combined with 2 µL of 5× TAPS-DMF buffer (50 mM TAPS, pH 8.5; 25 mM $MgCl_2$; 50% DMF) and 5 µL of prepared Tn5 beads in wash buffer. The mixture was briefly mixed at 15,000 rpm for 10 seconds and incubated at 55 °C for 10 minutes. Then, 10 µL of 0.6% SDS in wash buffer was added, mixed, and incubated again at 55 °C for 10 minutes. Samples were washed in 150 µL of wash buffer for at least 1 minute, followed by a second wash with 100 µL. The DNA-bead mix was then used directly for PCR using the Q5 High-Fidelity DNA Polymerase Kit (NEB, Cat. No. N0447). Each PCR reaction contained 5 µL 5× buffer, 0.25 µL Q5 polymerase, 0.5 µL 10 mM dNTPs, 11 µL water, 0.75 µL P5 adapter, and 7.5 µL P7 adapter. The PCR protocol included an initial extension at 72 °C for 10 minutes, followed by brief mixing, denaturation at 98 °C for 30 seconds, and 14 cycles of 98 °C for 15 seconds, 65 °C for 20 seconds, and 72 °C for 90 seconds. Library size was checked by running 4 µL of each sample on an agarose gel. Successfully amplified libraries were pooled and purified using SPRI beads (Sera-Mag Magnetic SpeedBeads) according to the manufacturer's instructions. Prior to sequencing, libraries were size-selected (300–700 bp) using the BluePippin system (Sage Science), and final quality control was performed with the Agilent 2100 Bioanalyzer (Agilent Technologies, Santa Clara, CA, USA).

Mapping of *H. arabidopsidis* sequences, variant calling and effector extraction: Following genomic DNA extraction and library preparation, whole-genome sequencing was performed on an Illumina NextSeq2000 platform (Illumina, San Diego, USA), generating 150 bp paired-end reads. Cleaned reads were then aligned to the *Arabidopsis thaliana* reference genome 495-1 using BWA-MEM (v0.7.17 Pham et al., 2023). Variant calling was conducted using a Snakemake-based pipeline incorporating the Genome Analysis Toolkit (GATK v4.2; https://github.com/ibebio/vc-gatk4-snakemake, Van der Auwera & O'Conner 2020) following best practices workflows. This included base quality score recalibration (BQSR), indel realignment, and joint genotyping across samples. Variants were filtered based on the following criteria: Phred quality score ≥ 30, read depth ≥ 5 and ≤ 30, minor allele frequency (MAF) ≥ 0.2, and a minimum call rate of 75% across samples. Low-quality and ambiguous calls were removed to ensure robustness in downstream analyses. To characterize effector gene diversity, consensus sequences of the isolates were generated using Miniprot (v. 2.16; Li, 2023), using an effector coordinate set curated from Asai et al. (2014). Coordinates were provided in BED format to guide mapping and extraction of effector gene regions from the variant call set. We then employed BEDtools (v2.31.1; Quinlan & Hall, 2010) to extract variant data for effector loci, and calculated population genetic statistics including nucleotide diversity (π), the number of polymorphic sites, and allele frequencies using VCFtools (v0.1.17; Danecek et al., 2011). These metrics provided insight into the extent of variation within effector genes across the *H. arabidopsidis* isolates. Optionally, the VCF files were converted to input formats for population structure and phylogenetic analysis. Pairwise genetic distances were computed, and population structure was inferred using PLINK (v.1.9.0 ; Purcell et al., 2007).

Phylogenetic tree

Amino acids- based maximum likelihood tree was inferred with LG substitution model and gamma distribution plus invariant for among sites rate variation; used bootstrap 1,000 by using IQ-TREE$_2$ (v. 2.4.0; Minh et al., 2020) and visualization in iTOL (v.5; Letunic & Bork 2021).

AlphaFold3 prediction and 7CRC comparison:

Filtered amino acid sequences of RPP1, obtained via Miniprot annotation, were submitted to AlphaFold Server (Abramson et al., 2024) using AlphaFold v3 to predict tetrameric protein structures with a seed number of 1. The predicted structures were subsequently uploaded into ChimeraX (v1.8; Meng et al., 2023), where they were aligned to the PDB: 7CRC using the MatchMaker tool with the Needleman-Wunsch algorithm for pairwise structure alignment.

Cloning:

For expression in *Pseudomonas fluorescens* strain Pf0-1 (Thomas et al., 2009; kindly provided by Prof. Thomas Lahaye, Univ. of Tübingen), *ATR1* sequences were PCR-amplified from *H. arabidopsidis* genomic DNA (kindly provided by Dr. Rebecca Schwab and Fiona Paul, MPI Tübingen), without the first 52 codons starting downstream of the RXLR motif ("∆52-ATR1"; Krasileva et al., 2010). Primers were designed with ~20 bp overlaps complementary to the pre-digested expression vector pLL791 (kindly provided by Dr. Lei Li, MPI Tübingen. Gibson Assembly was performed using the NEB Gibson Assembly Master Mix (Cat. #10229799) according to the manufacturer's protocol. In some cases, half of the recommended Master Mix volume was used to reduce reagent costs. PCR products were assembled into the EcoRI and SalI pre-digested pLL791 backbone, which contains the *avrRps4* promoter, sequences for an N terminal signal peptide from the bacterial effector AvrRps4 (Grassmann et al., 1999), and an HA epitope tag. The assembly reaction was incubated at 50°C for 1 h. Assembled DNA were transformed into *E. coli* DH5α via heat-shock at 42°C for 1 min, followed by cooling on ice for at least 2 min and recovery in LB medium for continuous shaking at 37°C (Hanahan 1983). Single colonies were picked, grown overnight at 37°C in 2 mL LB, and plasmids were extracted using the GeneJET Plasmid Miniprep Kit (Thermo Fisher, Cat. #K0503). Inserts were confirmed by Sanger sequencing using G-47540, G-47541 primers. Verified pLL791 derivatives were introduced into *P. fluorescens* Pf0-1 via triparental mating. *E. coli* DH5α carrying the *ATR1* construct, the recipient Pf0-1 strain, and the helper strain carrying the pRK2013 plasmid (Hall et al., 2023) were mixed on non-selective LB agar plates and incubated at 28°C for 2 days. Bacterial mixtures were then transferred to selective LB agar plates containing 50 µg/mL kanamycin, 25 µg/mL chloramphenicol, and 50 µg/mL tetracycline. After

another 2-day incubation at 28°C, colonies were screened by colony PCR and verified by Sanger sequencing.

For transient co-expression of ATR1 in *Nicotiana* spp., *ATR1* alleles were amplified with the same primers described above and cloned via Gibson Assembly into the SalI- and EcoRI-digested Gateway entry vector pJLBlue (reverse orientation). Verified constructs were subsequently recombined into the Gateway-compatible binary vector pGWB414 using the LR Clonase II enzyme mix (Thermo Fisher, Cat. #11791020), following the manufacturer's instructions. Final constructs were transformed into *Agrobacterium tumefaciens* GV3101 pMP90 (kindly provided by Prof. Jane Parker, Max Planck Institute for Plant Breeding Research) via electroporation at 2.2 kV. Cells were allowed to recover in LB without antibiotics for 2 h at 28°C before plating on selective LB agar containing 50 µg/mL rifampicin, 100 µg/mL spectinomycin, and 25 µg/mL gentamicin. Colonies were verified by colony PCR and sequencing before use in infiltration assays.

***Nicotiana* infections and Western blot:**

Three- to four-week-old *Nicotiana* spp. plants were used for *Agrobacterium*-mediated transient expression. *Agrobacterium tumefaciens* strain GV3101 pMP90 derivatives were inocula were grown in LB with 100 µg/mL spectinomycin, 25 µg/mL gentamicin, 50 µg/mL rifampicin for overnight at 28°C. Bacteria were harvested by centrifugation at 6,000 rpm (in Eppendorf Microcentrifuge Cat. No. 5424) for 3 min and resuspended by vortexing in infiltration buffer containing 10 mM $MgCl_2$, 10 mM MES/KOH (pH. 5.6) and 150 µM acetosyringone for *N. tabacum* and 150 nMacetosyringone for *N. benthamiana*. Resupended bacteria were incubated under continuous shaking for at least two more hours in the dark.

For *Nicotiana tabacum* cv. Petite Gerard (kindly provided by Prof. Jonathan Jones, The Sainsbury Laboratory), *A. tumefaciens* suspensions were adjusted to OD_{600} = 0.9 for each construct and mixed 1:1 by thorough vortexing. Prior to syringe infiltration, plants were re-watered to promote stomatal opening. Infiltrations were performed on the abaxial side of the leaf using 1 mL syringes (Braun; Cat. No. H999.1) without needles (Krasileva et al., 2010). Syringe infiltrated plants were maintained in under controlled growth conditions 12h light and dark period, and cell death symptoms were recorded approximately 3 days post-infiltration (dpi).

For *N. benthamiana* (kindly provided Dr. Farid El-Kasmi, Univ. of Tübingen), infiltrations were carried out with *A. tumefaciens* suspensions adjusted to OD_{600} = 0.35 for ATR1 constructs, OD_{600} = 0.75 for RPP1 constructs, and OD_{600} = 0.15 for the silencing suppressor P19 (also kindly provided by Dr. Farid El-Kasmi). Infiltrated plants were maintained in the dark, and cell death symptoms were recorded approximately 3 dpi (Li et al., 2008). For each leaf, a positive and a negative control were included. Up to seven RPP1/ATR1 combinations were tested per leaf, with up to two leaves per plant. If either control failed to produce the expected outcome, results from the corresponding plants were discarded. For all valid experimental batches, the number of leaves exhibiting cell death or no cell death was recorded and normalized by the total number of treated leaves to calculate response frequencies.

For protein analysis, leaf tissue was harvested at 2 dpi and processed for immunoblotting as previously described by Ma and colleagues (Ma et al., 2020). Protein was detected via Western blot using mouse-anti-c-Myc antibody (Sigma, Cat. No. M5546) and goat anti-mouse IgG antibody, peroxidase conjugated, H+L (Sigma, Cat. No. AP124P) for constructs derived from pGWB420::35S-RPP1-Myc, rat-anti-HA-peroxidase-conjugated antibody (Roche, Cat. No. 12013819001) for constructs derived from pGWB414::35S-ATR1-HA.

Pf0-1 and *Pst* DC3000 infection assay:

Pseudomonas fluorescens Pf0-1 strains, engineered with a functional type III secretion system (Thomas et al., 2009), and carrying AvrRpt2N-ATR1 constructs, were freshly grown on selective Luria-Broth (LB) agar plates. Bacterial cells were harvested and resuspended in 10 mM $MgCl_2$ to an optical density of OD_{600} = 0.2 for infiltration. Leaves of 5-week-old *Arabidopsis thaliana* plants were hand-infiltrated using a 1 mL needleless syringe. Plants were incubated under standard growth conditions 3 dpi to assess symptom development, indicated by hypersensitive response (HR)-associated tissue collapse.

For *in planta* bacterial growth assays, *Pseudomonas syringae* pv. *tomato* DC3000 (*Pst* DC3000) carrying either the empty vector AvrRps4N or AvrRps4N-ATR1 was grown similarly on selective LB agar plates. Cultures were resuspended in 10 mM $MgCl_2$ and adjusted to OD_{600} = 0.001 for infiltration. Leaves of 5-week-old *A. thaliana* were infiltrated as described and harvested at 0 days post-inoculation (dpi) and 3 dpi.

Infiltrated leaves were washed in 70 % Ethanol for 1 min and rinsed with sterile water followed by quick drying with tissue paper. Leaf discs (1 cm²) were homogenized in 1 mL sterile water with 2 glass beads (4-5 mm diameter) for 2 times 1 min in Qiagen TissueLyser. Followed by 1:10 serial dilution, 10 ul of water/bacteria suspension was plated on selective LB agar. Plates were incubated at 28 °C for 2 days before quantifying colony-forming units (CFUs) (Sohn et al., 2007).

Bulk segregant analysis:

Crosses consisted of DraIII-1 and Gel-1 or DraIII-1 with IP-Moa-0. For all the crosses DraIII-1 was the resistant parent. 10-day old plants from the F^2 generation were infected with *H. arabidopsidis* strains Emoy2, PH0458, PH0527, PH708, PH0919, PH1234 and PH1239 at a spore concentration of around 10 x 10^4. 10 days after infection plants were harvested in bulks of two (resistance and susceptible). These bulks were crushed with mortar and pestle followed by the CTAB DNA extraction method, as mentioned above just the volumes were increased by 2 x the volume. Libraries were prepared, as mentioned above and sequenced as mentioned above. After obtaining 50 X genome coverage. Short reads were mapped to TAIR10, similarly as described for *H. arabidopsidis*. QTLseqr (Mansfeld & Grumet 2018) was used for analysis and visualization, after following described instructions.

Sampling, DNA extraction, sequencing of *A. thaliana* plants from Moa population:

114 plants were collected around and at the site where IP-Moa-0 (NASC ID: CS77102) had been collected in 2013 by Carlos Alonso-Blanco (The 1001 Genome Consortium 2016; https://1001genomes.org/), focusing on *H. arabidopsidis* infected plants. DNA was extracted via CTAB buffer, libraries were prepared and sequenced as mentioned above. Short reads were mapped against the Gel-1 genome (Teasdale Murray et al., 2024). To ensure accurate coverage estimation, I applied multiple filtering steps to the aligned reads using SAMtools (Li et al., 2009) and BEDTools (Quinlan & Hall, 2010). First, I used samtools view with the -F 3596 flag to exclude reads that were unmapped, not primary alignments, failed quality checks, PCR duplicates, or secondary/supplementary alignments. I retained only reads with a mapping quality of at least 30 using the -q 30 parameters. The -h flag preserved the header for downstream processing. To further eliminate reads with soft or hard clipping, I piped

the output to awk, which removed alignments containing "H" or "S" in the CIGAR string, unless the line was a header line (starting with "@"). The resulting alignments were converted back to BAM format using samtools view -bo. For read depth analysis, I used bedtools genomecov with the -d option on the filtered BAM file to compute the per-base coverage across the genome. Coverage plots were produced with pyGenomeTracks (v3.0) (Lopez-Delisle et al., 2020).

List of plasmids:

Construct name	Species/Host strain	Insert	Backbone
pML012	*Escherichia coli* DH5α (lab stock)	Δ52-ATR1-Emoy2	pLL791 (lab stock)
pML013	Pf0-1 (Thomas et al., 2009)	Δ52-ATR1-Emoy2	pLL791
pML018	*E. coli* DH5α	Δ52-ATR1-708	pLL791
pML019	Pf0-1	Δ52-ATR1-708	pLL791
pML057	Pf0-1	ev	pLL791
pML072	*E.coli* DH5α	Δ52-ATR1-919	pLL791
pML073	Pf0-1	Δ52-ATR1-919	pLL791
pML080	*E. coli* DB3.1	ev	pGW414 (Addgene Cat. No. #74808)
pML087	*E. coli* DH5α	Δ52-ATR1-708	pJLBlue (rev) (lab stock)
pML177	*P. syringae* pv. *tomato* DC3000 (from Thomas Lahaye)	ev	pLL791
pML181	*Pst* DC3000	Δ52-ATR1-919	pLL791
pML183	*E.coli* DH5α	RPP1 WsB	pGWB414
pML186	*P. syringae* pv. *tomato* DC3000	Δ52-ATR1-708	pLL791
pML190	*A. tumefaciens* GV3101 pMP90 (from Jane Parker)	RPP- WsB	pGWB420 (Addgene Cat. No. #74814)
pML241	*E. coli* DH5α	Δ52-ATR1-919	pJLBlue (rev)
pML273	*E. coli* DH5α	RPP1-Gel1A	pGenDONR (lab stock)
pML274	*E. coli* DH5α	RPP1-Gel1B	pGenDONR
pML275	*E. coli* DH5α	RPP1-Gel1C	pGenDONR
pML276	*E. coli* DH5α	RPP1-Gel1D	pGenDONR
pML277	*E. coli* DH5α	RPP1-Gel1E	pGenDONR
pML278	*E. coli* DH5α	RPP1-Gel1F	pGenDONR
pML279	*E. coli* DH5α	RPP1-Gel1G	pGenDONR
pML280	*E. coli* DH5α	RPP1-Gel1H	pGenDONR
pML281	*E. coli* DH5α	RPP1-Gel1I	pGenDONR
pML282	*E. coli* DH5α	RPP1-Gel1J	pGenDONR
pML283	*E. coli* DH5α	RPP1-DraIIIA	pGenDONR

pML284	*E. coli* DH5α	RPP1-DraIIIB	pGenDONR
pML285	*E. coli* DH5α	RPP1-DraIIIC	pGenDONR
pML286	*E. coli* DH5α	RPP1-DraIIID	pGenDONR
pML287	*E. coli* DH5α	RPP1-DraIIIE	pGenDONR
pML288	*E. coli* DH5α	RPP1-Gel1A	pGWB420
pML289	*E. coli* DH5α	RPP1-Gel1B	pGWB420
pML290	*E. coli* DH5α	RPP1-Gel1C	pGWB420
pML291	*E. coli* DH5α	RPP1-Gel1D	pGWB420
pML292	*E. coli* DH5α	RPP1-Gel1E	pGWB420
pML293	*E. coli* DH5α	RPP1-Gel1F	pGWB420
pML294	*E. coli* DH5α	RPP1-Gel1G	pGWB420
pML295	*E. coli* DH5α	RPP1-Gel1H	pGWB420
pML296	*E. coli* DH5α	RPP1-Gel1I	pGWB420
pML297	*E. coli* DH5α	RPP1-Gel1J	pGWB420
pML298	*E. coli* DH5α	RPP1-DraIIIA	pGWB420
pML299	*E. coli* DH5α	RPP1-DraIIIB	pGWB420
pML300	*E. coli* DH5α	RPP1-DraIIIC	pGWB420
pML301	*E. coli* DH5α	RPP1-DraIIID	pGWB420
pML302	*E. coli* DH5α	RPP1-DraIIIE	pGWB420
pML303	*A. tumefaciens* GV3101 pMP90	RPP1-Gel1A	pGWB420
pML304	*A. tumefaciens* GV3101 pMP90	RPP1-Gel1B	pGWB420
pML305	*A. tumefaciens* GV3101 pMP90	RPP1-Gel1C	pGWB420
pML306	*A. tumefaciens* GV3101 pMP90	RPP1-Gel1D	pGWB420
pML307	*A. tumefaciens* GV3101 pMP90	RPP1-Gel1E	pGWB420
pML308	*A. tumefaciens* GV3101 pMP90	RPP1-Gel1F	pGWB420
pML309	*A. tumefaciens* GV3101 pMP90	RPP1-Gel1G	pGWB420
pML310	*A. tumefaciens* GV3101 pMP90	RPP1-Gel1H	pGWB420
pML311	*A. tumefaciens* GV3101 pMP90	RPP1-Gel1I	pGWB420
pML312	*A. tumefaciens* GV3101 pMP90	RPP1-Gel1J	pGWB420
pML313	*A. tumefaciens* GV3101 pMP90	RPP1-DraIIIA	pGWB420
pML314	*A. tumefaciens* GV3101 pMP90	RPP1-DraIIIB	pGWB420
pML315	*A. tumefaciens* GV3101 pMP90	RPP1-DraIIIC	pGWB420
pML316	*A. tumefaciens* GV3101 pMP90	RPP1-DraIIID	pGWB420
pML317	*A. tumefaciens* GV3101 pMP90	RPP1-DraIIIE	pGWB420

pML465	*A. tumefaciens* GV3101 pMP90	Δ52-ATR1-Cala2	pGWB414
pML466	*A. tumefaciens* GV3101 pMP90	Δ52-ATR1-Emoy2	pGWB414
pML467	*A. tumefaciens* GV3101 pMP90	Δ52-ATR1-708	pGWB414
pML470	*A. tumefaciens* GV3101 pMP90	Δ52-ATR1-919	pGWB414
pML472	*A. tumefaciens* GV3101 pMP90	Δ52-ATR1-1297	pGWB414
pML474	*P. syringae* pv. *tomato* DC3000	Δ52-ATR1-Emoy2	pLL791
pML475	*P. syringae* pv. *tomato* DC3000	Δ52-ATR1-Cala2	pLL791
pML476	*P. syringae* pv. *tomato* DC3000	Δ52-ATR1-919	pLL791
pML477	*E.coli* NEB beta	Δ52-ATR1-458	pGWB414
pML478	*P. syringae* pv. *tomato* DC3000	Δ52 458 ATR1	pLL791

Oligonucleotides:

Name	Sequence 5‘ → 3‘	Purpose
G-47540	CGCTTCGAGTTTCCTCATTC	*ATR1* amplification forward
G-47541	TCAGCTCCTGAACCTGAGTG	*ATR1* amplification reverse
G-47869	attgggcggaggtaaacgag GTCGAC TTCGGGCGTTGAG	pLL791 cloning
G-47870	ctggtacgtcgtacggatag GAATTC AACAGAATATATTCTCGAATACTCTTCCACGAGTTCCTC	pLL791 cloning
G-47976	attgggcggaggtaaacgag GTCGAC TCAATCGGGCGTTGAGAG	Delta52 ATR1 amplification after RxLR
G-48404	attgggcggaggtaaacgagAGACAGCTCTCGATGACG	Delta52 ATR1 amplification for cloning into pLL791

G-48405	ctggtacgtcgtacggatagAACAGAATATATTCTCGAATACTCTTCCAC	Delta52 ATR1 amplification for cloning into pLL791 reverse
G-47869	attgggcggaggtaaacgag GTCGAC TTCGGGCGTTGAG	Delta52 ATR1 amplification for cloning into pJLblue
G-47870	ctggtacgtcgtacggatag GAATTC AACAGAATATATTCTCGAATACTCTTCCACGAGTTCCTC	Delta52 ATR1 amplification for cloning into pJLblue reverse

2.10 References

Abramson, J., Adler, J., Dunger, J., Evans, R., Green, T., Pritzel, A., Ronneberger, O., Willmore, L., Ballard, A. J., Bambrick, J., Bodenstein, S. W., Evans, D. A., Hung, C. C., O'Neill, M., Reiman, D., Tunyasuvunakool, K., Wu, Z., Žemgulytė, A., Arvaniti, E., … Jumper, J. M. (2024). Accurate structure prediction of biomolecular interactions with AlphaFold 3. *Nature*, *630*(8016), 493–500. https://doi.org/10.1038/S41586-024-07487-W;TECHMETA=139,141;SUBJMETA=114,1305,154,2411,535,631;KWRD=DRUG+DISCOVERY,MACHINE+LEARNING,PROTEIN+STRUCTURE+PREDICTIONS,STRUCTURAL+BIOLOGY

Adachi, H., Contreras, M., Harant, A., Wu, C. H., Derevnina, L., Sakai, T., Duggan, C., Moratto, E., Bozkurt, T. O., Maqbool, A., Win, J., & Kamoun, S. (2019). An N-terminal motif in NLR immune receptors is functionally conserved across distantly related plant species. *ELife*, *8*. https://doi.org/10.7554/ELIFE.49956,

Ahn, H., Lin, X., Olave-Achury, A. C., Derevnina, L., Contreras, M. P., Kourelis, J., Wu, C., Kamoun, S., & Jones, J. D. G. (2023). Effector-dependent activation and oligomerization of plant NRC class helper NLRs by sensor NLR immune receptors Rpi-amr3 and Rpi-amr1 . *The EMBO Journal*, *42*(5). https://doi.org/10.15252/EMBJ.2022111484,

Alcázar, R., García, A. V., Parker, J. E., & Reymond, M. (2009). Incremental steps toward incompatibility revealed by Arabidopsis epistatic interactions modulating salicylic acid pathway activation. *Proceedings of the National Academy of Sciences of the United States of America*, *106*(1), 334–339. https://doi.org/10.1073/PNAS.0811734106,

Alcázar, R., von Reth, M., Bautor, J., Chae, E., Weigel, D., Koornneef, M., & Parker, J. E. (2014). Analysis of a Plant Complex Resistance Gene Locus Underlying Immune-Related Hybrid Incompatibility and Its Occurrence in Nature. *PLOS Genetics*, *10*(12), e1004848. https://doi.org/10.1371/JOURNAL.PGEN.1004848

Alonso-Blanco, C., Andrade, J., Becker, C., Bemm, F., Bergelson, J., Borgwardt, K. M. M., Cao, J., Chae, E., Dezwaan, T. M. M., Ding, W., Ecker, J. R. R., Exposito-Alonso, M., Farlow, A., Fitz, J., Gan, X., Grimm, D. G. G., Hancock, A. M. M., Henz, S. R. R., Holm, S., … Zhou, X. (2016). 1,135 Genomes Reveal the Global Pattern of Polymorphism in Arabidopsis thaliana. *Cell*, *166*(2), 481–491. https://doi.org/10.1016/J.CELL.2016.05.063/ATTACHMENT/D2E3D704-8EE7-4B34-B59C-81F2B4C47148/MMC2.PDF

Allen, R. L., Bittner-Eddy, P. D., Grenville-Briggs, L. J., Meitz, J. C., Rehmany, A. P., Rose, L. E., & Beynon, J. L. (2004). Host-parasite coevolutionary conflict between Arabidopsis and downy mildew. *Science*, *306*(5703), 1957–1960. https://doi.org/10.1126/science.1104022

Anderson, R., Deb, D., Withers, J., He, S. Y., & McDowell, J. (2019). An oomycete RXLR effector triggers antagonistic plant hormone crosstalk to suppress host immunity. *BioRxiv*, 561605. https://doi.org/10.1101/561605

Asai, S., Rallapalli, G., Piquerez, S. J. M., Caillaud, M. C., Furzer, O. J., Ishaque, N., Wirthmueller, L., Fabro, G., Shirasu, K., & Jones, J. D. G. (2014). Expression Profiling during Arabidopsis/Downy Mildew Interaction Reveals a Highly-Expressed Effector That Attenuates Responses to Salicylic Acid. *PLoS Pathogens*, *10*(10). https://doi.org/10.1371/JOURNAL.PPAT.1004443,

Bailey, K., Çevik, V., Holton, N., Byrne-Richardson, J., Sohn, K. H., Coates, M., Woods-Tör, A., Murat Aksoy, H., Hughes, L., Baxter, L., Jones, J. D. G., Beynon, J., Holub, E. B., & Tör, M. (2011). Molecular cloning of ATR5 Emoy2 from Hyaloperonospora arabidopsidis, an avirulence determinant that triggers RPP5-mediated defense in Arabidopsis. *Molecular Plant-Microbe Interactions*, *24*(7), 827–838. https://doi.org/10.1094/MPMI-12-10-0278,

Barragan, A. C., & Weigel, D. (2020). *Plant NLR Diversity: The Known Unknowns of Pan-NLRomes*. https://doi.org/10.1093/plcell/koaa002/5985533

Barragan, C. A., Wu, R., Kim, S. T., Xi, W., Habring, A., Hagmann, J., Van de Weyer, A. L., Zaidem, M., Ho, W. W. H., Wang, G., Bezrukov, I., Weigel, D., & Chae, E. (2019). RPW8/HR repeats control NLR activation in Arabidopsis thaliana. *PLOS Genetics*, *15*(7), e1008313. https://doi.org/10.1371/JOURNAL.PGEN.1008313

Bhandari, D. D., Lapin, D., Kracher, B., von Born, P., Bautor, J., Niefind, K., & Parker, J. E. (2019). An EDS1 heterodimer signalling surface enforces timely reprogramming of immunity genes in Arabidopsis. *Nature Communications 2019 10:1*, *10*(1), 1–13. https://doi.org/10.1038/s41467-019-08783-0

Birker, D., Heidrich, K., Takahara, H., Narusaka, M., Deslandes, L., Narusaka, Y., Reymond, M., Parker, J. E., & O'Connell, R. (2009). A locus conferring resistance to Colletotrichum higginsianum is shared by four geographically distinct Arabidopsis accessions. *Plant Journal*, *60*(4), 602–613. https://doi.org/10.1111/J.1365-313X.2009.03984.X,

Bittner-Eddy, P. D., & Beynon, J. L. (2001). The Arabidopsis Downy Mildew Resistance Gene, RPP13-Nd, Functions Independently of NDR1 and EDS1 and Does Not Require the Accumulation of Salicylic Acid. In *Molecular Plant-Microbe Interactions MPMI* (Vol. 14, Issue 3).

Bomblies, K., Lempe, J., Epple, P., Warthmann, N., Lanz, C., Dangl, J. L., & Weigel, D. (2007). Autoimmune response as a mechanism for a Dobzhansky-Muller-type incompatibility syndrome in plants. *PLoS Biology*, *5*(9), 1962–1972. https://doi.org/10.1371/JOURNAL.PBIO.0050236,

Bomblies, K., Yant, L., Laitinen, R. A., Kim, S. T., Hollister, J. D., Warthmann, N., Fitz, J., & Weigel, D. (2010). Local-Scale Patterns of Genetic Variability, Outcrossing, and Spatial Structure in Natural Stands of Arabidopsis thaliana. *PLOS Genetics*, *6*(3), e1000890. https://doi.org/10.1371/JOURNAL.PGEN.1000890

Busche, M., & Laflamme, B. (2024). From algae to apples: The structural and functional conservation of NLRs. *The Plant Cell*, *36*(7), 2453–2454. https://doi.org/10.1093/PLCELL/KOAE131

Caillaud, M. C., Asai, S., Rallapalli, G., Piquerez, S., Fabro, G., & Jones, J. D. G. (2013). A Downy Mildew Effector Attenuates Salicylic Acid–Triggered Immunity in Arabidopsis by Interacting with the Host Mediator Complex. *PLoS Biology*, *11*(12), e1001732. https://doi.org/10.1371/JOURNAL.PBIO.1001732

Castel, B., Ngou, P. M., Cevik, V., Redkar, A., Kim, D. S., Yang, Y., Ding, P., & Jones, J. D. G. (2019). Diverse NLR immune receptors activate defence via the RPW8-NLR NRG1. *New Phytologist*, *222*(2), 966–980. https://doi.org/10.1111/NPH.15659,

Cesari, S., Thilliez, G., Ribot, C., Chalvon, V., Michel, C., Jauneau, A., Rivas, S., Alaux, L., Kanzaki, H., Okuyama, Y., Morel, J. B., Fournier, E., Tharreau, D., Terauchi, R., & Kroj, T. (2013). The rice resistance protein pair RGA4/RGA5 recognizes the Magnaporthe oryzae effectors AVR-Pia and AVR1-CO39 by direct binding. *Plant Cell*, *25*(4), 1463–1481. https://doi.org/10.1105/TPC.112.107201,

Chen, S., Ma, T., Song, S., Li, X., Fu, P., Wu, W., Liu, J., Gao, Y., Ye, W., Dry, I. B., & Lu, J. (2021). Arabidopsis downy mildew effector HaRxLL470 suppresses plant immunity by attenuating the DNA-binding activity of bZIP transcription factor HY5. *New Phytologist*, *230*(4), 1562–1577. https://doi.org/10.1111/NPH.17280,

Chia, K. S., & Carella, P. (2023). Taking the lead: NLR immune receptor N-terminal domains execute plant immune responses. *New Phytologist*, *240*(2), 496–501. https://doi.org/10.1111/NPH.19170

Chia, K. S., Kourelis, J., Teulet, A., Vickers, M., Sakai, T., Walker, J. F., Schornack, S., Kamoun, S., & Carella, P. (2024). The N-terminal domains of NLR immune receptors exhibit structural and functional similarities across divergent plant lineages. *The Plant Cell*, *36*(7), 2491–2511. https://doi.org/10.1093/PLCELL/KOAE113

Chisholm, S. T., Coaker, G., Day, B., & Staskawicz, B. J. (2006). Host-microbe interactions: Shaping the evolution of the plant immune response. *Cell*, *124*(4), 803–814. https://doi.org/10.1016/j.cell.2006.02.008

Chou, S., Krasileva, K. V., Holton, J. M., Steinbrenner, A. D., Alber, T., & Staskawicz, B. J. (2011). Hyaloperonospora arabidopsidis ATR1 effector is a repeat protein with distributed recognition surfaces. *Proceedings of the National Academy of Sciences of the United States of America*, *108*(32), 13323–13328. https://doi.org/10.1073/PNAS.1109791108/SUPPL_FILE/SM01.AVI

Coates, M. E., & Beynon, J. L. (2010). *Hyaloperonospora arabidopsidis as a Pathogen Model*. https://doi.org/10.1146/annurev-phyto-080508-094422

Consortium, T. 1001 G. P., Alonso-Blanco, C. C., Ashkenazy, H., Baduel, P., Bao, Z., Becker, C., Caillieux, E., Colot, V., Crosbie, D., Oliveira, L. De, Fitz, J., Fritschi, K., Grigoreva, E., Guo, Y., Habring, A., Henderson, I., Hou, X.-H., Hu, Y., Igolkina, A., … Xian, W. (2024). The 1001G+ project: A curated collection of Arabidopsis thaliana long-read genome assemblies to advance plant research. *BioRxiv*, 2024.12.23.629943. https://doi.org/10.1101/2024.12.23.629943

Contreras, M. P., Lüdke, D., Pai, H., Toghani, A., & Kamoun, S. (2023). NLR receptors in plant immunity: making sense of the alphabet soup. *EMBO Reports*, *24*(10). https://doi.org/10.15252/EMBR.202357495,

Couto, D., & Zipfel, C. (2016). Regulation of pattern recognition receptor signalling in plants. In *Nature Reviews Immunology* (Vol. 16, Issue 9, pp. 537–552). Nature Publishing Group. https://doi.org/10.1038/nri.2016.77

Danecek, P., Auton, A., Abecasis, G., Albers, C. A., Banks, E., DePristo, M. A., Handsaker, R. E., Lunter, G., Marth, G. T., Sherry, S. T., McVean, G., & Durbin, R. (2011). The variant call format and VCFtools. *Bioinformatics*, *27*(15), 2156. https://doi.org/10.1093/BIOINFORMATICS/BTR330

Daskalov, A., Habenstein, B., Sabaté, R., Berbon, M., Martinez, D., Chaignepain, S., Coulary-Salin, B., Hofmann, K., Loquet, A., & Saupe, S. J. (2016). Identification of a novel cell death-inducing domain reveals that fungal amyloid-controlled programmed cell death is related to necroptosis. *Proceedings of*

the National Academy of Sciences of the United States of America, *113*(10), 2720–2725. https://doi.org/10.1073/PNAS.1522361113/SUPPL_FILE/PNAS.201522361SI.PDF
Deslandes, L., Olivier, J., Peeters, N., Feng, D. X., Khounlotham, M., Boucher, C., Somssich, I., Genin, S., & Marco, Y. (2003). Physical interaction between RRS1-R, a protein conferring resistance to bacterial wilt, and PopP2, a type III effector targeted to the plant nucleus. *Proceedings of the National Academy of Sciences of the United States of America*, *100*(13), 8024–8029. https://doi.org/10.1073/PNAS.1230660100,
Eastman, S., Smith, T., Zaydman, M. A., Kim, P., Martinez, S., Damaraju, N., DiAntonio, A., Milbrandt, J., Clemente, T. E., Alfano, J. R., & Guo, M. (2022). A phytobacterial TIR domain effector manipulates NAD+ to promote virulence. *New Phytologist*, *233*(2), 890–904. https://doi.org/10.1111/NPH.17805,
Ercolano, M. R., D'Esposito, D., Andolfo, G., & Frusciante, L. (2022). Multilevel evolution shapes the function of NB-LRR encoding genes in plant innate immunity. *Frontiers in Plant Science*, *13*, 1007288. https://doi.org/10.3389/FPLS.2022.1007288
Essuman, K., Milbrandt, J., Dangl, J. L., & Nishimura, M. T. (2022). Shared TIR enzymatic functions regulate cell death and immunity across the tree of life. *Science*, *377*(6605). https://doi.org/10.1126/SCIENCE.ABO0001/ASSET/8B18500A-D98C-4132-A20D-AE3FBA472A47/ASSETS/IMAGES/LARGE/SCIENCE.ABO0001-F6.JPG
Essuman, K., Summers, D. W., Sasaki, Y., Mao, X., DiAntonio, A., & Milbrandt, J. (2017). The SARM1 Toll/Interleukin-1 Receptor Domain Possesses Intrinsic NAD+ Cleavage Activity that Promotes Pathological Axonal Degeneration. *Neuron*, *93*(6), 1334-1343.e5. https://doi.org/10.1016/j.neuron.2017.02.022
Fabro, G., Steinbrenner, J., Coates, M., Ishaque, N., & Baxter, L. (2011). Multiple Candidate Effectors from the Oomycete Pathogen Hyaloperonospora arabidopsidis Suppress Host Plant Immunity. *PLoS Pathog*, *7*(11), 1002348. https://doi.org/10.1371/journal.ppat.1002348
Fabro, G., Steinbrenner, J., Coates, M., Ishaque, N., Baxter, L., Studholme, D. J., Körner, E., Allen, R. L., Piquerez, S. J. M., Rougon-Cardoso, A., Greenshields, D., Lei, R., Badel, J. L., Caillaud, M. C., Sohn, K. H., van den Ackerveken, G., Parker, J. E., Beynon, J., & Jones, J. D. G. (2011). Multiple candidate effectors from the oomycete pathogen hyaloperonospora arabidopsidis suppress host plant immunity. *PLoS Pathogens*, *7*(11). https://doi.org/10.1371/journal.ppat.1002348
Fraley, R. T., Rogers, S. G., Horsch, R. B., Sanders, P. R., Flick, J. S., Adams, S. P., Bittner, M. L., Brand, L. A., Fink, C. L., Fry, J. S., Galluppi, G. R., Goldberg, S. B., Hoffmann, N. L., & Woo, S. C. (1983). Expression of bacterial genes in plant cells. *Proceedings of the National Academy of Sciences*, *80*(15), 4803–4807. https://doi.org/10.1073/PNAS.80.15.4803
Förderer, A., & Kourelis, J. (2023). NLR immune receptors: structure and function in plant disease resistance. *Biochemical Society Transactions*, *51*(4), 1473. https://doi.org/10.1042/BST20221087
Förderer, A., Li, E., Lawson, A. W., Deng, Y. nan, Sun, Y., Logemann, E., Zhang, X., Wen, J., Han, Z., Chang, J., Chen, Y., Schulze-Lefert, P., & Chai, J. (2022). A wheat resistosome defines common principles of immune receptor channels. *Nature*, *610*(7932), 532–539. https://doi.org/10.1038/S41586-022-05231-W,
Gassmann, W., Hinsch, M. E., & Staskawicz, B. J. (1999). The Arabidopsis RPS4 bacterial-resistance gene is a member of the TIR-NBS-LRR family of disease-resistance genes. *The Plant Journal*, *20*(3), 265–277. https://doi.org/10.1046/J.1365-313X.1999.00600.X
Gordon A. 2002. Analysis of the RPP1 resistance gene cluster in Arabidopsis accession Niederzenz (Nd-1). PhD thesis, University of Birmingham, Birmingham, UK.
Goritschnig, S., Steinbrenner, A. D., Grunwald, D. J., & Staskawicz, B. J. (2016). Structurally distinct Arabidopsis thaliana NLR immune receptors recognize tandem WY domains of an oomycete effector. *New Phytologist*, *210*(3), 984–996. https://doi.org/10.1111/NPH.13823
Hackl, T., Duponchel, S., Barenhoff, K., Weinmann, A., & Fischer, M. G. (2021). Virophages and retrotransposons colonize the genomes of a heterotrophic flagellate. *ELife*, *10*. https://doi.org/10.7554/ELIFE.72674
Hacquard, S., Spaepen, S., Garrido-Oter, R., & Schulze-Lefert, P. (2017). Interplay Between Innate Immunity and the Plant Microbiota. *Annual Review of Phytopathology*, *55*(1), 565–589. https://doi.org/10.1146/annurev-phyto-080516-035623
Hall, S. A., Allen, R. L., Baumber, R. E., Baxter, L. A., Fisher, K., Bittner-Eddy, P. D., Rose, L. E., Holub, E. B., & Beynon, J. L. (2009). Maintenance of genetic variation in plants and pathogens involves complex networks of gene-for-gene interactions. *Molecular Plant Pathology*, *10*(4), 449–457. https://doi.org/10.1111/J.1364-3703.2009.00544.X;WGROUP:STRING:PUBLICATION
Harant, A., Pai, H., Sakai, T., Kamoun, S., & Adachi, H. (2022a). A vector system for fast-forward studies of the HOPZ-ACTIVATED RESISTANCE1 (ZAR1) resistosome in the model plant Nicotiana benthamiana. *Plant Physiology*, *188*(1), 70–80. https://doi.org/10.1093/PLPHYS/KIAB471,

Harvey, S., Kumari, P., Lapin, D., Griebel, T., Hickman, R., Guo, W., Zhang, R., Parker, J. E., Beynon, J., Denby, K., & Steinbrenner, J. (2020). Downy Mildew effector HaRxL21 interacts with the transcriptional repressor TOPLESS to promote pathogen susceptibility. *PLOS Pathogens*, *16*(8), e1008835. https://doi.org/10.1371/JOURNAL.PPAT.1008835

Haverkort, A. J., Struik, P. C., Visser, R. G. F., & Jacobsen, E. (2009). Applied Biotechnology to Combat Late Blight in Potato Caused by Phytophthora Infestans. *Potato Research*, *52*, 249–264. https://doi.org/10.1007/s11540-009-9136-3

Hoffmann, M. H. (2002). Biogeography of Arabidopsis thaliana (L.) Heynh. (Brassicaceae). *Journal of Biogeography*, *29*(1), 125–134. https://doi.org/10.1046/J.1365-2699.2002.00647.X

Horsefield, S., Burdett, H., Zhang, X., Manik, M. K., Shi, Y., Chen, J., Qi, T., Gilley, J., Lai, J. S., Rank, M. X., Casey, L. W., Gu, W., Ericsson, D. J., Foley, G., Hughes, R. O., Bosanac, T., Von Itzstein, M., Rathjen, J. P., Nanson, J. D., … Kobe, B. (2019). NAD+ cleavage activity by animal and plant TIR domains in cell death pathways. *Science*, *365*(6455), 793–799. https://doi.org/10.1126/SCIENCE.AAX1911,

Huang, S., Jia, A., Song, W., Hessler, G., Meng, Y., Sun, Y., Xu, L., Laessle, H., Jirschitzka, J., Ma, S., Xiao, Y., Yu, D., Hou, J., Liu, R., Sun, H., Liu, X., Han, Z., Chang, J., Parker, J. E., & Chai, J. (2022). Identification and receptor mechanism of TIR-catalyzed small molecules in plant immunity. *Science*, *377*(6605). https://doi.org/10.1126/SCIENCE.ABQ3297/SUPPL_FILE/SCIENCE.ABQ3297_MDAR_REPRODUCIBILITY_CHECKLIST.PDF

Hulin, M. T., Hill, L., Jones, J. D. G., & Ma, W. (2023). Pangenomic analysis reveals plant NAD+ manipulation as an important virulence activity of bacterial pathogen effectors. *Proceedings of the National Academy of Sciences of the United States of America*, *120*(7), e2217114120. https://doi.org/10.1073/PNAS.2217114120

Jacob, F., Vernaldi, S., & Maekawa, T. (2013). Evolution and Conservation of Plant NLR Functions. *Frontiers in Immunology*, *4*(SEP), 297. https://doi.org/10.3389/FIMMU.2013.00297

Jacob, P., Kim, N. H., Wu, F., El-Kasmi, F., Chi, Y., Walton, W. G., Furzer, O. J., Lietzan, A. D., Sunil, S., Kempthorn, K., Redinbo, M. R., Pei, Z. M., Wan, L., & Dangl, J. L. (2021). Plant “helper” immune receptors are Ca2+-permeable nonselective cation channels. *Science (New York, N.Y.)*, *373*(6553), 420. https://doi.org/10.1126/SCIENCE.ABG7917

Jia, A., Huang, S., Song, W., Wang, J., Meng, Y., Sun, Y., Xu, L., Laessle, H., Jirschitzka, J., Hou, J., Zhang, T., Yu, W., Hessler, G., Li, E., Ma, S., Yu, D., Gebauer, J., Baumann, U., Liu, X., … Chai, J. (n.d.). *TIR-catalyzed ADP-ribosylation reactions produce signaling molecules for plant immunity*. https://doi.org/10.1126/science.abq8180

Jiménez-Guerrero, I., Pérez-Montaño, F., Medina, C., Ollero, F. J., & López-Baena, F. J. (2015). NopC is a rhizobium-specific type 3 secretion system effector secreted by sinorhizobium (ensifer) fredii HH103. *PLoS ONE*, *10*(11), 1–17. https://doi.org/10.1371/journal.pone.0142866

Jones, J. D. G., & Dangl, J. L. (2006). The plant immune system. In *Nature* (Vol. 444, Issue 7117, pp. 323–329). Nature Publishing Group. https://doi.org/10.1038/nature05286

Jubic, L. M., Saile, S., Furzer, O. J., El Kasmi, F., & Dangl, J. L. (2019). Help wanted: helper NLRs and plant immune responses. *Current Opinion in Plant Biology*, *50*, 82–94. https://doi.org/10.1016/j.pbi.2019.03.013

Karasov, T. L., Kniskern, J. M., Gao, L., Deyoung, B. J., Ding, J., Dubiella, U., Lastra, R. O., Nallu, S., Roux, F., Innes, R. W., Barrett, L. G., Hudson, R. R., & Bergelson, J. (2014). The long-term maintenance of a resistance polymorphism through diffuse interactions. *Nature*, *512*(7515), 436–440. https://doi.org/10.1038/NATURE13439,

Kee, H. S., Lei, R., Nemri, A., & Jones, J. D. G. (2007). The Downy Mildew Effector Proteins ATR1 and ATR13 Promote Disease Susceptibility in Arabidopsis thaliana. *The Plant Cell*, *19*(12), 4077. https://doi.org/10.1105/TPC.107.054262

Koch, E., & Slusarenko, A. (1990). Arabidopsis is susceptible to infection by a downy mildew fungus. *The Plant Cell*, *2*(5), 437. https://doi.org/10.1105/TPC.2.5.437

Kourelis, J., Marchal, C., Posbeyikian, A., Harant, A., & Kamoun, S. (2023). NLR immune receptor–nanobody fusions confer plant disease resistance. *Science*, *379*(6635), 934–939. https://doi.org/10.1126/SCIENCE.ABN4116/SUPPL_FILE/SCIENCE.ABN4116_MDAR_REPRODUCIBILITY_CHECKLIST.PDF

Krasileva, K. V., Zheng, C., Leonelli, L., Goritschnig, S., Dahlbeck, D., & Staskawicz, B. J. (2011). Global analysis of Arabidopsis/downy mildew interactions reveals prevalence of incomplete resistance and rapid evolution of pathogen recognition. *PLoS ONE*, *6*(12). https://doi.org/10.1371/journal.pone.0028765

Lai, Y., & Eulgem, T. (2018). Transcript-level expression control of plant NLR genes. *Molecular Plant Pathology*, *19*(5), 1267–1281. https://doi.org/10.1111/MPP.12607,
Lapin, D., Bhandari, D. D., & Parker, J. E. (2020). Origins and Immunity Networking Functions of EDS1 Family Proteins. *Annual Review of Phytopathology*, *58*, 253–276. https://doi.org/10.1146/ANNUREV-PHYTO-010820-012840,
Lee, S. K., Song, M. Y., Seo, Y. S., Kim, H. K., Ko, S., Cao, P. J., Suh, J. P., Yi, G., Roh, J. H., Lee, S., An, G., Hahn, T. R., Wang, G. L., Ronald, P., & Jeon, J. S. (2009). Rice Pi5-Mediated Resistance to Magnaporthe oryzae Requires the Presence of Two Coiled-Coil–Nucleotide-Binding–Leucine-Rich Repeat Genes. *Genetics*, *181*(4), 1627–1638. https://doi.org/10.1534/GENETICS.108.099226
Letunic, I., & Bork, P. (2021). Interactive tree of life (iTOL) v5: An online tool for phylogenetic tree display and annotation. *Nucleic Acids Research*, *49*(W1), W293–W296. https://doi.org/10.1093/NAR/GKAB301,
Li, H., Handsaker, B., Wysoker, A., Fennell, T., Ruan, J., Homer, N., Marth, G., Abecasis, G., & Durbin, R. (2009). The Sequence Alignment/Map format and SAMtools. *Bioinformatics*, *25*(16), 2078–2079. https://doi.org/10.1093/BIOINFORMATICS/BTP352,
Li, L., & Weigel, D. (2021). One Hundred Years of Hybrid Necrosis: Hybrid Autoimmunity as a Window into the Mechanisms and Evolution of Plant-Pathogen Interactions. *Annual Review of Phytopathology*, *59*, 213–237. https://doi.org/10.1146/ANNUREV-PHYTO-020620-114826,
Liu, F., Yang, Z., Wang, C., You, Z., Martin, R., Qiao, W., Huang, J., Jacob, P., Dangl, J. L., Carette, J. E., Luan, S., Nogales, E., & Staskawicz, B. J. (2024). Activation of the helper NRC4 immune receptor forms a hexameric resistosome. *Cell*, *187*(18), 4877-4889.e15. https://doi.org/10.1016/J.CELL.2024.07.013/ASSET/E1D30BB7-44A0-44AD-8807-3903FD90B04C/MAIN.ASSETS/GR1_LRG.JPG
Liu, N., Hake, K., Wang, W., Zhao, T., Romeis, T., & Tang, D. (2017). Calcium-dependent protein kinase5 associates with the truncated NLR protein TIR-NBS2 to contribute to exo70B1-mediated immunity. *Plant Cell*, *29*(4), 746–759. https://doi.org/10.1105/TPC.16.00822,
Liu, Y., Zhang, Y. M., Tang, Y., Chen, J. Q., & Shao, Z. Q. (2023). The evolution of plant NLR immune receptors and downstream signal components. *Current Opinion in Plant Biology*, *73*, 102363. https://doi.org/10.1016/J.PBI.2023.102363
Locci, F., & Parker, J. E. (2024). Plant NLR immunity activation and execution: a biochemical perspective. *Open Biology*, *14*(1). https://doi.org/10.1098/RSOB.230387;WGROUP:STRING:PUBLICATION
Lopez-Delisle, L., Rabbani, L., Wolff, J., Bhardwaj, V., Backofen, R., Grüning, B., Ramírez, F., & Manke, T. (2020). pyGenomeTracks: reproducible plots for multivariate genomic datasets. *Bioinformatics*, *37*(3), 422. https://doi.org/10.1093/BIOINFORMATICS/BTAA692
Lucke, M., Correa, M. G., & Levy, A. (2020). The Role of Secretion Systems, Effectors, and Secondary Metabolites of Beneficial Rhizobacteria in Interactions With Plants and Microbes. *Frontiers in Plant Science*, *11*. https://doi.org/10.3389/FPLS.2020.589416
Ma, S., Lapin, D., Liu, L., Sun, Y., Song, W., Zhang, X., Logemann, E., Yu, D., Wang, J., Jirschitzka, J., Han, Z., Schulze-Lefert, P., Parker, J. E., & Chai, J. (2020). Direct pathogen-induced assembly of an NLR immune receptor complex to form a holoenzyme. *Science*, *370*(6521). https://doi.org/10.1126/SCIENCE.ABE3069/SUPPL_FILE/ABE3069_REPRODUCIBILITY_CHECKLIST.PDF
Maekawa, T., Kufer, T. A., & Schulze-Lefert, P. (2011). NLR functions in plant and animal immune systems: so far and yet so close. *Nature Immunology 2011 12:9*, *12*(9), 817–826. https://doi.org/10.1038/ni.2083
Macho, A. P., & Zipfel, C. (2014). Plant PRRs and the activation of innate immune signaling. In *Molecular Cell* (Vol. 54, Issue 2, pp. 263–272). Cell Press. https://doi.org/10.1016/j.molcel.2014.03.028
Maidment, J. H. R., Shimizu, M., Bentham, A. R., Vera, S., Franceschetti, M., Longya, A., Stevenson, C. E. M., De la Concepcion, J. C., Białas, A., Kamoun, S., Terauchi, R., & Banfield, M. J. (2023). Effector target-guided engineering of an integrated domain expands the disease resistance profile of a rice NLimmune receptor. *ELife*, *12*. https://doi.org/10.7554/ELIFE.81123
Magwene, P. M., Willis, J. H., & Kelly, J. K. (2011). The statistics of bulk segregant analysis using next generation sequencing. *PLoS Computational Biology*, *7*(11). https://doi.org/10.1371/JOURNAL.PCBI.1002255,
Mansfeld, B. N., & Grumet, R. (2018). QTLseqr: An R Package for Bulk Segregant Analysis with Next-Generation Sequencing. *The Plant Genome*, *11*(2). https://doi.org/10.3835/PLANTGENOME2018.01.0006,
Manik, M. K., Shi, Y., Li, S., Zaydman, M. A., Damaraju, N., Eastman, S., Smith, T. G., Gu, W., Masic, V., Mosaiab, T., Weagley, J. S., Hancock, S. J., Vasquez, E., Hartley-Tassell, L., Kargios, N., Maruta, N., Lim, B. Y. J., Burdett, H., Landsberg, M. J., … Kobe, B. (2022). Cyclic ADP ribose isomers:

Production, chemical structures, and immune signaling. *Science*, *377*(6614). https://doi.org/10.1126/SCIENCE.ADC8969/SUPPL_FILE/SCIENCE.ADC8969_DATA_S1_TO_S4.ZIP

Maqbool, A., Saitoh, H., Franceschetti, M., Stevenson, C. E. M., Uemura, A., Kanzaki, H., Kamoun, S., Terauchi, R., & Banfield, M. J. (2015). Structural basis of pathogen recognition by an integrated HMA domain in a plant NLR immune receptor. *ELife*, *4*(AUGUST2015). https://doi.org/10.7554/ELIFE.08709,

Martin, R., Qi, T., Zhang, H., Liu, F., King, M., Toth, C., Nogales, E., & Staskawicz, B. J. (2020). Structure of the activated ROQ1 resistosome directly recognizing the pathogen effector XopQ. *Science*, *370*(6521). https://doi.org/10.1126/SCIENCE.ABD9993/SUPPL_FILE/ABD9993-MARTIN-SM.PDF

McDowell, J. M. (2013). Genomic and transcriptomic insights into lifestyle transitions of a hemi-biotrophic fungal pathogen. *New Phytologist*, *197*(4), 1032–1034. https://doi.org/10.1111/NPH.12141,

Meng, E. C., Goddard, T. D., Pettersen, E. F., Couch, G. S., Pearson, Z. J., Morris, J. H., & Ferrin, T. E. (2023). UCSF ChimeraX: Tools for structure building and analysis. *Protein Science*, *32*(11), e4792. https://doi.org/10.1002/PRO.4792

Minh, B. Q., Schmidt, H. A., Chernomor, O., Schrempf, D., Woodhams, M. D., Von Haeseler, A., Lanfear, R., & Teeling, E. (2020). IQ-TREE 2: New Models and Efficient Methods for Phylogenetic Inference in the Genomic Era. *Molecular Biology and Evolution*, *37*(5), 1530–1534. https://doi.org/10.1093/MOLBEV/MSAA015,

Narusaka, M., Shirasu, K., Noutoshi, Y., Kubo, Y., Shiraishi, T., Iwabuchi, M., & Narusaka, Y. (2009). RRS1 and RPS4 provide a dual Resistance-gene system against fungal and bacterial pathogens. *Plant Journal*, *60*(2), 218–226. https://doi.org/10.1111/J.1365-313X.2009.03949.X,

Ngou, B. P. M., Ahn, H. K., Ding, P., & Jones, J. D. G. (2021). Mutual potentiation of plant immunity by cell-surface and intracellular receptors. *Nature*, *592*(7852), 110–115. https://doi.org/10.1038/S41586-021-03315-7,

Ngou, B. P. M., Heal, R., Wyler, M., Schmid, M. W., & Jones, J. D. G. (2022). Concerted expansion and contraction of immune receptor gene repertoires in plant genomes. *Nature Plants*, *8*(10), 1146–1152. https://doi.org/10.1038/S41477-022-01260-5,

Nimma, S., Gu, W., Maruta, N., Li, Y., Pan, M., Saikot, F. K., Lim, B. Y. J., McGuinness, H. Y., Zaoti, Z. F., Li, S., Desa, S., Manik, M. K., Nanson, J. D., & Kobe, B. (2021). Structural Evolution of TIR-Domain Signalosomes. *Frontiers in Immunology*, *12*, 784484. https://doi.org/10.3389/FIMMU.2021.784484/BIBTEX

Nishimura, M. T., Anderson, R. G., Cherkis, K. A., Law, T. F., Liu, Q. L., Machius, M., Nimchuk, Z. L., Yang, L., Chung, E. H., El Kasmi, F., Hyunh, M., Nishimura, E. O., Sondek, J. E., & Dangl, J. L. (2017). TIR-only protein RBA1 recognizes a pathogen effector to regulate cell death in Arabidopsis. *Proceedings of the National Academy of Sciences of the United States of America*, *114*(10), E2053–E2062. https://doi.org/10.1073/PNAS.1620973114,

Nobori, T., Monell, A., Lee, T. A., Sakata, Y., Shirahama, S., Zhou, J., Nery, J. R., Mine, A., & Ecker, J. R. (2025). A rare PRIMER cell state in plant immunity. *Nature 2025 638:8049*, *638*(8049), 197–205. https://doi.org/10.1038/s41586-024-08383-z

Ofir, G., Herbst, E., Baroz, M., Cohen, D., Millman, A., Doron, S., Tal, N., Malheiro, D. B. A., Malitsky, S., Amitai, G., & Sorek, R. (2021). Antiviral activity of bacterial TIR domains via immune signalling molecules. *Nature*, *600*(7887), 116–120. https://doi.org/10.1038/S41586-021-04098-7,

Okuyama, Y., Kanzaki, H., Abe, A., Yoshida, K., Tamiru, M., Saitoh, H., Fujibe, T., Matsumura, H., Shenton, M., Galam, D. C., Undan, J., Ito, A., Sone, T., & Terauchi, R. (2011). A multifaceted genomics approach allows the isolation of the rice Pia-blast resistance gene consisting of two adjacent NBS-LRR protein genes. *Plant Journal*, *66*(3), 467–479. https://doi.org/10.1111/J.1365-313X.2011.04502.X,

Peart, J. R., Mestre, P., Lu, R., Malcuit, I., & Baulcombe, D. C. (2005). NRG1, a CC-NB-LRR protein, together with N, a TIR-NB-LRR protein, mediates resistance against tobacco mosaic virus. *Current Biology*, *15*(10), 968–973. https://doi.org/10.1016/j.cub.2005.04.053

Pham, M., Tu, Y., & Lv, X. (2023). Accelerating BWA-MEM Read Mapping on GPUs. *ICS ... : Proceedings of the ... ACM International Conference on Supercomputing. International Conference on Supercomputing*, *2023*, 155. https://doi.org/10.1145/3577193.3593703

Pieterse, C. M. J., Van der Does, D., Zamioudis, C., Leon-Reyes, A., & Van Wees, S. C. M. (2012). Hormonal Modulation of Plant Immunity. *Annual Review of Cell and Developmental Biology*, *28*(1), 489–521. https://doi.org/10.1146/annurev-cellbio-092910-154055

Pieterse, C. M. J., Zamioudis, C., Berendsen, R. L., Weller, D. M., Van Wees, S. C. M., Bakker, P. A. H. M., Nl, C. M. J. P., Nl, C. Z., Nl, R. L. B., Nl, S. V., & Nl, P. A. H. M. B. (2014). *Induced Systemic Resistance by Beneficial Microbes*. https://doi.org/10.1146/annurev-phyto-082712-102340

Prigozhin, D. M., & Krasileva, K. V. (2021). Analysis of intraspecies diversity reveals a subset of highly variable plant immune receptors and predicts their binding sites. *The Plant Cell*, *33*(4), 998–1015. https://doi.org/10.1093/PLCELL/KOAB013

Pruitt, R. N., Locci, F., Wanke, F., Zhang, L., Saile, S. C., Joe, A., Karelina, D., Hua, C., Fröhlich, K., Wan, W. L., Hu, M., Rao, S., Stolze, S. C., Harzen, A., Gust, A. A., Harter, K., Joosten, M. H. A. J., Thomma, B. P. H. J., Zhou, J. M., … Nürnberger, T. (2021). The EDS1–PAD4–ADR1 node mediates Arabidopsis pattern-triggered immunity. *Nature 2021 598:7881*, *598*(7881), 495–499. https://doi.org/10.1038/s41586-021-03829-0

Purcell, S., Neale, B., Todd-Brown, K., Thomas, L., Ferreira, M. A. R., Bender, D., Maller, J., Sklar, P., De Bakker, P. I. W., Daly, M. J., & Sham, P. C. (2007). PLINK: A tool set for whole-genome association and population-based linkage analyses. *American Journal of Human Genetics*, *81*(3), 559–575. https://doi.org/10.1086/519795

Rehmany, A. P., Gordon, A., Rose, L. E., Allen, R. L., Armstrong, M. R., Whisson, S. C., Kamoun, S., Tyler, B. M., Birch, P. R. J., & Beynon, J. L. (2005). Differential Recognition of Highly Divergent Downy Mildew Avirulence Gene Alleles by RPP1 Resistance Genes from Two Arabidopsis Lines. *The Plant Cell*, *17*(6), 1839. https://doi.org/10.1105/TPC.105.031807

Quinlan, A. R., & Hall, I. M. (2010). BEDTools: A flexible suite of utilities for comparing genomic features. *Bioinformatics*, *26*(6), 841–842. https://doi.org/10.1093/BIOINFORMATICS/BTQ033,

Sang, Y., & Macho, A. P. (2017). Analysis of PAMP-triggered ROS burst in plant immunity. *Methods in Molecular Biology*, *1578*, 143–153. https://doi.org/10.1007/978-1-4939-6859-6_11,

Schreiber, K. J., Bentham, A., Williams, S. J., Kobe, B., & Staskawicz, B. J. (2016). Multiple Domain Associations within the Arabidopsis Immune Receptor RPP1 Regulate the Activation of Programmed Cell Death. *PLOS Pathogens*, *12*(7), e1005769. https://doi.org/10.1371/journal.ppat.1005769

Schultink, A., Qi, T., Lee, A., Steinbrenner, A. D., & Staskawicz, B. (2017). Roq1 mediates recognition of the Xanthomonas and Pseudomonas effector proteins XopQ and HopQ1. *Plant Journal*, *92*(5), 787–795. https://doi.org/10.1111/TPJ.13715;PAGE:STRING:ARTICLE/CHAPTER

Seong, K., Seo, E., Witek, K., Li, M., & Staskawicz, B. (2020). Evolution of NLR resistance genes with noncanonical N-terminal domains in wild tomato species. *New Phytologist*, *227*(5), 1530–1543. https://doi.org/10.1111/NPH.16628

Shirsekar, G., Devos, J., Latorre, S. M., Blaha, A., Dias, M. Q., Gonz Alez Hernando, A., Lundberg, D. S., Burbano, H. A. A., Fenster, C. B., & Weigel, D. (n.d.). *Multiple Sources of Introduction of North American Arabidopsis thaliana from across Eurasia*. https://doi.org/10.1093/molbev/msab268

Shumate, A., & Salzberg, S. L. (2021). Liftoff: accurate mapping of gene annotations. *Bioinformatics*, *37*(12), 1639–1643. https://doi.org/10.1093/BIOINFORMATICS/BTAA1016

Singh, D. P., Singh, H. B., & Prabha, R. (2017). Plant-microbe interactions in agro-ecological perspectives. In *Plant-Microbe Interactions in Agro-Ecological Perspectives* (Vol. 1). Springer Singapore. https://doi.org/10.1007/978-981-10-5813-4

Sohn, K. H., Hughes, R. K., Piquerez, S. J., Jones, J. D. G., & Banfield, M. J. (2012). Distinct regions of the Pseudomonas syringae coiled-coil effector AvrRps4 are required for activation of immunity. *Proceedings of the National Academy of Sciences of the United States of America*, *109*(40), 16371–16376. https://doi.org/10.1073/PNAS.1212332109/-/DCSUPPLEMENTAL

Sohn, K. H., Lei, R., Nemri, A., & Jones, J. D. G. (n.d.). *The Downy Mildew Effector Proteins ATR1 and ATR13 Promote Disease Susceptibility in Arabidopsis thaliana W*. https://doi.org/10.1105/tpc.107.054262

Song, W., Liu, L., Yu, D., Bernardy, H., Jirschitzka, J., Huang, S., Jia, A., Jemielniak, W., Acker, J., Laessle, H., Wang, J., Shen, Q., Chen, W., Li, P., Parker, J. E., Han, Z., Schulze-Lefert, P., & Chai, J. (2024). Substrate-induced condensation activates plant TIR domain proteins. *Nature 2024 627:8005*, *627*(8005), 847–853. https://doi.org/10.1038/s41586-024-07183-9

Soylu, E. M., & Soylu, S. (2003). Light and electron microscopy of the compatible interaction between Arabidopsis and the downy mildew pathogen Peronospora parasitica. *Journal of Phytopathology*, *151*(6), 300–306. https://doi.org/10.1046/J.1439-0434.2003.00723.X;REQUESTEDJOURNAL:JOURNAL:14390434;PAGE:STRING:ARTICLE/CHAPTER

Steinbrenner, A. D., Goritschnig, S., & Staskawicz, B. J. (2015). Recognition and Activation Domains Contribute to Allele-Specific Responses of an Arabidopsis NLR Receptor to an Oomycete Effector Protein. *PLOS Pathogens*, *11*(2), e1004665. https://doi.org/10.1371/journal.ppat.1004665

Steuernagel, B., Witek, K., Krattinger, S. G., Ramirez-Gonzalez, R. H., Schoonbeek, H. J., Yu, G., Baggs, E., Witek, A. I., Yadav, I., Krasileva, K. V., Jones, J. D. G., Uauy, C., Keller, B., Ridout, C. J., & Wulff, B. B. H. (2020). The NLR-annotator tool enables annotation of the intracellular immune receptor repertoire. *Plant Physiology*, *183*(2), 468–482. https://doi.org/10.1104/PP.19.01273,

Takagi, H., Abe, A., Yoshida, K., Kosugi, S., Natsume, S., Mitsuoka, C., Uemura, A., Utsushi, H., Tamiru, M., Takuno, S., Innan, H., Cano, L. M., Kamoun, S., & Terauchi, R. (2013). QTL-seq: Rapid mapping of quantitative trait loci in rice by whole genome resequencing of DNA from two bulked populations. *Plant Journal*, *74*(1), 174–183. https://doi.org/10.1111/TPJ.12105,

Tanaka, M., Mori, H., Kayasuga, R., & Kawabata, K. (2015). Induction of creatine kinase release from cultured osteoclasts via the pharmacological action of aminobisphosphonates. *SpringerPlus*, *4*(1). https://doi.org/10.1186/S40064-015-0848-3

Tamulaitiene, G., Sabonis, D., Sasnauskas, G., Ruksenaite, A., Silanskas, A., Avraham, C., Ofir, G., Sorek, R., Zaremba, M., & Siksnys, V. (2024). Activation of Thoeris antiviral system via SIR2 effector filament assembly. *Nature*, *627*(8003), 431–436. https://doi.org/10.1038/S41586-024-07092-X;TECHMETA=101,16,28,29,80,82,83;SUBJMETA=45,535,631;KWRD=BIOCHEMISTRY,STRUCTURAL+BIOLOGY

Thomas, W. J., Thireault, C. A., Kimbrel, J. A., & Chang, J. H. (2009). Recombineering and stable integration of the Pseudomonas syringae pv. syringae 61 hrp/hrc cluster into the genome of the soil bacterium Pseudomonas fluorescens Pf0-1. *Plant Journal*, *60*(5), 919–928. https://doi.org/10.1111/J.1365-313X.2009.03998.X,

Teasdale, L. C., Murray, K. D., Collenberg, M., Contreras-Garrido, A., Schlegel, T., van Ess, L., Jüttner, J., Lanz, C., Deusch, O., Fitz, J., Mencia, R., van Velthoven, R., Drost, H.-G., Weigel, D., Shirsekar, G., & Fe, S. (2024). Pangenomic context reveals the extent of intraspecific plant NLR evolution. *BioRxiv*, 2024.09.02.610789. https://doi.org/10.1101/2024.09.02.610789

Tian, D., Traw, M. B., Chen, J. Q., Kreitman, M., & Bergelson, J. (2003). Fitness costs of R-gene-mediated resistance in Arabidopsis thaliana. *Nature*, *423*(6935), 74–77. https://doi.org/10.1038/NATURE01588;KWRD=SCIENCE

Todesco, M., Kim, S. T., Chae, E., Bomblies, K., Zaidem, M., Smith, L. M., Weigel, D., & Laitinen, R. A. E. (2014). Activation of the Arabidopsis thaliana Immune System by Combinations of Common ACD6 Alleles. *PLOS Genetics*, *10*(7), e1004459. https://doi.org/10.1371/JOURNAL.PGEN.1004459

Van Damme, M., Andel, A., Huibers, R. P., Panstruga, R., Weisbeek, P. J., & Van Den Ackerveken, G. (2005). Identification of Arabidopsis loci required for susceptibility to the downy mildew pathogen Hyaloperonospora parasitica. *Molecular Plant-Microbe Interactions*, *18*(6), 583–592. https://doi.org/10.1094/MPMI-18-0583

Van der Auwera, G., O'Connor, B., & Safari. (2020). Genomics in the Cloud: Using Docker, GATK, and WDL in Terra. *O'Reilly Media*, 300.

Van De Weyer, A.-L., Monteiro, F., Furzer, O. J., Dangl, J. L., Weigel, D., & Bemm, F. (2019). A Species-Wide Inventory of NLR Genes and Alleles in Arabidopsis thaliana. *Cell*, *178*, 1260-1272.e14. https://doi.org/10.1016/j.cell.2019.07.038

Wan, W.-L., Kim, G., Kim, N., Tan, Y. Y., Watari, M., Charoennit, N., Lee, R. R. Q., Phang, I. R. K., Wang, J., Liew, Y. Y., Hu, D., Ng, S. K., Zhang, Y., Jang, I.-C., Song, J.-J., & Chae, E. (2025). Structural determinants of DANGEROUS MIX 3, an alpha/beta hydrolase that triggers NLR-mediated genetic incompatibility in plants. *Molecular Cell*, *85*(14), 2776-2795.e8. https://doi.org/10.1016/J.MOLCEL.2025.06.021

Wang, W., Zhang, Y., Wen, Y., Berkey, R., Ma, X., Pan, Z., Bendigeri, D., King, H., Zhang, Q., & Xiao, S. (2013). A comprehensive mutational analysis of the arabidopsis resistance protein RPW8.2 reveals key amino acids for defense activation and protein targeting. *Plant Cell*, *25*(10), 4242–4261. https://doi.org/10.1105/TPC.113.117226,

Wang, G., Roux, B., Feng, F., Guy, E., Li, L., Li, N., Zhang, X., Lautier, M., Jardinaud, M. F., Chabannes, M., Arlat, M., Chen, S., He, C., Noël, L. D., & Zhou, J. M. (2015). The Decoy Substrate of a Pathogen Effector and a Pseudokinase Specify Pathogen-Induced Modified-Self Recognition and Immunity in Plants. *Cell Host and Microbe*, *18*(3), 285–295. https://doi.org/10.1016/j.chom.2015.08.004

Wein, T., & Sorek, R. (n.d.). *Bacterial origins of human cell-autonomous innate immune mechanisms*. https://doi.org/10.1038/s41577-022-00705-4

Wick, R. R., Judd, L. M., Gorrie, C. L., & Holt, K. E. (2017). Unicycler: Resolving bacterial genome assemblies from short and long sequencing reads. *PLoS Computational Biology*, *13*(6). https://doi.org/10.1371/JOURNAL.PCBI.1005595,

Win, J., Chaparro-Garcia, A., Belhaj, K., Saunders, D. G. O., Yoshida, K., Dong, S., Schornack, S., Zipfel, C., Robatzek, S., Hogenhout, S. A., & Kamoun, S. (2012). Effector biology of plant-associated organisms: Concepts and perspectives. *Cold Spring Harbor Symposia on Quantitative Biology*, *77*, 235–247. https://doi.org/10.1101/SQB.2012.77.015933,

Wirthmueller, L., Asai, S., Rallapalli, G., Sklenar, J., Fabro, G., Kim, D. S., Lintermann, R., Jaspers, P., Wrzaczek, M., Kangasjärvi, J., MacLean, D., Menke, F. L. H., Banfield, M. J., & Jones, J. D. G. (2018). Arabidopsis downy mildew effector HaRxL106 suppresses plant immunity by binding to

RADICAL-INDUCED CELL DEATH1. *New Phytologist*, *220*(1), 232–248. https://doi.org/10.1111/NPH.15277,
Witek, K., Jupe, F., Witek, A. I., Baker, D., Clark, M. D., & Jones, J. D. G. (2016). Accelerated cloning of a potato late blight–resistance gene using RenSeq and SMRT sequencing. *Nature Biotechnology 2016 34:6*, *34*(6), 656–660. https://doi.org/10.1038/nbt.3540
Wlodzimierz, P., Rabanal, F. A., Burns, R., Naish, M., Primetis, E., Scott, A., Mandáková, T., Gorringe, N., Tock, A. J., Holland, D., Fritschi, K., Habring, A., Lanz, C., Patel, C., Schlegel, T., Collenberg, M., Mielke, M., Nordborg, M., Roux, F., … Henderson, I. R. (2023). Cycles of satellite and transposon evolution in Arabidopsis centromeres. *Nature 2023 618:7965*, *618*(7965), 557–565. https://doi.org/10.1038/s41586-023-06062-z
Woodward, A. W., & Bartel, B. (2018). Biology in Bloom: A Primer on the Arabidopsis thaliana Model System. *Genetics*, *208*(4), 1337. https://doi.org/10.1534/GENETICS.118.300755
Xiao, Y., Wu, X., Wang, Z., Ji, K., Zhao, Y., Zhang, Y., & Wan, L. (2025). Activation and inhibition mechanisms of a plant helper NLR. *Nature 2025 639:8054*, *639*(8054), 438–446. https://doi.org/10.1038/s41586-024-08517-3
Yang, L., Teixeira, P. J. P. L., Biswas, S., Finkel, O. M., He, Y., Salas-Gonzalez, I., English, M. E., Epple, P., Mieczkowski, P., & Dangl, J. L. (2017). Pseudomonas syringae Type III Effector HopBB1 Promotes Host Transcriptional Repressor Degradation to Regulate Phytohormone Responses and Virulence. *Cell Host and Microbe*, *21*(2), 156–168. https://doi.org/10.1016/j.chom.2017.01.003
Yang, Y., Furzer, O. J., Fensterle, E. P., Lin, S., Zheng, Z., Kim, N. H., Wan, L., & Dangl, J. L. (2024). Paired plant immune CHS3-CSA1 receptor alleles form distinct hetero-oligomeric complexes. *Science*, *383*(6684), 719–730. https://doi.org/10.1126/SCIENCE.ADK3468/SUPPL_FILE/SCIENCE.ADK3468_MDAR_REPRODUCIBILITY_CHECKLIST.PDF
Yu, X. Q., Niu, H. Q., Liu, C., Wang, H. L., Yin, W., & Xia, X. (2024). PTI-ETI synergistic signal mechanisms in plant immunity. *Plant Biotechnology Journal*, *22*(8), 2113. https://doi.org/10.1111/PBI.14332
Yuan, B., Zhai, C., Wang, W., Zeng, X., Xu, X., Hu, H., Lin, F., Wang, L., & Pan, Q. (2011). The Pik-p resistance to Magnaporthe oryzae in rice is mediated by a pair of closely linked CC-NBS-LRR genes. *Theoretical and Applied Genetics*, *122*(5), 1017–1028. https://doi.org/10.1007/S00122-010-1506-3,
Zhai, C., Zhang, Y., Yao, N., Lin, F., Liu, Z., Dong, Z., Wang, L., & Pan, Q. (n.d.). *Function and Interaction of the Coupled Genes Responsible for Pik-h Encoded Rice Blast Resistance*. https://doi.org/10.1371/journal.pone.0098067

3.1 MANUSCRIPT

The Expanding Landscape of RPP1: Domain-Level Diversity, Functional Insights, and RPP1 truncations

AUTHOR CONTRIBUTIONS

Miriam Lucke: Designed the study, performed all experiments, some with the help of work study students, performed all data analyses, wrote the first draft of the manuscript.

Zhigui Bao: Performed quality control on *A. thaliana* genomes, provided context and code for analyses, discussed and provided ideas.

Luisa Teasdale: Provided annotation data for analysis, discussed and provided ideas.

Mohamed El-Walid: Discussed and provided ideas, helped to set up code for analyses.

Detlef Weigel: Designed and supervised the study, discussed results and interpretations, major editing of the manuscript.

Haim Ashkenazy: Helped with study design, suggested experiments, provided code and pipelines, discussed results and interpretations.

Rebecca Schwab: Designed the study, suggested experiments, discussed results and interpretations, contributed to the first draft of the manuscript.

STATUS IN PUBLICATION PROCESS
Close to submission to bioRxiv.

3.2 Abstract

Plant genes encoding NLR (nucleotide-binding leucine-rich repeat) proteins have exceptional sequence, copy number and allelic diversity. Previous efforts have identified the *RPP1 (RECOGNITION OF PERONOSPORA PARASITICA 1*) locus from *Arabidopsis thaliana* as one of the most extreme, but it has been unclear how much of its full diversity has already been uncovered. Full-length RPP1 proteins have an N-terminal Toll/interleukin-1 receptor (TIR) domain, a nucleotide-binding adaptor shared by APAF-1, R proteins, and CED-4 (NB-ARC) domain, leucine rich repeats (LRRs), and a C-terminal jelly roll/Ig-like domain (C-JID), which in some well-characterized RPP1 variants binds the ARABIDOPSIDIS THALIANA RECOGNIZED 1 (ATR1) effector from the oocyte *Hyaloperonospora arabidopsidis*. The *RPP1* locus is also notable for having spawned several alleles that cause hybrid incompatibility due inappropriate activation of the immune system when combined with specific alleles at other *A. thaliana* loci. Making use of over two hundred long-read based genome assemblies, we systematically annotated hundreds of new *RPP1* variants. Most accessions carry two to five genes encoding full-length RPP1 proteins, often with additional copies encoding proteins that lack at least one of the functional domains. The loci are arranged in genomic regions that can cover dozens to hundreds of kilobases. Structural modeling suggests that most full-length RPP1 proteins have the ability to form oligomeric resistosomes. *In planta* functional assays indicated that some of the representative variants forming large clusters indeed can recognize ATR1 variants. Altogether, our work offers new resources and hypotheses for dissecting NLR evolution, regulation, and deployment across natural populations.

3.3 Introduction

RECOGNITION OF PERNOSOPORA PARASITICA 1 (*RPP1*), initially identified in the *Arabidopsis thaliana* Nd-1 accession as the locus conferring resistance to the isolates Emoy2 and Hiks1 of the oomycete pathogen *Hyaloperonospora arabidopsidis* (Holub et al., 1995; Holub & Beynon, 1997; Tor et al., 1994), is a prime example of allele-specific function of disease resistance genes. Extensive investigations by numerous laboratories have revealed a large degree of functional diversity of the encoded protein in different *A. thaliana* accessions - as well as a similar degree of functional diversity in its counterpart, the protein it recognizes to initiate resistance, the effector protein ARABIDOPSIDIS THALIANA RECOGNIZED 1 (ATR1) of *H. arabidopsidis* (Reignault et al. 1996; Botella et al., 1998; Chou et al., 2011; Mishra et al., 2015; Prigozhin & Krasileva, 2021; Rehmany et al., 2005). Incompatible interactions, where an *A. thaliana* RPP1 protein variant recognizes the ATR1 effector variant delivered by the infecting *H. arabidopsidis* pathogen, leads to effective disease resistance, accompanied by a hypersensitive response as a striking visible symptom. The interaction can be recapitulated in transient expression experiments in tobacco, where hypersensitive responses are easily detectable upon co-expression of the two protein partners (Krasileva et al. 2010).

Several strands of research have subsequently led to a thorough understanding of the molecular function of the RPP1 protein as well as the high degree of diversity of the encoding genetic locus. Culminating with the resolution of the $RPP1^{WsB}$ structure through cryo-EM studies (Ma et al., 2020), and including numerous earlier reports dissecting the role of RPP1 subdomains (Steinbrenner et al., 2012, 2015; Krasileva et al., 2010, 2011; Goritschnig et al., 2016), structure-function studies suggest the following model of RPP1 function: Upon effector recognition of ATR1 at the leucine-rich-repeat (LRR) domain, conformational activation leads to RPP1 tetramerization through the nucleotide-binding (NB)/ helix-domain1 /winged-helix-domain (NOD) module. This holoenzyme forms active sites at asymmetric Toll-interleukin-1 receptors (TIR) homodimers, for NAD+ hydrolysis (Ma et al., 2020).

The high degree of allelic diversity including copy number variation at the *RPP1* locus was recognized early on (Botella et al., 1998, Gordon, 2002, Goritschnig et al., 2016). This was not only observed in the *RPP1* locus but also in many other NLR loci that these are driven by gene rearrangements, duplications, and transposon

insertions, which posed challenges for the identification of allelic diversity (McDowell et al., 1998; Baumgarten et al., 2003; Meyers et al., 2003; Leister 2004). However, the *RPP1* locus is one of the few loci with the highest copy number and described as hypervariable (Lee & Chae 2020; Prigozhin & Krasileva 2021). This work was subsequently extended from the accessions in which *RPP1*-mediated disease resistance had been first defined by genetic crosses through extensive structure-function studies in transient expression systems (Goritschnig et al., 2012).

In parallel, *RPP1* emerged as a central factor in intraspecific hybrid incompatibility due to genetic mismatches within the immune system and between the immune system and non-immune proteins (Bomblies et al. 2007; Alcázar et al. 2010; Chae et al. 2014; Alcázar et al. 2014; Alcázar et al. 2009; Tran et al. 2017; Wan et al. 2025; Ordon et al. 2021; Stuttmann et al. 2016). The *RPP1* locus includes *DANGEROUS MIX 2* (*DM2*) genes, NLRs known for their role in hybrid incompatibility (Bomblies et al., 2007; Chae et al., 2014; Lei & Weigel, 2021). The DM2/RPP1 resistosome can be activated by multiple mechanisms, besides the recognition of the *H. arabidopsidis* effector ATR1 (Rehmany et al., 2005; Krasileva et al., 2010): interaction with the DM1 NLR (Bomblies 2007; Tran 2017); with DM3, a prolyl aminopeptidase that regulates proline homeostasis (Chae 2014; Ghifari et al., 2020; Wan et al., 2025) and other regulatory proteins such as SRF3 a receptor kinase (Alcázar et al., 2010; 2014), OASTL-A1 an acetylserine(thiol) lyase (Tahir et al., 2013), and EDS1 fusion proteins (Stuttmann 2016).

The complete sequence of an entire *RPP1* locus became only available with the release of the *A. thaliana* Col-0 reference genome, which revealed presence of a bipartite superlocus, with two gene pairs separated by about 150 kb (The Arabidopsis Genome Initiative 2000). The *RPP1* was painstakingly reconstructed in a few additional accessions using BAC and fosmid clones and Sanger sequencing, which showed that other accessions often had many more *RPP1* genes, with a complex evolutionary history (Alcázar et al. 2009; Chae et al. 2014). The complexity of the locus precluded its complete analysis using short reads, even though short read coverage was already helpful for demonstrating that specific *RPP1* copies were typically rare in the global *A. thaliana* population (Chae et al. 2014). Enrichment of *NLR* sequences coupled with long-read sequencing (Ren-seq) indicated that most accessions had six to ten copies, but at least one accession had 17 copies (Lee & Chae, 2020; Van De

Weyer et al., 2019). Ren-seq also identified the IP-Moa-0 accession as potentially lacking the entire *RPP1* locus (Lee and Chae 2020).

With long-read sequencing having become more affordable, more and more *A. thaliana* genome assemblies are available now and can be used to study complex loci (Michael et al. 2018; Jiao and Schneeberger 2020; Wlodzimierz et al. 2023; Kang et al. 2023; Lian et al. 2024; Teasdale et al. 2024; Alonso-Blanco et al. 2024). We seized this opportunity to study diversity at the *A. thaliana RPP1* locus. We describe over 900 distinct RPP1 protein variants that carry the functionally relevant TIR, NB-ARC and LRR domains. Structural modeling and experimental tests suggest that a majority of these proteins can potentially function to activate immune responses, with most accessions encode at least one potentially functional variant.

3.4 Results

Using genomic resources from 262 *Arabidopsis thaliana* accessions, we investigated the diversity of the *RPP1* locus, aiming to better understand the radiations that contribute to its extensive sequence variation (Prigozhin & Krasileva, 2021; Lee & Chae, 2020). By identifying representative variants, we sought to associate distinct functional roles, particularly among those that recognize the effector ATR1. Beyond effector recognition, we explored how sequence diversity correlates with copy number variation and the presence of altered or truncated RPP1 forms. Ultimately, we also asked whether, despite this high diversity, shared structural or functional features could be identified across accessions.

3.4.1 A high level of within-species diversity at the *RPP1* locus

To assess species-wide diversity at the *RPP1* locus, we made use of the extensive whole-genome information available for *A. thaliana* through the 1001 Genomes Plus resource (Alonso-Blanco et al. 2024). We selected 262 *A. thaliana* accessions with high-quality assemblies (Supplementary Table 1 Sheet 1; Alonso-Blanco et al. 2024). Starting with the four RPP1 protein sequences from Araport11 and a total of 93 sequences from 17 accessions with high-quality NLR annotation (Teasdale et al., 2024), I searched for homologous sequences with Miniprot (Li, 2023), which identified 1,317 *RPP1* homologs encoding proteins that were at least 1,000 amino acids long and contained the TIR, NB-ARC and LRR domains. All 1,311 sequences were subjected to a Blast search against the TAIR10 gene set from Araport11. Only one RPP1 homolog, from the Tibet-0 accession, did not match the four RPP1 proteins from Araport11 (Supplementary Figure 3.1). An additional 395 sequences carried likely truncations or deletions, resulting in an overall data set of 1,712 RPP1 proteins. We first focus on the full-length copies.

We discovered that the majority of accessions carry two to five (155/262) copies per genome, less than described by Lee and Chae (Lee & Chae, 2020) (Figure 3.1A, B). We confirmed the absence of *RPP1* genes in IP-Moa-0 (Lee and Chae 2020). The size of the superlocus was up to 800 kb (median 90.2 kb), and the maximum *RPP1* (full-length) gene copy number was 14 (Figure 3.1 A,B & Supplementary Table 3.1 Sheet 2). 4. This is fewer than described by (Lee and Chae 2020), which may be due

to differences in annotation approach or errors due to the use of Ren-seq data, which allow only assembly of individual genes and not entire loci.

We also found conserved non-NLR genes within the *RPP1* locus. Generally, we observed that the locus can be divided into different gene regions, based on the large gene content within that locus. For instance, in Col-0 we detected that between *RPP1* there can be up to 10 genes between the different copies. Therefore, we used conserved genes flanking *RPP1* to define three distinct genomic regions within that locus (Figure 3.1 B): the left region A had only up to one *RPP1* copy, and the middle region B contained up to two copies. The majority of *RPP1* genes were located in the 3' region C, which corresponds to the region identified as the *RPP1* locus proper in previous publications (Reignault et al. 1996; Botella et al. 1998; Alcázar et al. 2009; Chae et al. 2014) (Figure 3.1 C and Supplementary Figure 3.2). The uneven distribution of *RPP1* homologs is very apparent in IP-Rel-13, which has 14 *RPP1* copies, all in region C (Figure 3.1B, D).

Eight accessions (BELC-C10, BELC-C12, Db-1, Kew-1, IP-Cer-6, Bon-1, ET-86-4, IP-Rel-13) carried identical duplicated *RPP1* copies and one accession (IP-Rel-13) identical triplicated *RPP1* copies (without any SNPs or indels in either the exons or introns) with sequence identity sometimes extending to intergenic regions (Figure 3.1D). Of these apparently very recent duplications 15 were in region C and two in region B (Supplementary Figure 3.3). Suggesting region C may be a hotspot for recent *RPP1* duplications.

Our dataset contained 119 accessions that were originally collected in very close proximity to at least one other accession (same collection site; 56 sites with two to five accessions each), affording us a potential opportunity to examine very short-term evolutionary trends at the *RPP1* locus. We found that the entire *RPP1* locus (including introns and intergenic sequences) was identical or close to identical in 19 same-site pairs; an additional two pairs had the same gene repertoire with differences in the locus structure. In 37 accession groups, the *RPP1* locus differed in both structure and *RPP1* homolog content. Highlighting the coexistence of local conservation and diversification at the *RPP1* locus.

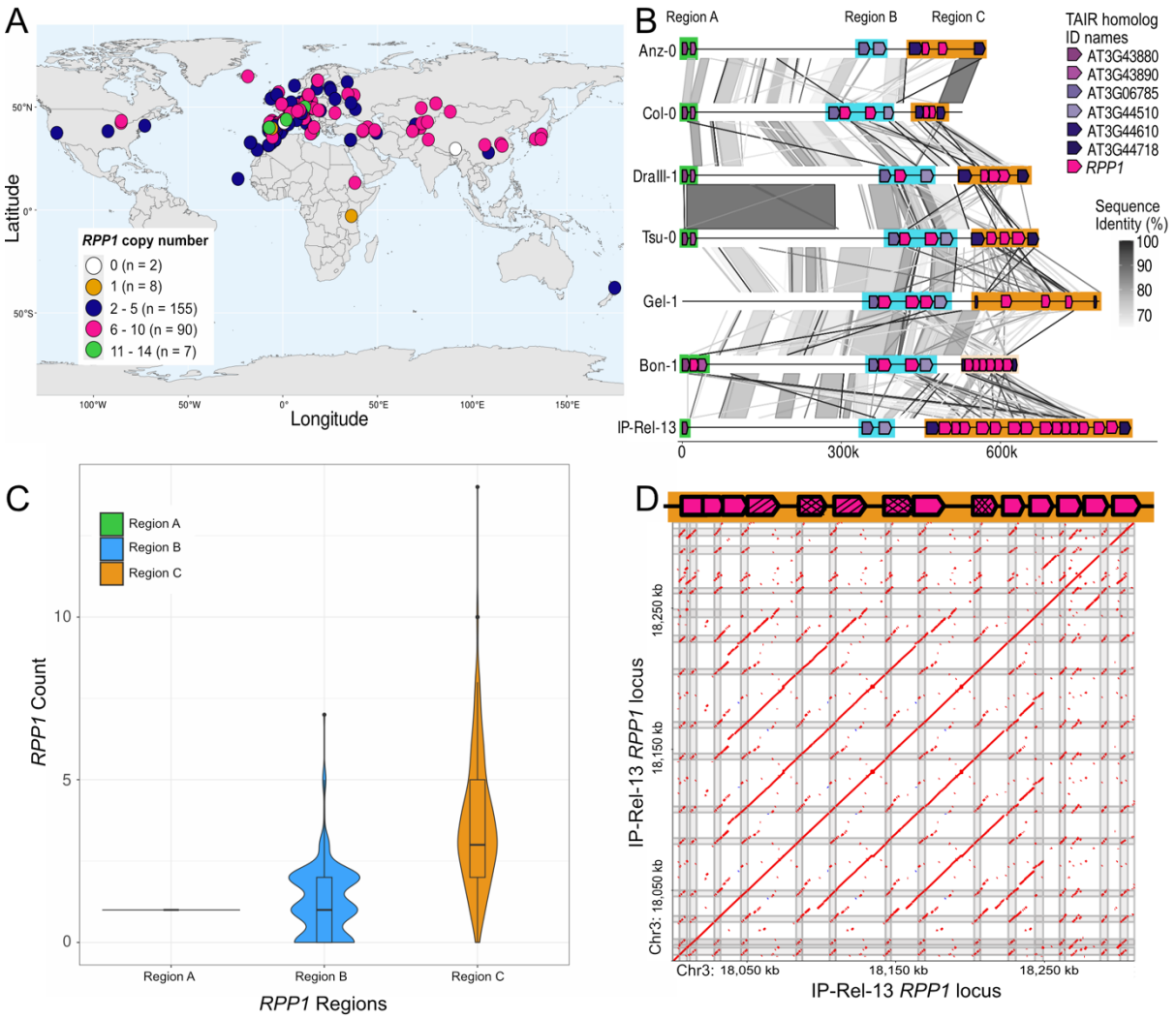

Figure 3.1: *RPP1* locus diversity and structure. A) Collection sites of 262 *A. thaliana* accessions and their *RPP1* copy numbers. n indicates the number of accessions in the respective category. B) Within the *RPP1* locus, we identified *RPP1* genes along with their neighboring anchor genes arranged in consecutive genomic order, using TAIR homolog ID names for consistent annotation across accessions. The locus can be subdivided into highlighted regions A, B and C based on conserved flanking non-*RPP1* genes. Syntenic regions with sequence identity above 70 % are in increasingly darker shades of grey. These seven accessions were chosen as representatives to highlight the complexity of this locus. C) Distribution of *RPP1* copy numbers per accession, separated by regions A, B and C. D) Self-alignment of IP-Rel-13 region C indicates both longer and shorter duplications (lines off the center diagonal). Identical sequences are indicated in red; corresponding duplicated and triplicated identical *RPP1* copies are highlighted as striped and checkered boxes above.

3.4.2 Widespread sequence identity among RPP1 variants and subdomains

Turning to the level of individual genes and the proteins they encode, we first generated a maximum likelihood phylogenetic tree from all predicted 1,317 full-length proteins, including the well-studied WsB allele (Botella et al., 1998; Ma et al., 2020; Rehmany et al., 2005; Schreiber et al., 2016) as well as two RPP1 homologs from *Arabidopsis lyrata* as outgroups (Figure 3.2A, Kolesnikova et al., 2023). The phylogenetic intermixing of RPP1 variants from regions B and C, including those from the same *A. thaliana* accession, indicates that diversification within the *RPP1* locus is not confined to distinct genomic subregions. (Figure 3.2 A). Genes encoded by genes in region A, when present, formed a distinct branch on the phylogenetic tree, indicating a very early split (Figure 3.2 B).

Systematic analyses identified in the entire dataset 582 protein sequences with one or more identical partners. They correspond to 208 distinct sequences that were found in up to 14 copies. Nine were from within-accession duplications and triplications, as described above, and four originated from identical protein repertoires in accessions from the same collection site, as also described above.

One hundred and ninety-five protein variants were shared by at least two accessions originating from different places, with an average distance of 154 kilometers between them. Looking at those more closely revealed a large group of 12 accessions, including RRS10, KBS-Mac-74, 14INRCT07, 15INRCT09, LI-EF-011, LI-EF-018, and Pent-46, all members of the N. American HPG1 lineage; (Exposito-Alonso et al., 2018; Shirsekar et al., 2021), SALE-A-10, SALE-A-12, MONT-B-12, and NAUV-B-7 from Southwest France), and Sq-1 from England, that shared identical nucleotide sequences along most of the 116 kb big *RPP1* locus (Figure 3.3C, Supplementary Figure 3.6). While this was not too surprising for HPG1 accessions given their extensive genome-wide similarity (Exposito-Alonso et al., 2018), it was unexpected for the European accessions. The predominant HPG1 lineage appears to have stronger ancestry from Upper and Eastern France than from Northwestern Europe or the British Isles, despite the latter being a major source of multiple introductions (Exposito-Alonso; Becker, et al., 2018; Shirsekar et al., 2021). The 12 accessions are genetically closely related, as expected from their geographic proximity (Supplementary Figure 3.5; Exposito-Alonso et al., 2018; Shirsekar et al., 2021), but in a genome-wide Principal Component Analysis they are interspersed with other

accessions that do not share a closely related *RPP1* cluster. Tul-0 and Yo-0 from N. America and previously reported to be very similar to another N. American accession, RRS10 accession from HPG1, (Lian et al., 2024), shared large fractions, but not the entirety of RPP1 homologs with the other 12 accessions (Figure. 3.3 B). Another identical RPP1 variant was found in FERR-A-8 and BARA-C-5 from France, Edi-0 from Scotland, and also N13 (Russia). While the first three are close to each other throughout the genome, N13 is not (Supplementary Figure 3.5).

Seven hundred and thirty-five RPP1 sequences were found only once in the entire dataset. We found that many of these proteins, which are unique when their entire sequence is considered, nevertheless share 100% identity in one or more NLR domains with other RPP1 homologs: of 838 TIR domains that had one or more identical partners, 256 were from this 'unique' set. Similarly, 501 LRR and 729 NB-ARC domains, of which are 154 LRR and 388 NB-ARC domains found in the 'unique' RPP1 set had identical partners (Supplementary Table 3.1 Sheet 3).

We used this extensive domain sequence identity to define common and less common RPP1 variants: we ranked all domain variants by their observed frequency (lowest rank being most common) and subsequently assigned these rank scores to each RPP1 protein in our dataset (Supplementary Table 3.1 Sheet 3). The most common TIR, the most common NB-ARC, the most common LRRs and the most common C-JID were not found in combination. Eight hundred and ninety-eight RPP1 proteins contained one or more domains that ranked in the bottom 5% of frequency scores (Figure 3.2C, Supplementary Table 3.1 Sheet 3). The well-studied $RPP1^{WsB}$ variant is not composed of particularly frequent RPP1 domains; its domains ranked 18 (out of 226 TIR domains), 14 (of 244 NB-ARCs), 32 (of 238 LRRs), and 45 (of 238 C-JIDs).

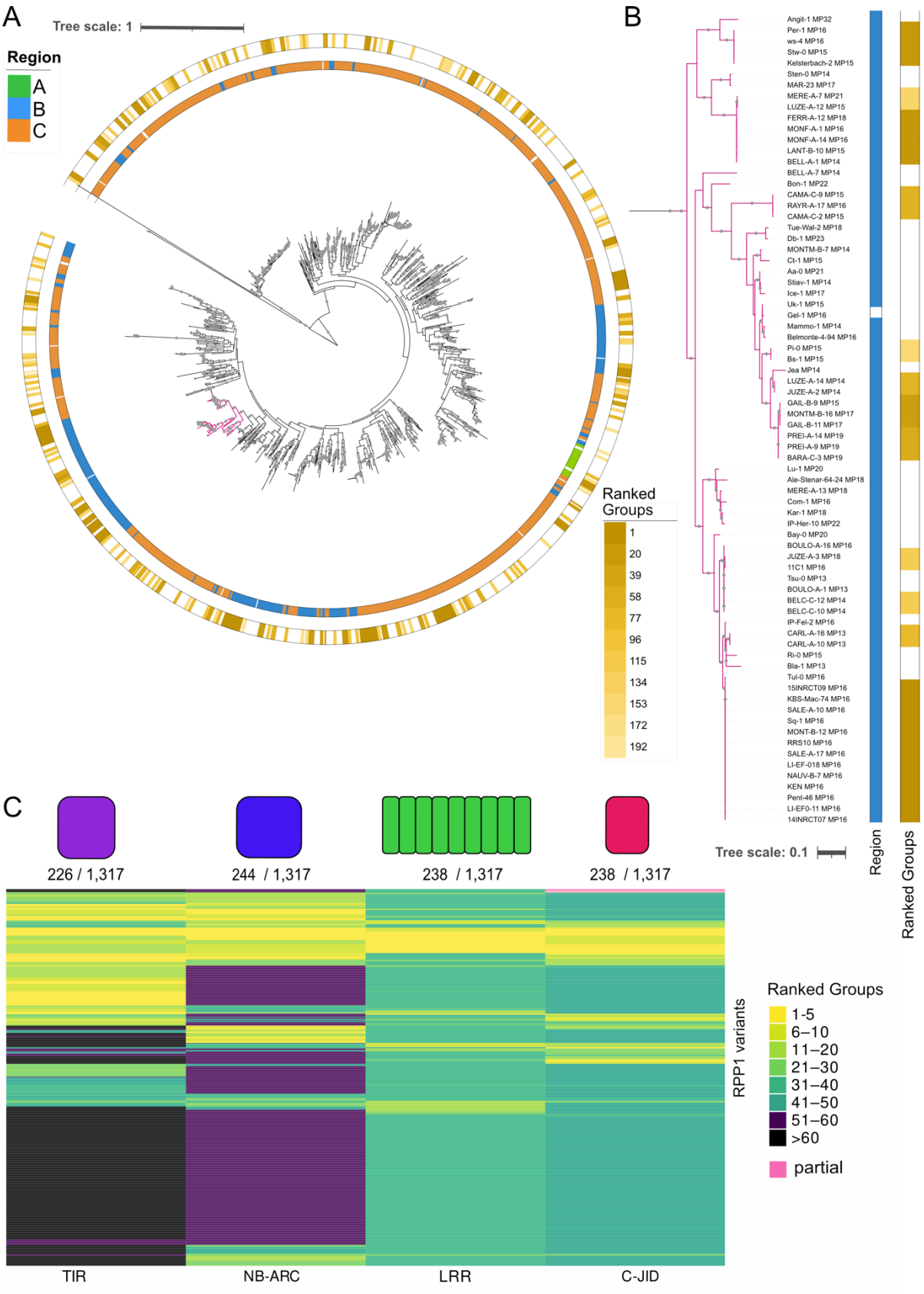

Figure 3.2: Extensive sequence identity among RPP1 proteins and subdomains. A) Maximum-likelihood tree of 1,317 full-length RPP1 proteins based on their complete protein sequences (LG substitution model and gamma distribution plus constant site rates; 1,000

bootstraps). *Arabidopsis lyrata* sequences were used as outgroups. Locations of encoding genes in the three defined *RPP1* supercluster subregions A, B and C are indicated in green, blue and orange (inner circle). Prevalence of protein variants (rank of group size of identical RPP1 homologs) is shown in the outer circle. B) Magnification of tree section highlighted in pink and indicated with an arrow A). C) Diagram of RPP1 and the number of unique variants for each domain among all full-length proteins. Each row represents one of the 1,175 proteins with at least one domain that is identical in at least one other protein. Sixteen C-JIDs were lacking the C terminus. Proteins were clustered hierarchically.

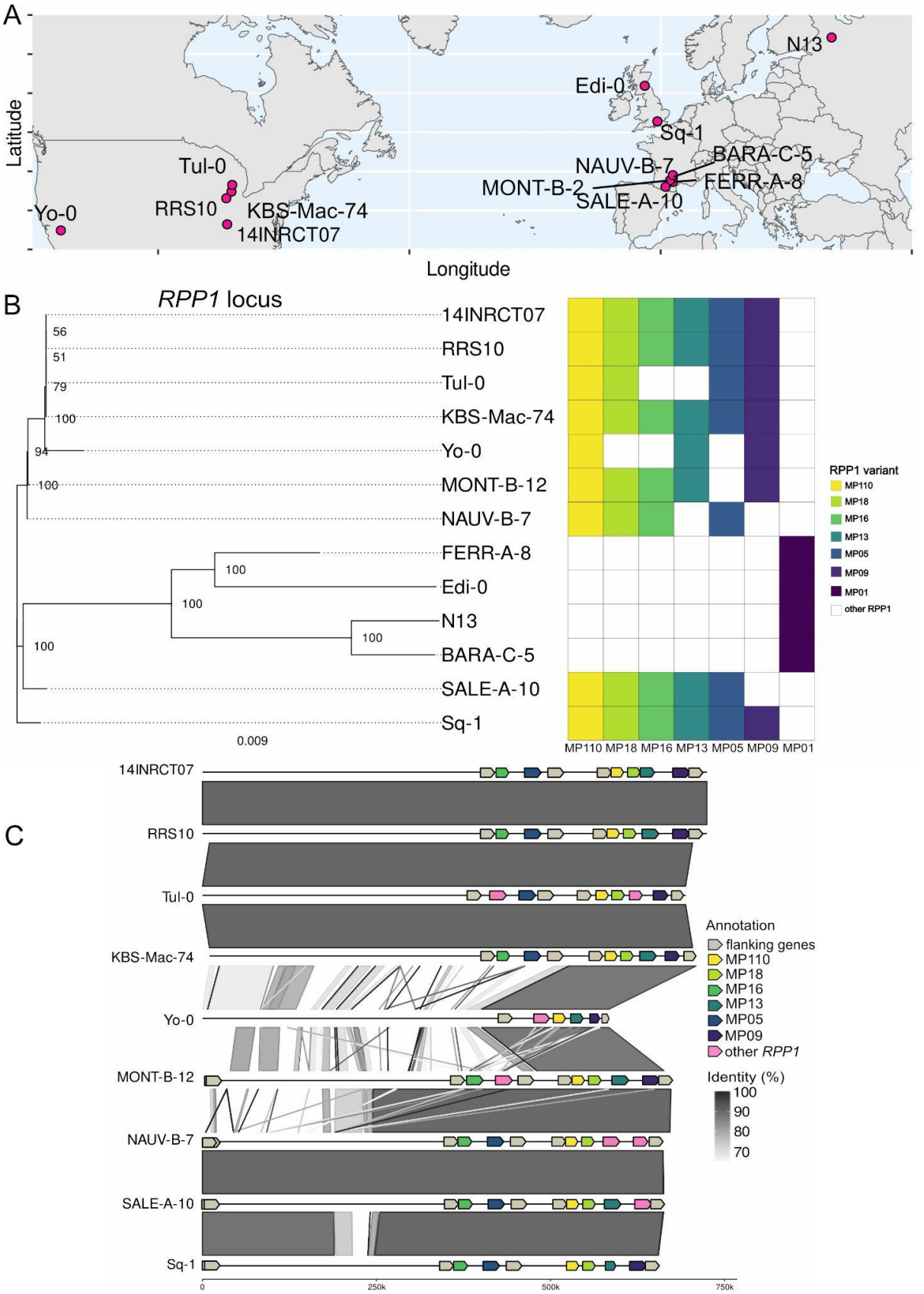

Figure 3.3: Identical RPP1 variants from accessions with different geographical origins. A) Geographical origin of accessions that share the most common RPP1 variant. B) Graphical representation of unique protein sequences that were found in several of these accessions

(right) and maximum-likelihood tree built from DNA sequences of the corresponding entire *RPP1* locus (lengths 49 to 164 kb). C) Extent of collinearity of a subset of *RPP1* loci shown in B.

3.4.3 Many RPP1 variants resemble known alleles in structure and function

In an effort to judge functionality of RPP1 proteins, we first compared their sequences to those of known functional RPP1 variants, RPP1^{NdA}, RPP1^{EstA}, RPP1^{ZdrA}, RPP1^{ZdrE}, RPP1^{WsB} and RPP1^{WsC}, which are all closely related in sequence up to ~80 % sequence identity (Goritschnig et al., 2016; Ma et al., 2020), as well as RPP1^{WsA} (Goritschnig et al., 2016), which is diverged in sequence and only shares 48 % sequence identity, particularly in the NB-ARC, LRR and C-JID domains, from the first five.

We began by examining key residues previously identified as being essential for RPP1 function or located at key positions in well-described interfaces in the RPP1 resistosome (Bernoux et al., 2011; Ma et al., 2020; Schreiber et al., 2016; Williams et al., 2014). This included in the TIR domain the catalytical site for NAD^+ hydrolysis, the BB-loop involved in protein multimerization, the AE interface for self-association and the αA and αE helices with roles in domain folding (positions S102, H103, K111, G112, I121, A122, E158, S244, L247, N248 in the reference accession WsB), and in the NB-ARC domain the P-loop (N316, D327, E372, TTE motif) relevant for ADP nucleotide binding.

Compared to the sequence of RPP1^{WsB}, most substitutions or deletions, a total of 415 in 1,317 proteins, were in residues in the P-loop. We did not identify any of the specific amino acid substitutions previously shown to impair ATR1 recognition by full-length RPP1^{WsB} (Ma et al., 2020). Many proteins, 263, had both the N316D and D327N substitutions, which, when found together, may preserve the integrity of the nucleotide-binding pocket for ADP binding (Ma et al., 2020; Zhou et al. 2015). An 182-amino-acid deletion in the P-loop region in RPP1-MP59$^{CAMA-C-2}$, RPP1-MP59$^{CAMA-C-9}$, RPP1-MP104$^{IP-Rel-13}$ and RPP1-MP63$^{RAYR-A-9}$ likely leads to complete loss of the nucleotide binding interface.

In the TIR domain, critical residues I121, S102, and H103 (Williams et al., 2014) were missing in RPP1-MP59$^{IP-San-6}$ and RPP1-MP59$^{IP-San-9}$, potentially disrupting TIR homodimerization.

Altogether, 536 RPP1 proteins carried one or more substitution or insertions/deletions in residues previously described as functionally relevant for tetramerization (Bernoux et al., 2011; Ma et al., 2020; Schreiber et al., 2016; Williams

et al., 2014) The results are summarized in Table 3.1; a comprehensive overview is provided in Supplementary Table 3.1 Sheet 4 (Supplementary Table 3.1 Sheet 4).

Table 3.1: **Substitutions and insertions/deletions reported in RPP1^{WsB} at residues with known activity in different RPP1 proteins**. "-" indicates missing amino acids (gaps). Frequency of observations is indicated by (n). References for functional tests of the relevant residues are provided on the far right.

Position	Described substitution (RPP1^{XXXX})	Observed substitution	Functional region	References
I121	I121E (RPP1^{I121E})	I121M: n = 80 I121R: n = 1 I121-: n = 1	BB-loop	Ma et al.,2020
A222	A222E (RPP1^{A222E})	A222T: n = 32 A222-: n = 2	BB-loop	Ma et al.,2020
E158	E158A/Q (RPP1$^{E158A/Q}$)	E158-: n = 3	BB-loop	Ma et al.,2020
S102	S102D (RPP1^{S102D})	S102E: n = 1 S102-: n = 2	AE interface	Williams et al., 2014
H103	H103A (RPP1^{H103A})	H103D: n = 1 H103-: n = 2	AE interface	Williams et al., 2014
N316	N316 (RPP1^{N316})	-: n = 5 N316D: n = 358	P-loop	Ma et al.,2020
D327	D327 (RPP1^{D327})	-:n = 4 D327K: n = 2 D327N: n = 265	P-loop	Ma et al.,2020
E372	E372 (RPP1^{E372})	-: n = 6 E372D: n= 21	P-loop	Ma et al.,2020
TTE/Q	T398, T340, E341 (RPP1^{T398}; RPP1^{T340}; RPP1^{E341})	- - - : n = 12 I - -:n = 3 PTE: n = 2 TE -: n = 2	P-loop	Ma et al.,2020
αE helix	K111; G112 (RPP1^{K111}; RPP1^{G112})	- - : n = 11	TIR	Ma et al.,2020

αA helix	S244; S247I; N248 (RPP1^{S244}; RPP^{S247}; RPP1^{N248})	- - -: n = 1	TIR	Ma et al.,2020

In order to assess the overall protein architecture of RPP1 variants, we modeled their structure based on AlphaFold3 (Abramson et al., 2024). For this, we first reduced the complexity of our protein dataset and formed 64 similarity clusters using DIAMOND DeepClust (Buchfink et al., 2023) with a protein similarity and query of 80%. The largest cluster had 348 members, and thirty clusters had at least five members. All clusters with RPP1 members of known activity in *H. arabidopsidis* resistance have multiple members, with RPP1^{WsA} and RPP1^{WsC} defining the second largest cluster with 148 members. The RPP1^{NdA} cluster has 23, the RPP1^{WsB} cluster 25, and the RPP1^{ZdrE} cluster 19, and the cluster defined by RPP1^{EstA} and RPP1^{ZdrA} has a total of 11 members (Figure 3.4A. Supplementary Table 3.1 Sheet 5).

RPP1^{WsB} forms a tetramer when activated upon binding to its cognate effector ATR1^{Emoy2}, with the entire complex known as a resistosome (Ma et al., 2020). We therefore used AlphaFold3 (Abramson et al., 2024) to model tetramer structures of our cluster representatives, including RPP1^{WsB} itself. To assess the structural plausibility of tetramer formation in the absence of ATR1, we specified a 4:0 stoichiometry in the input, effectively simulating ligand-independent oligomerization. This enabled us to compare predicted inter-subunit interfaces across variants. We first inspected the retrieved structure models visually, together with the accompanying confidence scores (Supplementary Figure 3.7). Based on visual inspection several structures deviated markedly from the RPP1^{WsB} structure, e.g., exhibited a substantially altered overall domain arrangement (e.g. RPP1-MP104$^{IP\text{-}Rel\text{-}13}$) or low pLDDT (predicted local distance difference test) scores across the LRR domain (e.g. RPP1-MP83$^{BROU\text{-}A\text{-}2}$). To systematically compare structural similarities without introducing reference bias, we applied an all-against-all structural alignment approach (Zhang et al., 2022). The resulting Template Modeling (TM) scores quantify the extent of shared structural features between protein pairs. A TM-score of 1 indicates identical structures, while scores between 0.5 and 0.45 suggest that the proteins share a common global fold or topology (Zhang et al., 2022). For each protein structure we calculated the average TM-score across all models. The resulting average template modeling (TM) scores

were high in most of our structure models (Figure 3.4 A), which gave us confidence that they may indeed be functional and able to form protein tetramers. Average TM scores were, however, below 0.5 for RPP1-MP104$^{IP\text{-}Rel\text{-}13}$, RPP1-MP63$^{RAYR\text{-}A\text{-}9}$, RPP1-MP19$^{IP\text{-}Ini\text{-}0}$, RPP1-MP108$^{IP\text{-}Bus\text{-}0}$, RPP1-MP23^{Zin9}, and RPP1-MP25$^{IP\text{-}Piq\text{-}0}$. For two of these, RPP1-MP63$^{RAYR\text{-}A\text{-}9}$ and RPP1-MP104$^{IP\text{-}Rel\text{-}13}$, this was already obvious by visual inspection, as large parts of the P-loop are missing. The best scores were 0.73 for RPP1-MP182$^{Jm\text{-}0}$ and RPP1-MP68$^{MERE\text{-}A\text{-}7}$. In addition to the TM-score, we also considered the size of each sequence cluster, which may correlate with structural conservation.

As a direct test of protein functionality, we expressed several RPP1 proteins *in planta* in combination with different ATR1 variants. We first inspected a phylogenetic tree built from full-length protein sequences (Figure 3.4 A) to select representatives of divergent branches and with varying TM scores. As several similarity clusters had representatives encoded by the Gel-1 accession, we started with those, and expressed them transiently in tobacco leaves, with or without ATR1 effector variants, including the well-known Emoy2 variant recognized by RPP1^{WsB} and the well-known Cala2 variant not recognized by RPP1^{WsB}, looking for macroscopic cell death (Krasileva et al., 2010). RPP1-MP22$^{Gel\text{-}1}$, which has a low average TM score of 0.49 (similarity cluster contains 107 members), never induced visible cell death, neither when expressed alone nor when co-expressed with ATR1 effectors (Figure 3.4 B and Supplementary Figure 3.8). Neither did RPP1-MP106$^{Gel\text{-}1}$, with a high TM score of 0.68 (cluster contains only 2 members). RPP1-MP21$^{Gel\text{-}1}$, with a high TM score of 0.71 (cluster contains 148 members), was autoactive, and both RPP1-MP16$^{Gel\text{-}1}$ with a high TM score of 0.67 (cluster contains 88 members) and RPP1-MP17$^{Gel\text{-}1}$, with an TM score of 0.52 (largest cluster, containing 348 members), induced cell death when co-expressed with several ATR1 effector variants (Figure 3.4 B).

With at least three potentially active RPP1 variants in the Gel-1 accession, of which at least one recognized the ATR1^{Emoy2} effector, we expected that the Gel-1 accession would respond with leaf wilting or necrosis when delivering g ATR1^{Emoy2} with *Pseudomonas fluorescent* (Pf0-1; Thomas et al., 2009). This was, however, not the case (Figure 3.4 C). Similarly, the *H. arabidopsidis* isolate Emoy2 sporulated well when inoculated on Gel-1 seedlings, indicating that ATR1^{Emoy2} was apparently not recognized in Gel-1 (Supplementary Table 3.2).

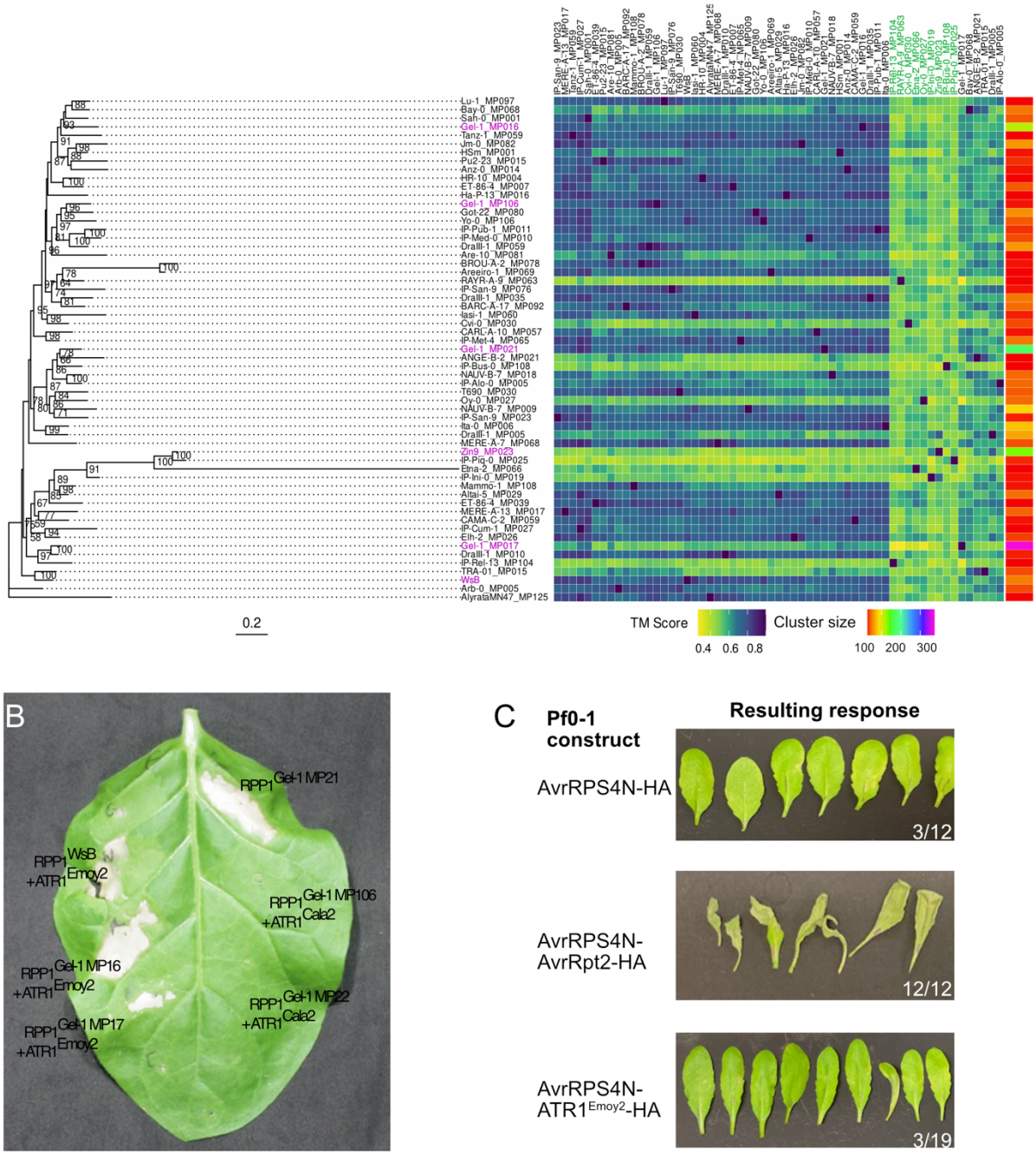

Figure 3.4: ***In planta* activity tests of selected RPP1 representatives.** A) Maximum likelihood tree (only bootstrap values above 40 are shown) of full-length protein sequences of cluster representatives (left) and their TM scores resulting from all-against-all structural alignment, for better visualization the x-axis was sorted by hierarchical clustering (right). Variants highlighted in pink were used for *in plant* tests, cluster size refers to Diamond DeepClust clusters. B) Example of co-expression of RPP1 and ATR1 variants in *Nicotiana tabacum*, 3 dpi. $RPP1^{WsB}$ in combination with $ATR1^{Emoy2}$ served as positive control. C) *Arabidopsis thaliana* Gel-1 leaves infiltrated with Pf0-1 delivering a negative control

(AvrRPS4N-HA), a positive control (AvrRPS4N-AvrRpt2-HA) or the ATR1^{Emoy2} effector (AvrRPS2N-ATR1^{Emoy2}-HA). Numbers indicate the fraction of leaves with wilting symptoms 3 dpi. Infiltrations were repeated at least three times with 12-20 leaves each.

3.4.4 Identification of truncated RPP1 variants

In the initial Miniprot-based search for RPP1 homologs, we identified 395 that lacked TIR, NB-ARC or LRR domains or were shorter than 1,000 amino acids, usually because of drastically reduced LRR repeats (see above). We will refer to such unusual RPP1 proteins as ‘truncated’.

Truncated RPP1 homologs were encoded in the genomes of 190 (of 262) accessions, with up to eight truncated RPP1s encoded in a single genome. On average, each genome encoded 6 RPP1 homologs, of which approximately 25% were truncated (Figure 3.5 A). The most common architecture among truncated RPP1 homologs was TIR/NB-ARC, lacking the entire LRRs and C-JID (138 proteins) and TIR-only (117 proteins).

To assess whether TIR-only forms might be autoactive, we asked whether they had the K98R, I100F, or K228S substitutions previously reported to induce autoactivity in experimentally truncated RPP1 variants (Schreiber et al., 2016b). 43 TIR-only proteins, or about one third, contained either K98R, I100F, K228S, or a combination of these (Figure 3.5 B). In the TIR/NB-ARC proteins, this was the case for an even higher fraction, 48/177. It is therefore not unlikely that many of the truncated proteins could be autoactive – if they are indeed expressed.

One accession encoding several truncated RPP1 proteins is Gel-1. The *RPP1* locus in this accession encodes an NB-ARC only variant (in region B), two TIR-only variants and a TIR/NB-ARC/C-JID variant (in Region C). One of the TIR-only variant carries the K98R and I100F substitutions associated with autoactivity (Figure 3.5 C).

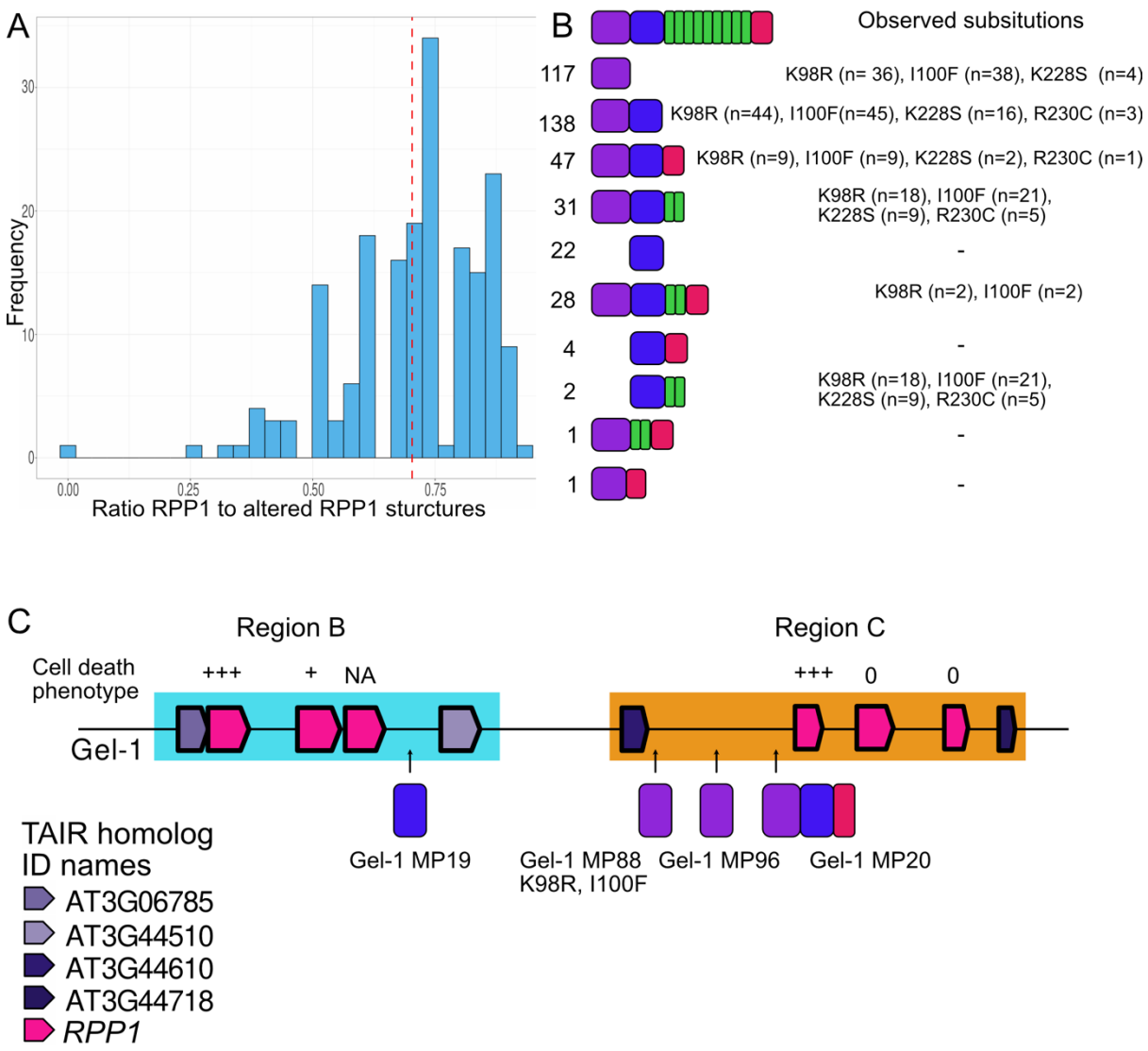

Figure 3.5: **Truncated RPP1 variants.** A) Fraction of truncated RPP1 homologs in each accession (red line indicates average). B) Diagram of domain architectures and presence of substitutions associated before with autoactivity. C) Left part of the *RPP1* locus highlighting genes encoding truncated RPP1 variants. Cell death phenotypes shown on top correspond to results obtained with coexpression with ATR1 variants Emoy2 and/or Cala2 in *N. tabacum* .

3.5 Discussion

We have identified analyzed the genomes of 262 *A. thaliana* accessions, each of which encodes on average five full-length RPP1 proteins, for a total of 1,317 full-length RPP1 proteins corresponding to over 900 unique sequences. Structural modeling and *in planta* assays suggest that many of them are indeed functional proteins. We also describe extensive variation at the *RPP1* locus, including copy number variation and the presence of shorter *RPP1* genes that do not encode all of the canonical RPP1 domains. Our insights provide a new baseline for understanding natural variation of *RPP1* function in pathogen defense and hybrid incompatibility.

RPP1 variants

Numerous studies (Bomblies et al., 2007; Chae et al.; 2014, Tran et al., 2017; Botella et al., 1998; Goritschnig et al., 2016; Rehmany et al., 2005; Schreiber et al., 2016a; Stuttmann et al., 2016; Alcázar et al., 2010; 2014; Tahir et al., 2013; Stuttmann et al., 2016) have identified and described allele-specificity of RPP1 function, and mapped and characterized, through mutational analyses, specific residues required for effector recognition and initiation of a signaling cascade leading to activation of (auto)immunity. This revealed early on that different accessions of *Arabidopsis thaliana* carry different RPP1 repertoires (Botella et al., 1998; Holub et al., 1994; Gordon, 2002; Goritschnig et al., 2016), and also that individual accessions may carry RPP1 variants with different specificities (Chae et al., 2014; Stuttmann et al., 2016; Tran et al., 2017; Alcázar et al., 2010; 2014; Tahir et al., 2013). Our study greatly expands the known RPP1 repertoire of the species and enables future systematic studies of receptor/interactor (effector) specificity, building on natural diversity and taking knowledge of frequency of alleles and their geographic distribution into account.

Evolutionarily meaningful tests of interaction with ATR1 variants of course require a comprehensive collection of natural ATR1 alleles, which is now becoming available through a range-wide collection of *H. arabidopsidis* strains (Rebecca Schwab, pers. communication). We have already tested several RPP1 variants from the Gel-1 accession against over 10 ATR1 alleles from isolates collected across Europe (Supplemental Figure 3.8). Expanding such experimental tests will not only reveal important residues needed for effector recognition, but also reveal the

geographical co-existence or mutual exclusion of RPP1/ATR variants with alternative allele specificities.

Another interesting aspect is the presence of genes encoding RPP1 proteins with altered domain architectures, completely missing TIR, NB-ARC or LRR domains, in more than half of the accessions we have investigated (Figure 3.5). It has been reported (Schreiber et al., 2016) that TIR-only domains can autonomously induce cell death in transient expression assays when carrying particular amino acid substitutions (K98R, I100F, K228S). We identified several such proteins and also observed autoactive full-length alleles from the Gel-1 accession (Figure 3.4B). Systematic studies are needed to reveal whether such non-canonical RPP1 variants may contribute to resistance signaling. Such contribution may be negative, e.g., by preventing the formation of functional RPP1 tetramers or by competing for signaling components (e.g., EDS1 or ADR1/NRG1 modules: Bhandari et al., 2019; Lapin et al., 2020; Stuttmann et al., 2016). A potentially related example comes from the NLR pair RPS4/RRS1-R, where weak autoactivity of RPS4 can be suppressed by RRS1-R (Huh et al., 2017; Wirthmueller et al., 2007). Similarly, other studies have shown that stacking multiple NLRs does not always enhance resistance and can even result in mutual suppression. For instance, the CC-NLR *Pm3* in wheat can interfere with resistance against *Blumeria graminis* f. sp. *tritici* when different *Pm3* alleles are combined (Strinweis et al., 2014). Contributions may also be positive when elevating basal immunity, including through NLR interactions similar to those leading to autoimmunity at low temperatures (Bomblies & Weigel, 2010; Li & Weigel 2021).

The Gel-1 accession encodes four RPP1 proteins that lack at least one functional domain (Figure 3.5C). At the same time, Gel-1 does not respond as expected to an ATR1 effector that one of its RPP1 variants can recognize when the two proteins are taken out of the native context and co-expressed in tobacco (Figure 3.4 B,C). While we currently cannot provide a mechanistic explanation for this observation, interference between RPP1 variants, including those with missing domains, is a possibility that can be tested. As it has been discussed for several crop plants that the LRR domain can suppress immune receptors (Stirnweis et al., 2014; Du et al., 2012). Another explanation could be that relevant alleles are not necessarily expressed, when needed. Given the heterogeneity of *A. thaliana* natural habitats and differential induction of NLR genes upon (a)biotic stresses (Fick et al., 2022; Yang et al., 2021), basal NLR expression may indeed vary considerably between accessions.

RPP1 locus diversity

Genes encoding proteins that lack at least one functional domain must have arisen from full-length copies. Given the high copy number of *RPP1* genes in most *Arabidopsis thaliana* accessions, it is not unexpected to observe a large number of truncated variants. Early studies of the *RPP1* locus reported the presence of truncated genes within the cluster (Goritschnig et al., 2016). Similarly, the *RPP5* resistance locus, another highly polymorphic NLR cluster, was shown to contain truncated gene copies (Noël et al., 1999; Parker et al., 1997). Some of these truncated forms can function as negative regulators of immune signaling, as demonstrated for *RPP5*-related genes (Yang & Hua, 2004). More broadly, genome-wide surveys of natural *Arabidopsis thaliana* accessions have revealed that truncation of NLR genes is a widespread feature (Van de Weyer et al., 2019; Chao et al., 2011). This phenomenon is not restricted to *A. thaliana*; for example, the *Mla* powdery mildew resistance locus in barley also contains truncated NLRs (Seeholzer et al., 2010). Surprisingly, we observed a high level of nucleotide identity at the *RPP1* locus between accessions that are otherwise distantly related across the rest of the genome. This is unexpected given that RPP1 has previously been described as a hypervariable and highly polymorphic NLR (Prigozhin & Krasileva 2021; Lee & Chae 2020) Of particular interest will be accessions that were originally collected at the same place and that are closely related throughout the genome, but that have greatly differed *RPP1* repertoires (see above). These could potentially provide examples for rapid diversification - either through recombination or other mutational processes. Do they lead to differing RPP1 specificities? Do they co-exist with ATR1 effectors that are recognized by different RPP1 receptors? Is ATR1 diversity higher in places with rapidly diversifying RPP1 specificities? These and other questions will help us understand diversification of NLR loci in plant genomes.

3.6 Supplementary Information

Supplementary Table 1, available on Zenodo:

Sheet 1: Total number of *RPP1* in all 262 accessions and their coordinates.

Sheet 2: Calculation of locus size.

Sheet 3: RPP1 domains and their ranks.

Sheet 4: Substitutions and deletions at known residues in RPP1.

Sheet 5: Protein cluster of representatives their TM-Scores and cluster size

Supplementary fasta file: All annotated RPP1 sequences, available on Zenodo:

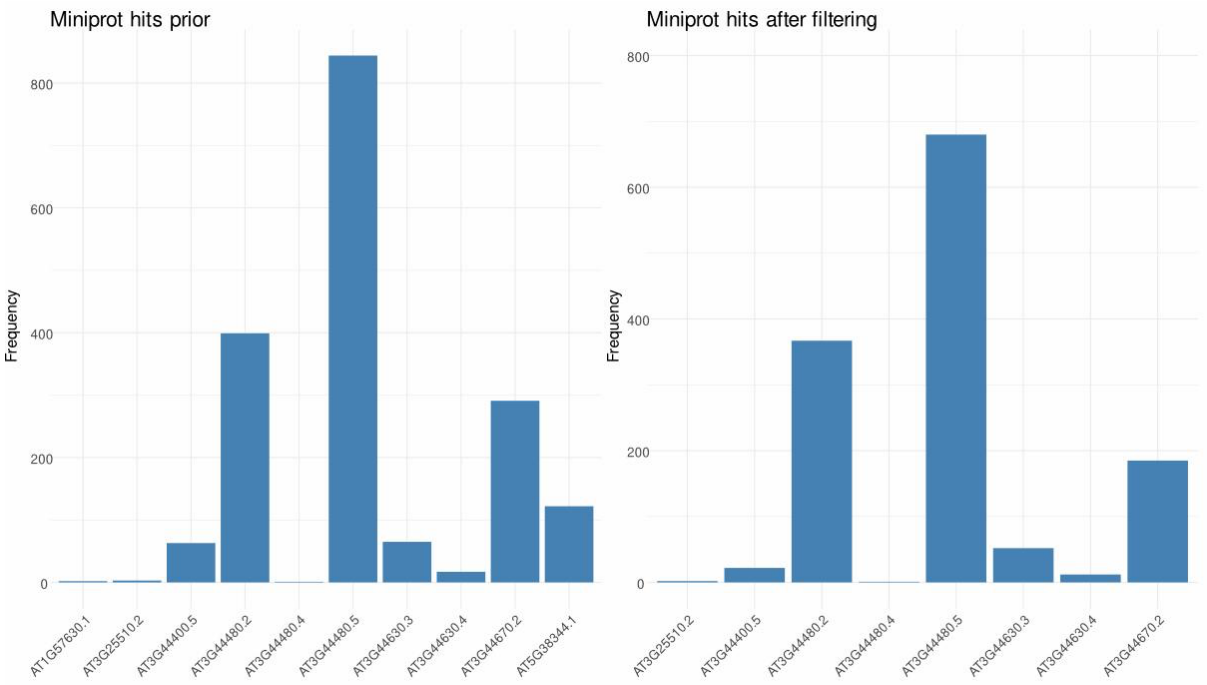

Supplementary Figure 3.1: Validation of annotated RPP1. Diamond blastp of Miniprot v.16 amino acid predicted, after removing sequences shorter than 1000 amino acids, removal of additional mutations within the genome. The two sequences matching AT3G25510.2 are IP-Moa and Tibet. Therefore, these sequences were removed for further analysis

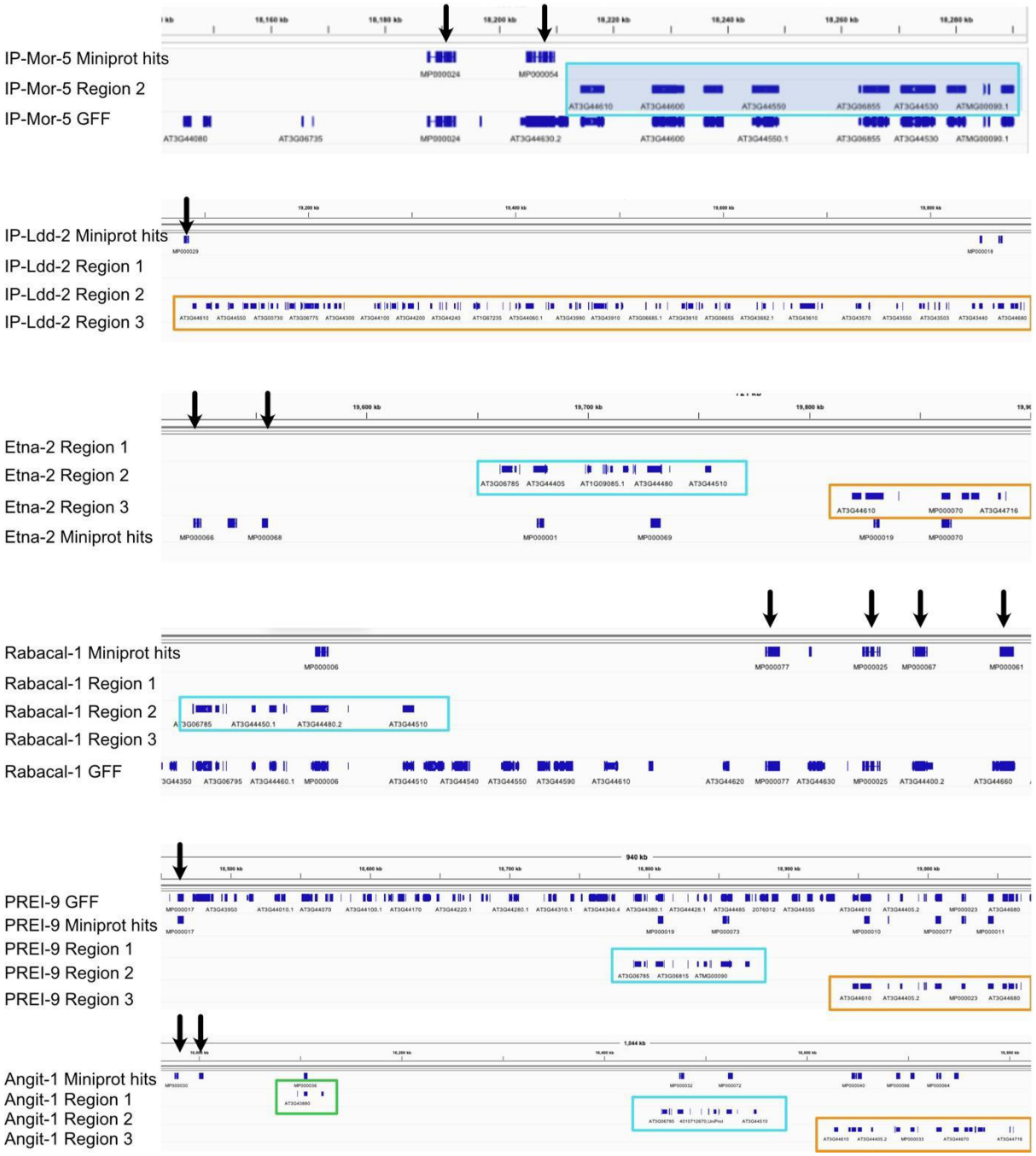

Supplementary Figure 3.2: *RPP1* copies detected outside of the *RPP1* locus. Genomes with *RPP1* adjacent to the anchor genes that define the *RPP1* locus. Arrows indicate Miniprot hits that are not located within the regions A, B, or C. Regions were highlighted in green for region A, blue for region B, and orange for region C.

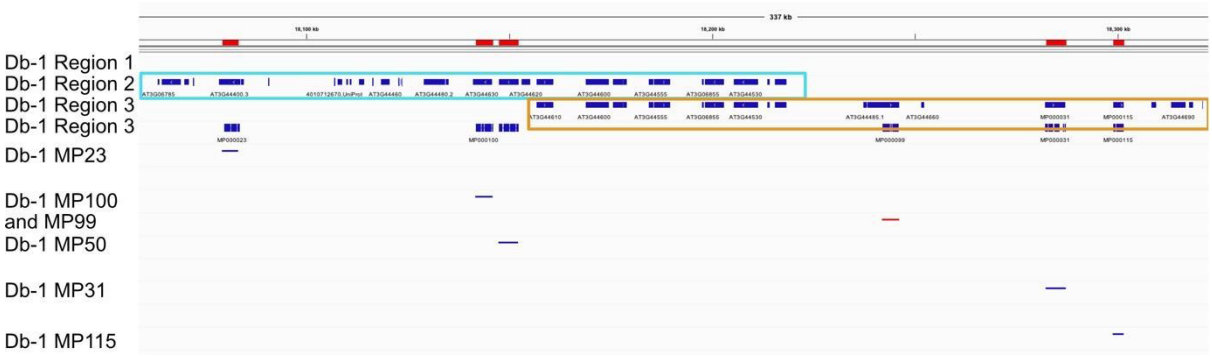

Supplementary Figure 3.3: *RPP1* duplications across different regions of the *RPP1* locus. *RPP1* regions B and C from accession Db-1 visualized in IGV. Highlighted in red are *RPP1* copies. Marked are the regions B and C in blue and orange, respectively. *RPP1-MP100* and *RPP1-MP99* are duplicated between both regions and in region C is a gene inversion of *RPP1-MP99*.

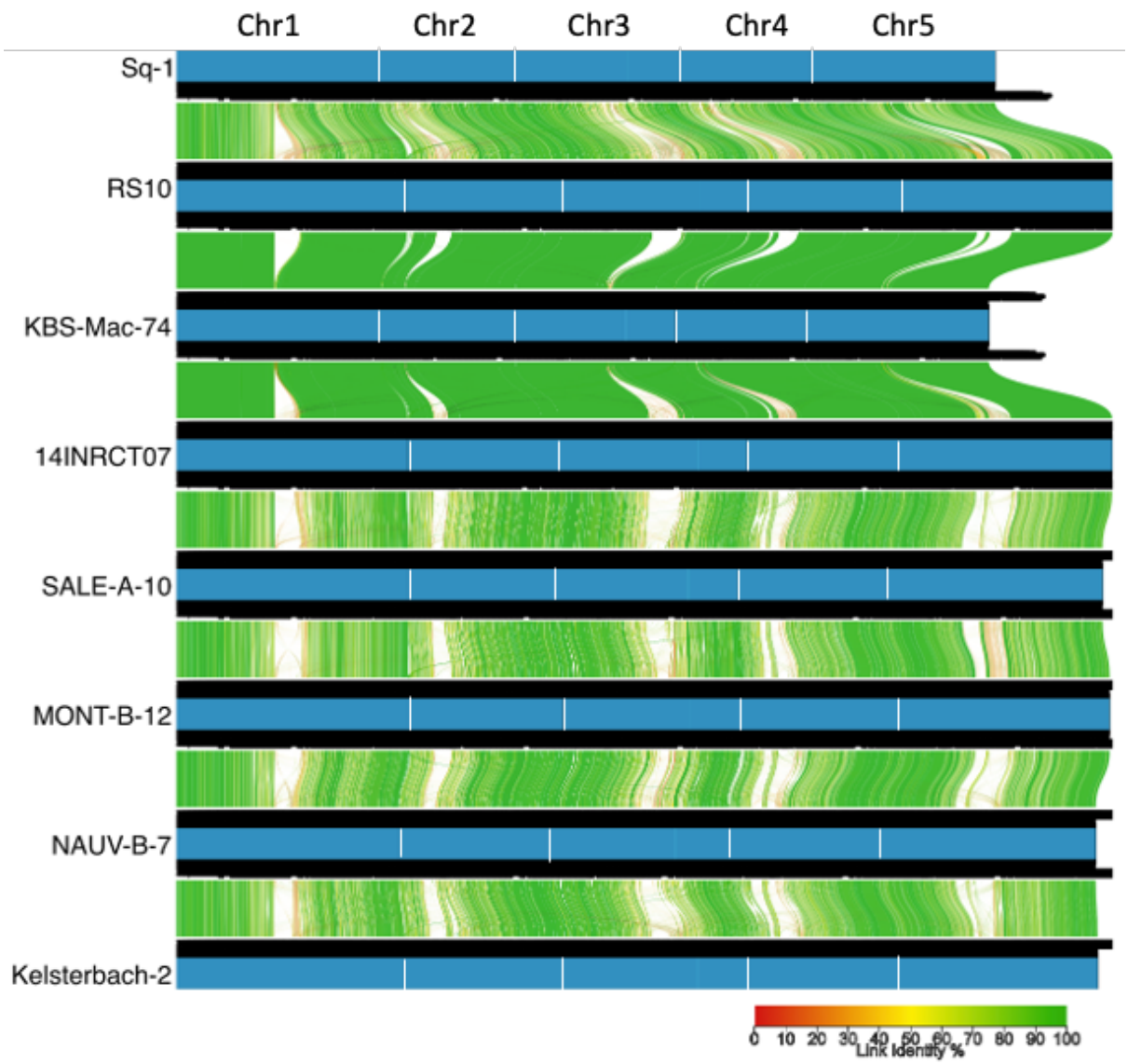

Supplementary Figure 3.4: Whole genome alignments. Selected genome were aligned with minimap2 and visualized in AliView. Sequence differences and similarities are indicated with synteny links ranging from 0 -100 % in identity. White regions without links correspond to centromeres. Chromosomes were marked with black frames and separators in white indicate chromosome breaks.

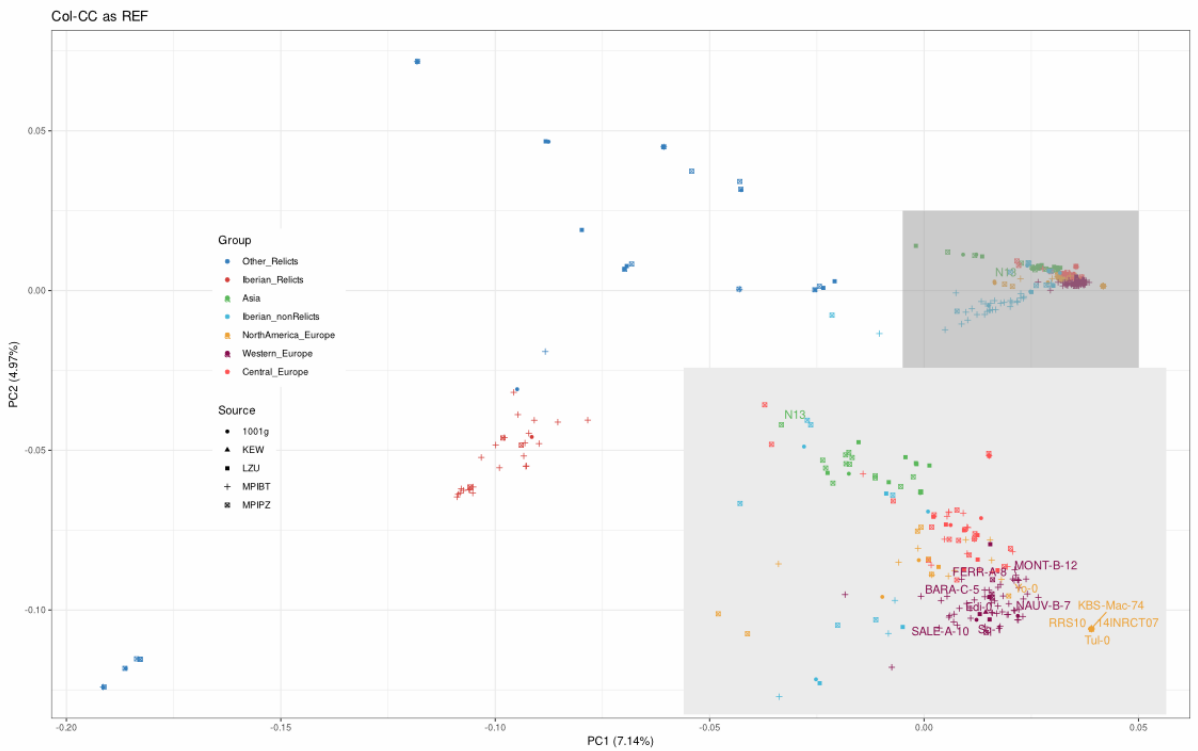

Supplementary Figure 3.5: Diversity of *A. thaliana* genomes used in this stuy. A Principal Component (PC) Analysis was performed based on biallelic SNPs from whole genome alignments of 262 assemblies to the Col-CC reference genome (GCA_028009825.2, TAIR12). Colors indicate previously defined admixture groups (1001 Genomes Consortium 2016), shapes sequencing platforms. BAC, TAIR10 reference genome; ONT-HiFi, hybrid assembly from multiple Col-0 accessions. Highlighted are accessions with similar or identical *RPP1* locus and content (Adapted from Consortium 2024).

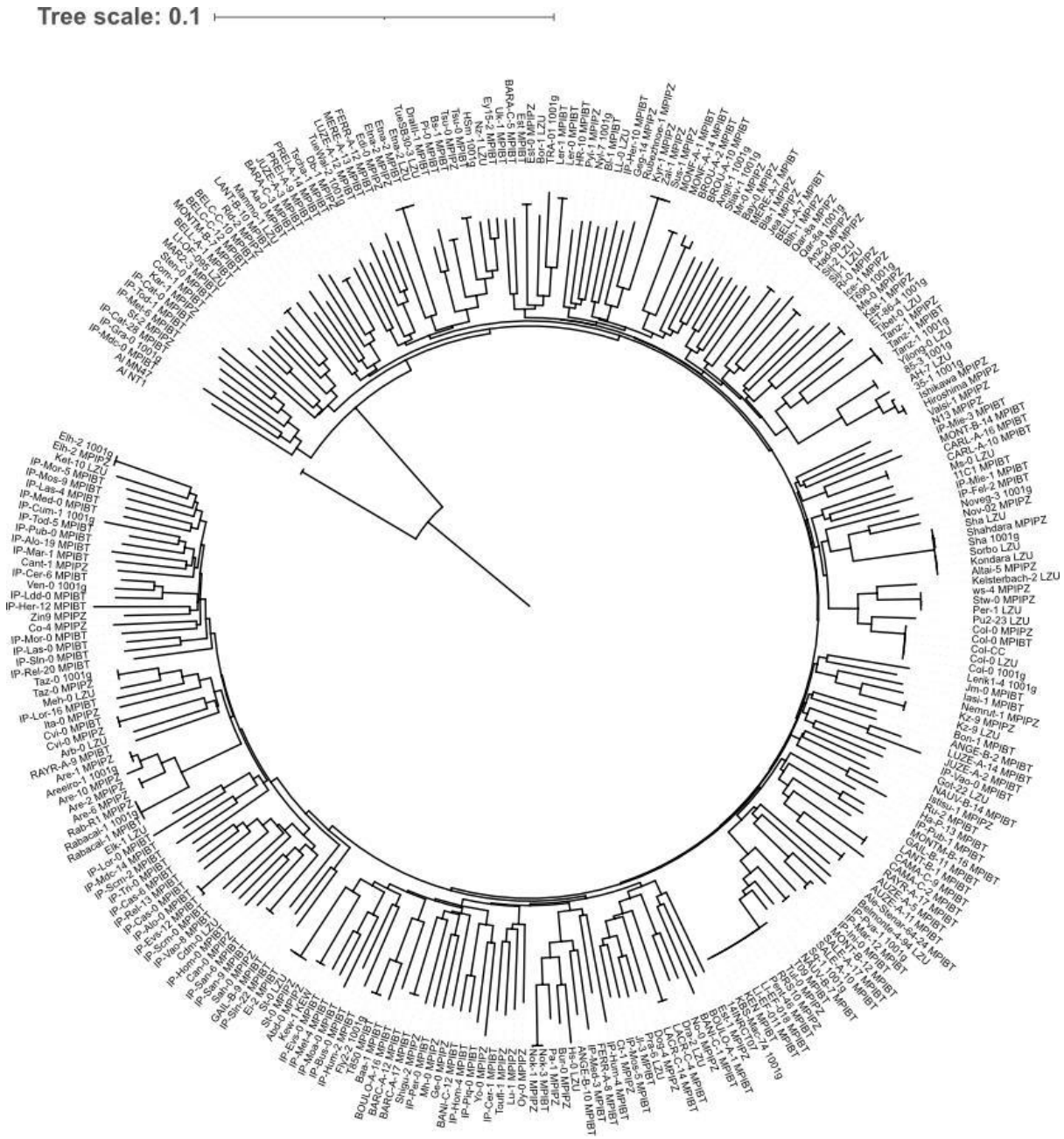

Supplementary Figure 3.6: Locus diversity of *RPP1*. Alignment of *RPP1* locus flanking AT3G43920 and AT4G44880. Included were *A. lyrata* NT1 and *A. lyrata* MN47 as outgroups. Neighbor-Joining tree was visualized with iTOL.

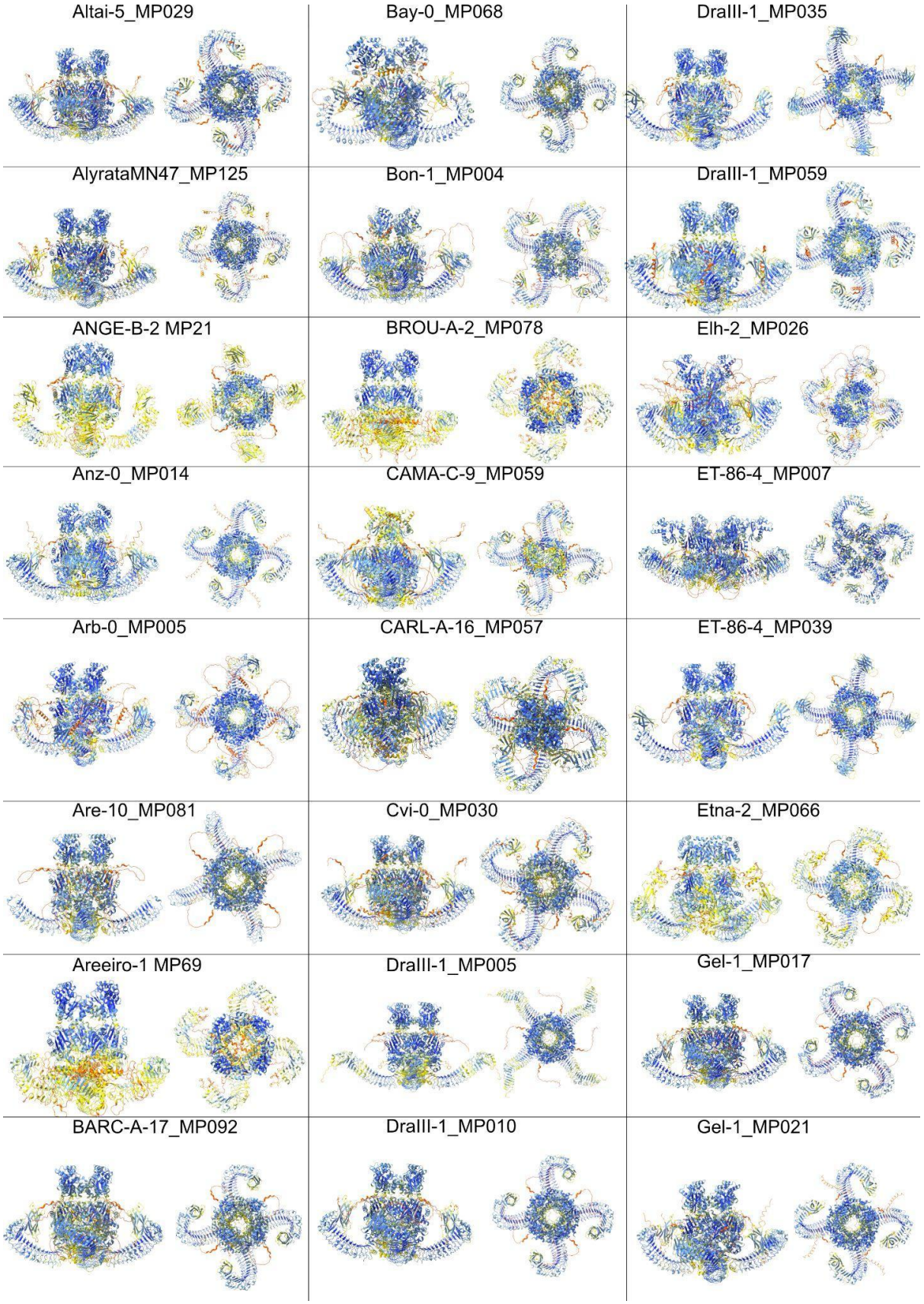
Altai-5_MP029
Bay-0_MP068
DraIII-1_MP035
AlyrataMN47_MP125
Bon-1_MP004
DraIII-1_MP059
ANGE-B-2 MP21
BROU-A-2_MP078
Elh-2_MP026
Anz-0_MP014
CAMA-C-9_MP059
ET-86-4_MP007
Arb-0_MP005
CARL-A-16_MP057
ET-86-4_MP039
Are-10_MP081
Cvi-0_MP030
Etna-2_MP066
Areeiro-1 MP69
DraIII-1_MP005
Gel-1_MP017
BARC-A-17_MP092
DraIII-1_MP010
Gel-1_MP021

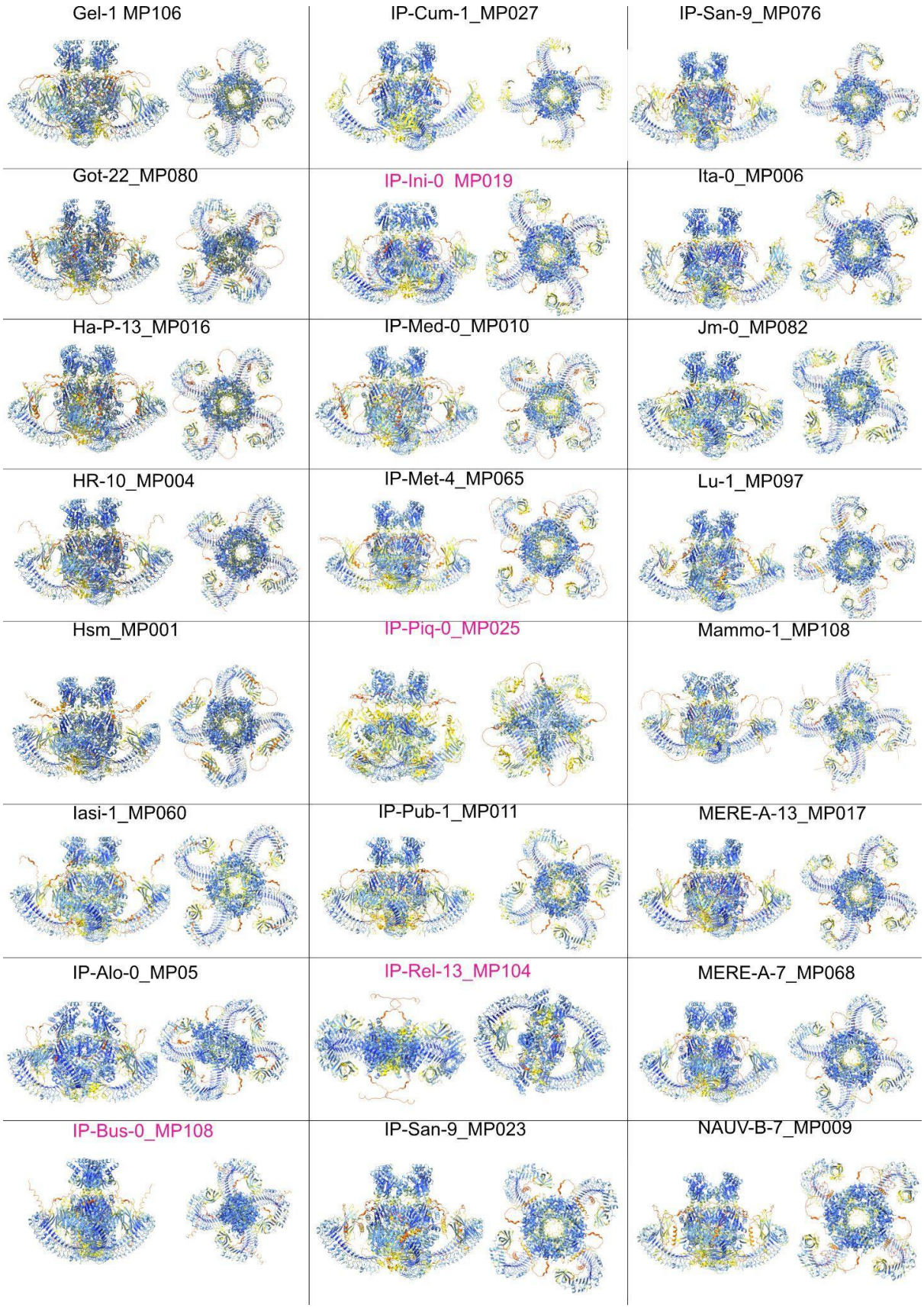
Gel-1 MP106
IP-Cum-1_MP027
IP-San-9_MP076
Got-22_MP080
IP-Ini-0 MP019
Ita-0_MP006
Ha-P-13_MP016
IP-Med-0_MP010
Jm-0_MP082
HR-10_MP004
IP-Met-4_MP065
Lu-1_MP097
Hsm_MP001
IP-Piq-0_MP025
Mammo-1_MP108
Iasi-1_MP060
IP-Pub-1_MP011
MERE-A-13_MP017
IP-Alo-0_MP05
IP-Rel-13_MP104
MERE-A-7_MP068
IP-Bus-0_MP108
IP-San-9_MP023
NAUV-B-7_MP009

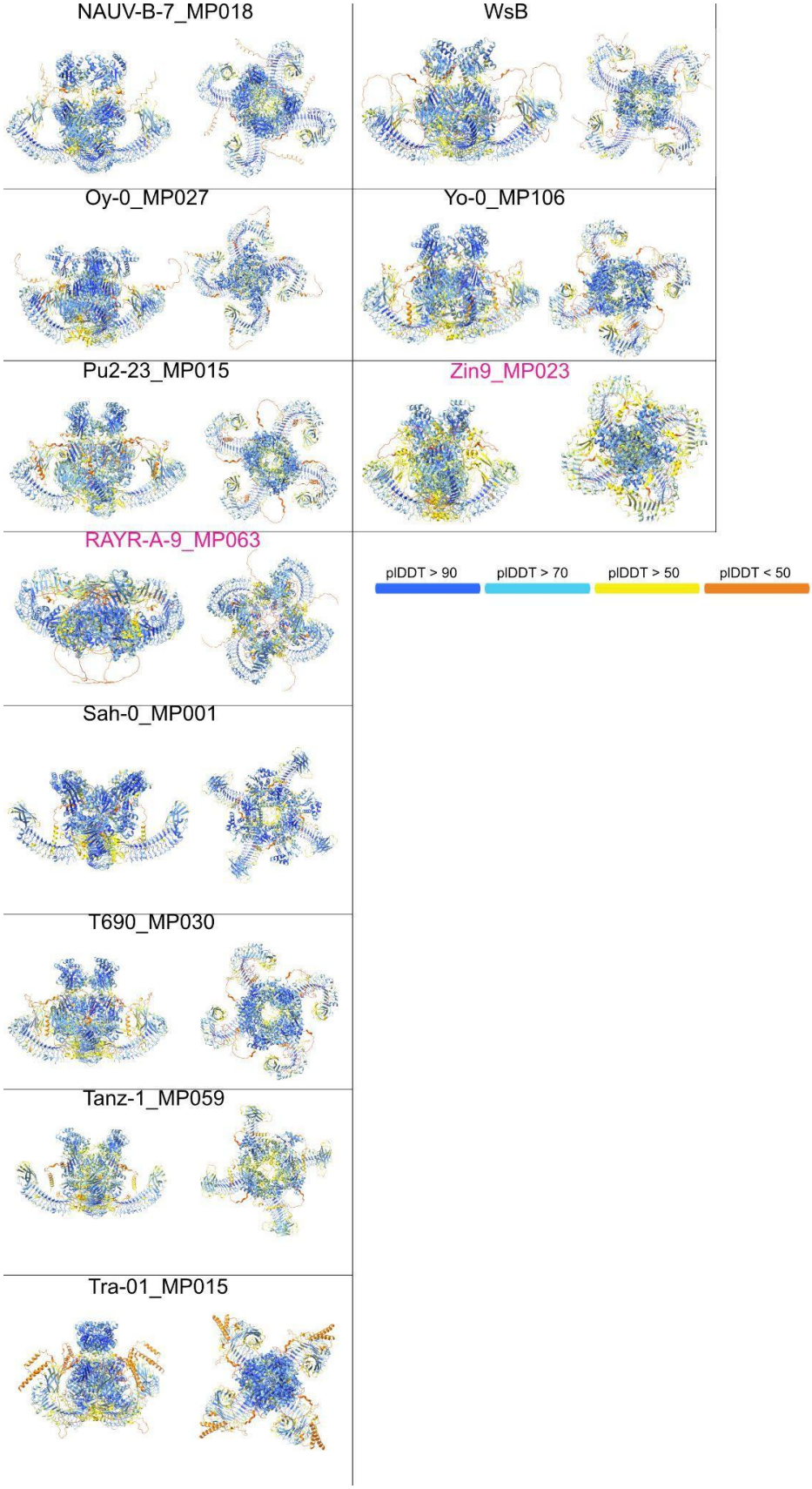

Supplementary Figure 3.7: RPP1 models predicted with AlphaFold3. Structural models of RPP1 representatives were generated using AlphaFold3 to assess model reproducibility,

with the random seed set to 1. Structures are colored by plDDT scores from AlphaFold3 and visualized in ChimeraX.

Supplementary Table 3.2: Resistance and susceptibility of *A. thaliana* accession Gel-1 when infected with different *H. arabidopsidis* isolates. Infections were repeated at least 3 times with 5 - 20 seedlings.

H. arabidopsidis isolates	Gel-1 (R=Resistance; S=Susceptibility)
Cala2	S
Emoy2	S
PH0068-1	S
PH0124-1	S
PH0129-1	S
PH0133-1	S
PH0147-1	S
PH0163-1	S
PH0320-1	S
PH0458-1	R
PH0459-1	S
PH0466-1	S
PH0477-1	S
PH0495-1	S
PH0511-1	S
PH0527-3	S
PH0538	R
PH0566-1	S
PH0682-1	S
PH0708-1	weak S
PH0733-1	R
PH0736	R
PH0745-1	R
PH0883-1	S
PH0885-1	S
PH0900-1	S
PH0919-1	S
PH0920-1	S
PH1032	R
PH1034	S
PH1109-1	S
PH1192	R
PH1199	S

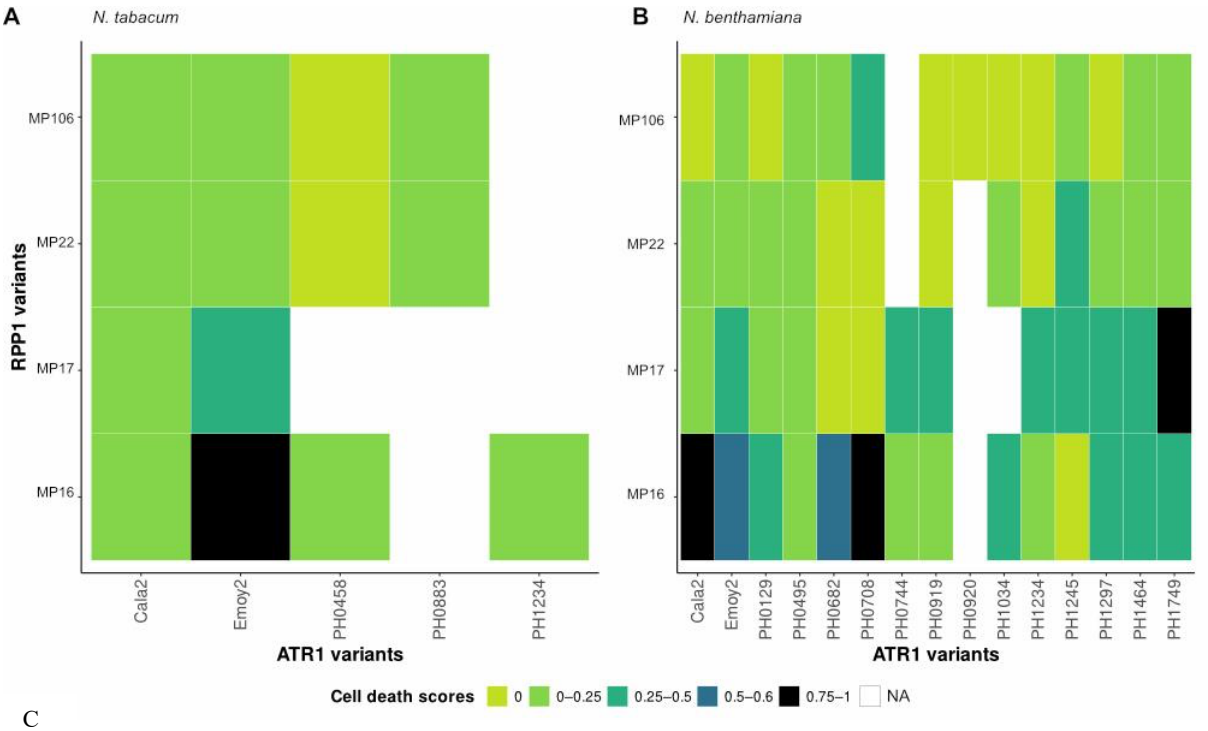

C

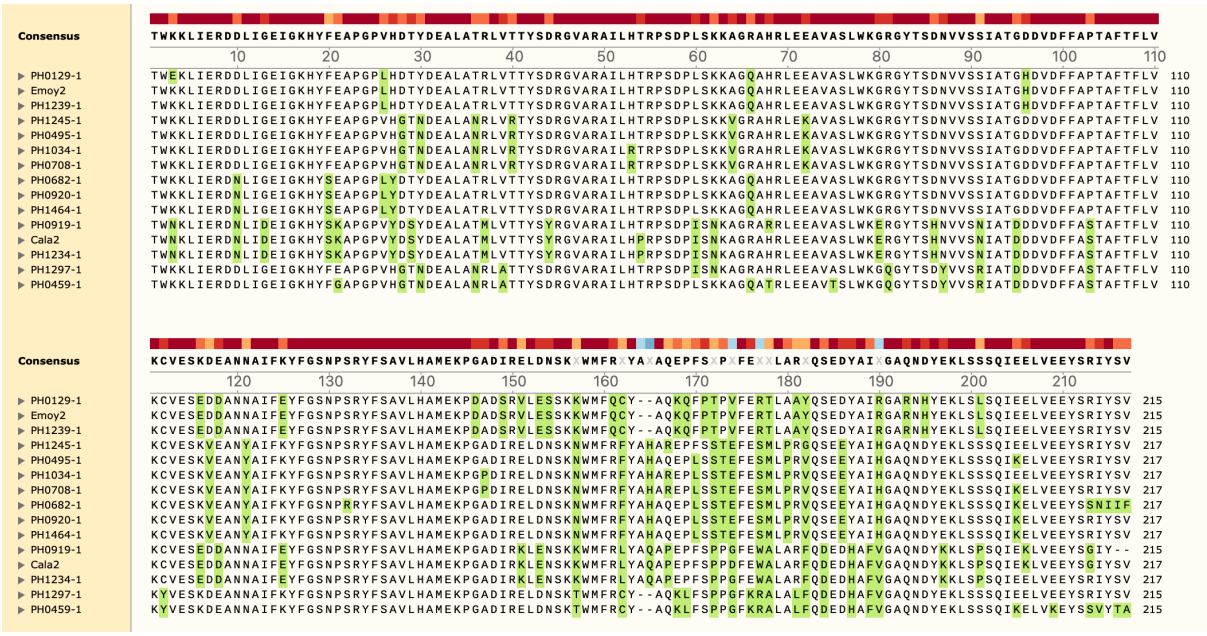

Supplementary Figure 3.8: Results from co-expression of RPP1 and ATR1 variants in *Nicotiana sp*. RPP1 proteins from Gel-1 were co-expressed with different ATR1 variants in (A) *N. tabacum* or (B) *N. benthamiana*, with at least three replicates per experiment. Cell death scores indicate the summarized cell death of each combination. Insufficient replicates or no data indicated in white (NA). C) Protein sequence alignment of tested ATR1 variants, with amino acid variation highlighted in green.

3.7 Material and Methods

Annotation of *RPP1*:

Genomes were initially annotated using Liftoff v2.0 (Shumate & Salzberg, 2021), transferring gene models from the Araport11 reference annotation (Cheng et al., 2016). Protein-coding genes in the *RPP1* locus were further annotated using Miniprot v0.12 (Li, 2023), using in addition to Araport11 sequences RPP1 proteins, excluding truncated copies variants, from 17 genomes with high-quality NLR annotation (Teasdale et al., 2024). Genomes were aligned with Minimap2 (Li, 2021), and results were visualized with GGGenomes (Hackl et al., 2021).

Clustering of RPP1 proteins:

Proteins were clustered with DIAMONDDeepClust with 80% sequence coverage and 80% identity (v.2.1.11 ; Buchfink et al., 2023). Sequences were globally aligned with MAFFT (Katoh et al., 2002). Phylogenetic trees were generated from amino acid sequence alignments with maximum likelihood inferred with an LG substitution model and gamma distribution and constant site rates; with 1,000 bootstraps (v.2.4.0; Minh et al., 2020). Trees were visualized in iTOL (v.5; Letunic & Bork, 2021). RPP1 proteins in *A. lyrata* accessions were annotated as mentioned above and used as outgroups.

AlphaFold predictions and visualization in ChimeraX:

Tetrameric assemblies of RPP1 protein variants were predicted using AlphaFold3 (Abramson et al., 2024), with the random seed fixed at 1 to ensure reproducibility across runs. Structural predictions were performed in multimer mode with the stoichiometry explicitly set to four chains to model tetrameric assemblies. Resulting structures were visualized and analyzed using ChimeraX (v1.8; Meng et al., 2023).

Structure alignments US-align:

Structural models were aligned using the Universal Structural (US) alignment algorithm described by Zhang et al. (2022). Pairwise structural comparisons were performed among all predicted RPP1 models, including self-alignments, using default parameters.

Softwares, visualization and statistics:

Statistical analyses and their visualization used RStudio Pro 2024.04.2 with R v4.4.0 (Hornik and R Core Team; 2024). Read mappings were visualized in IGV v2.15.4 (Robinson et al., 2023). Multiple sequence alignments were visualized in AliView (v1.27.; Larsson, 2014).

Dotplot:

Dotplots were generated with re-DOT-able (v.11.0.12; https://www.bioinformatics.babraham.ac.uk/projects/redotable/). Input sequences were provided as a multifasta file.

LRR annotation:

LRRs in RPP1 proteins from IP-Rel-13 were annotated with LLRpredictor (Martin et al., 2020).

PFAM annotation:

InterProScan (v. 5.75; Blum et al., 2021), was used on all RPP1 proteins with default parameters.

Cloning:

For expression in *Pseudomonas fluorescens* strain Pf0-1 (Thomas et al., 2009; kindly provided by Prof. Thomas Lahaye, Univ. of Tübingen), *ATR1* sequences were PCR-amplified from *H. arabidopsidis* genomic DNA (kindly provided by Dr. Rebecca Schwab and Fiona Paul, MPI Tübingen), without the first 52 codons starting downstream of the RXLR motif ("Δ52-ATR1"; Krasileva et al., 2010). Primers were designed with ~20 bp overlaps complementary to the pre-digested expression vector pLL791 (kindly provided by Dr. Lei Li, MPI Tübingen. Gibson Assembly was performed using the NEB Gibson Assembly Master Mix (Cat. #10229799) according to the manufacturer's protocol. In some cases, half of the recommended Master Mix volume was used to reduce reagent costs. PCR products were assembled into the EcoRI and SalI pre-digested pLL791 backbone, which contains the *avrRps4* promoter, sequences for an N terminal signal peptide from the bacterial effector AvrRps4 (Grassmann et al., 1999), and an HA epitope tag. The assembly reaction was incubated at 50°C for 1 h. Assembled DNA were transformed into *E. coli* DH5α via heat-shock at 42°C for 1 min,

followed by cooling on ice for at least 2 min and recovery in LB medium for continuous shaking at 37°C (Hanahan 1983). Single colonies were picked, grown overnight at 37°C in 2 mL LB, and plasmids were extracted using the GeneJET Plasmid Miniprep Kit (Thermo Fisher, Cat. #K0503). Inserts were confirmed by Sanger sequencing using G-47540, G-47541 primers. Verified pLL791 derivatives were introduced into *P. fluorescens* Pf0-1 via triparental mating. *E. coli* DH5α carrying the *ATR1* construct, the recipient Pf0-1 strain, and the helper strain carrying the pRK2013 plasmid (Hall et al., 2023) were mixed on non-selective LB agar plates and incubated at 28°C for 2 days. Bacterial mixtures were then transferred to selective LB agar plates containing 50 µg/mL kanamycin, 25 µg/mL chloramphenicol, and 50 µg/mL tetracycline. After another 2-day incubation at 28°C, colonies were screened by colony PCR and verified by Sanger sequencing.

For transient co-expression of ATR1 in *Nicotiana* spp., *ATR1* alleles were amplified with the same primers described above and cloned via Gibson Assembly into the SalI- and EcoRI-digested Gateway entry vector pJLBlue (reverse orientation). Verified constructs were subsequently recombined into the Gateway-compatible binary vector pGWB414 using the LR Clonase II enzyme mix (Thermo Fisher, Cat. #11791020), following the manufacturer's instructions. Final constructs were transformed into *Agrobacterium tumefaciens* GV3101 pMP90 (kindly provided by Prof. Jane Parker, Max Planck Institute for Plant Breeding Research) via electroporation at 2.2 kV. Cells were allowed to recover in LB without antibiotics for 2 h at 28°C before plating on selective LB agar containing 50 µg/mL rifampicin, 100 µg/mL spectinomycin, and 25 µg/mL gentamicin. Colonies were verified by colony PCR and sequencing before use in infiltration assays.

Infection assays:

***Nicotiana sp.* infection and protein blot:**

Three- to four-week-old *Nicotiana* spp. plants were used for *Agrobacterium*-mediated transient expression. *Agrobacterium tumefaciens* strain GV3101 pMP90 derivatives were inocula were grown in LB with 100 µg/mL spectinomycin, 25 µg/mL gentamicin, 50 µg/mL rifampicin for overnight at 28°C. Bacteria were harvested by centrifugation at 6,000 rpm (in Eppendorf Microcentrifuge Cat. No. 5424) for 3 min and resuspended by vortexing in infiltration buffer containing 10 mM $MgCl_2$, 10 mM MES/KOH (pH. 5.6) and 150 µM acetosyringone for *N. tabacum* and 150 nMacetosyringone for *N.*

benthamiana. Resupended bacteria were incubated under continuous shaking for at least two more hours in the dark.

For *Nicotiana tabacum* cv. Petite Gerard (kindly provided by Prof. Jonathan Jones, The Sainsbury Laboratory), *A. tumefaciens* suspensions were adjusted to OD_{600} = 0.9 for each construct and mixed 1:1 by thorough vortexing. Prior to syringe infiltration, plants were re-watered to promote stomatal opening. Infiltrations were performed on the abaxial side of the leaf using 1 mL syringes (Braun; Cat. No. H999.1) without needles (Krasileva et al., 2010). Syringe infiltrated plants were maintained in under controlled growth conditions 12h light and dark period, and cell death symptoms were recorded approximately 3 days post-infiltration (dpi).

For *N. benthamiana* (kindly provided Dr. Farid El-Kasmi, Univ. of Tübingen), infiltrations were carried out with *A. tumefaciens* suspensions adjusted to OD_{600} = 0.35 for ATR1 constructs, OD_{600} = 0.75 for RPP1 constructs, and OD_{600} = 0.15 for the silencing suppressor P19 (also kindly provided by Dr. Farid El-Kasmi). Infiltrated plants were maintained in the dark, and cell death symptoms were recorded approximately 3 dpi (Li et al., 2008). For each leaf, a positive and a negative control were included. Up to seven RPP1/ATR1 combinations were tested per leaf, with up to two leaves per plant. If either control failed to produce the expected outcome, results from the corresponding plants were discarded. For all valid experimental batches, the number of leaves exhibiting cell death or no cell death was recorded and normalized by the total number of treated leaves to calculate response frequencies.

For protein analysis, leaf tissue was harvested at 2 dpi and processed for immunoblotting as previously described by Ma and colleagues (Ma et al., 2020). Protein was detected via Western blot using mouse-anti-c-Myc antibody (Sigma, Cat. No. M5546) and goat anti-mouse IgG antibody, peroxidase conjugated, H+L (Sigma, Cat. No. AP124P) for constructs derived from pGWB420::35S-RPP1-Myc, rat-anti-HA-peroxidase-conjugated antibody (Roche, Cat. No. 12013819001) for constructs derived from pGWB414::35S-ATR1-HA.

Pf0-1 infection assay:

Pf0-1 strains, engineered with a functional type III secretion system (Thomas et al., 2009), and carrying AvrRpt2N-ATR1 constructs, were freshly grown on selective LB agar plates. Bacterial cells were harvested and resuspended in 10 mM $MgCl_2$ to an

optical density of OD_{600} = 0.2 for infiltration. Leaves of 5-week-old *A. thaliana* plants were hand-infiltrated using a 1 mL needleless syringe. Plants were incubated for 20–24 hours under short day growth conditions (8 h light and 16 h dark) to assess symptom development, indicated by hypersensitive response (HR)-associated tissue collapse.

Plasmids:

Glycerol name	Species	Insert	Backbone
pML012	*Escherichia coli* DH5α (lab stock)	Δ52-ATR1-Emoy2	pLL791 (lab stock)
pML013	Pf0-1 (Thomas et al., 2009)	Δ52-ATR1-Emoy2	pLL791
pML018	*E.coli* DH5α	Δ52-ATR1-708	pLL791
pML019	Pf0-1	Δ52-ATR1-708	pLL791
pML057	Pf0-1	ev	pLL791
pML072	*E.coli* DH5α	Δ52-ATR1-919	pLL791
pML073	Pf0-1	Δ52-ATR1-919	pLL791
pML080	E.COLI DB3.1	ev	pGW414 (Addgene Cat. No. #74808)
pML087	*E.coli* DH5α	Δ90-ATR1-708	pJLBlue (R) (lab stock)
pML177	*Pst*. DC3000	ev	pLL791
pML181	*Pst* DC3000	Δ52-ATR1-919	pLL791
pML183	*E.coli* DH5α	RPP1-WsB	pGWB414
pML186	DC3000	Δ52-ATR1-708	pLL791
pML190	*A. tumefaciens* GV3101 pMP90	RPP1-WsB	pGWB420 (Addgene Cat. No. #74814)
pML241	*E.coli* DH5α	Δ52-ATR1-919	pJLBlue (R)
pML273	*E.coli* DH5α	RPP1-MP16-Gel1	pGenDONR (lab stock)
pML274	*E.coli* DH5α	RPP1-MP17-Gel-1	pGenDONR
pML279	*E.coli* DH5α	RPP1-MP21-Gel-1	pGenDONR
pML281	*E.coli* DH5α	RPP1-MP22-Gel-1	pGenDONR
pML282	*E.coli* DH5α	RPP1-MP106-Gel-1	pGenDONR
pML288	*E.coli* DH5α	RPP1-MP16-Gel1	pGWB420
pML289	*E.coli* DH5α	RPP1-MP17-Gel-1	pGWB420
pML294	*E.coli* DH5α	RPP1-MP21-Gel-1	pGWB420
pML296	*E.coli* DH5α	RPP1-MP22-Gel-1	pGWB420
pML297	*E.coli* DH5α	RPP1-MP106-Gel-1	pGWB420
pML303	*A. tumefaciens* GV3101 pMP90	RPP1-MP16-Gel1	pGWB420
pML304	*A. tumefaciens* GV3101 pMP90	RPP1-MP17-Gel-1	pGWB420

pML309	*A. tumefaciens* GV3101 pMP90	RPP1-MP21-Gel-1	pGWB420
pML311	*A. tumefaciens* GV3101 pMP90	RPP1-MP22-Gel-1	pGWB420
pML312	*A. tumefaciens* GV3101 pMP90	RPP1-MP106-Gel-1	pGWB420
pML465	*A. tumefaciens* GV3101 pMP90	Δ52-ATR1-Cala2	pGWB414
pML466	*A. tumefaciens* GV3101 pMP90	Δ52-ATR1-Emoy2	pGWB414
pML467	*A. tumefaciens* GV3101 pMP90	Δ52-ATR1-708	pGWB414
pML470	*A. tumefaciens* GV3101 pMP90	Δ52-ATR1-919	pGWB414
pML472	*A. tumefaciens* GV3101 pMP90	Δ52-ATR1-1297	pGWB414
pML474	*Pst* Dc3000	Δ52-ATR1-Emoy2	pLL791
pML475	*Pst* Dc3000	Δ52-ATR1-Cala2	pLL791
pML476	*Pst* Dc3000	Δ52-ATR1-919	pLL791
pML477	*E.coli* NEB beta	Δ52-ATR1-458	pGWB414
pML478	*Pst* Dc3000	Δ52-ATR1-458	pLL791

List of used oligos:

Name	Sequence 5‘ → 3‘	Purpose
G-47540	CGCTTCGAGTTTCCTCATTC	*ATR1* amplification forward
G-47541	TCAGCTCCTGAACCTGAGTG	*ATR1* amplification reverse
G-47869	attgggcggaggtaaacgag GTCGAC TTCGGGCGTTGAG	pLL791 cloning
G-47870	ctggtacgtcgtacggatag GAATTC AACAGAATATATTCTCGAATACTCTTCCACGAGTTCCTC	pLL791 cloning
G-47976	attgggcggaggtaaacgag GTCGAC TCAATCGGGCGTTGAGAG	Δ52 *ATR1* amplification forward

G-48404	attgggcggaggtaaacgagAGACAGCTCTCGATGACG	*ATR1* amplification forward for pJLblue cloning
G-48405	ctggtacgtcgtacggatagAACAGAATATATTCTCGAATACTCTTCCAC	*ATR1* amplification reverse for pJLblue cloning

3.8 References

Abramson, J., Adler, J., Dunger, J., Evans, R., Green, T., Pritzel, A., Ronneberger, O., Willmore, L., Ballard, A. J., Bambrick, J., Bodenstein, S. W., Evans, D. A., Hung, C. C., O'Neill, M., Reiman, D., Tunyasuvunakool, K., Wu, Z., Žemgulytė, A., Arvaniti, E., … Jumper, J. M. (2024). Accurate structure prediction of biomolecular interactions with AlphaFold 3. *Nature*, *630*(8016), 493–500. https://doi.org/10.1038/S41586-024-07487-W;TECHMETA=139,141;SUBJMETA=114,1305,154,2411,535,631;KWRD=DRUG+DISCOVERY,MACHINE+LEARNING,PROTEIN+STRUCTURE+PREDICTIONS,STRUCTURAL+BIOLOGY

Alcázar, R., García, A. V., Parker, J. E., & Reymond, M. (2009). Incremental steps toward incompatibility revealed by Arabidopsis epistatic interactions modulating salicylic acid pathway activation. *Proceedings of the National Academy of Sciences of the United States of America*, *106*(1), 334–339. https://doi.org/10.1073/PNAS.0811734106,

Alcázar, R., von Reth, M., Bautor, J., Chae, E., Weigel, D., Koornneef, M., & Parker, J. E. (2014). Analysis of a Plant Complex Resistance Gene Locus Underlying Immune-Related Hybrid Incompatibility and Its Occurrence in Nature. *PLoS Genetics*, *10*(12), e1004848. https://doi.org/10.1371/JOURNAL.PGEN.1004848

Alonso-Blanco, C., Andrade, J., Becker, C., Bemm, F., Bergelson, J., Borgwardt, K. M. M., Cao, J., Chae, E., Dezwaan, T. M. M., Ding, W., Ecker, J. R. R., Exposito-Alonso, M., Farlow, A., Fitz, J., Gan, X., Grimm, D. G. G., Hancock, A. M. M., Henz, S. R. R., Holm, S., … Zhou, X. (2016). 1,135 Genomes Reveal the Global Pattern of Polymorphism in Arabidopsis thaliana. *Cell*, *166*(2), 481–491. https://doi.org/10.1016/J.CELL.2016.05.063/ATTACHMENT/D2E3D704-8EE7-4B34-B59C-81F2B4C47148/MMC2.PDF

Baumgarten, A., Cannon, S., Spangler, R., & May, G. (2003). Genome-level evolution of resistance genes in Arabidopsis thaliana. *Genetics*, *165*(1), 309–319. https://doi.org/10.1093/GENETICS/165.1.309,

Bernoux, M., Ve, T., Williams, S., Warren, C., Hatters, D., Valkov, E., Zhang, X., Ellis, J. G., Kobe, B., & Dodds, P. N. (2011). Structural and Functional Analysis of a Plant Resistance Protein TIR Domain Reveals Interfaces for Self-Association, Signaling, and Autoregulation. *Cell Host & Microbe*, *9*(3), 200. https://doi.org/10.1016/J.CHOM.2011.02.009

Bhandari, D. D., Lapin, D., Kracher, B., von Born, P., Bautor, J., Niefind, K., & Parker, J. E. (2019). An EDS1 heterodimer signalling surface enforces timely reprogramming of immunity genes in Arabidopsis. *Nature Communications 2019 10:1*, *10*(1), 1–13. https://doi.org/10.1038/s41467-019-08783-0

Bittner-Eddy, P., Can, C., Gunn, N., Pinel, M., Tör, M., Crute, I., Holub, E. B., & Beynon, J. (1999). Genetic and physical mapping of the RPP13 locus, in arabidopsis, responsible for specific recognition of several Peronospora parasitica (downy mildew) isolates. *Molecular Plant-Microbe Interactions*, *12*(9), 792–802. https://doi.org/10.1094/MPMI.1999.12.9.792

Blum, M., Chang, H. Y., Chuguransky, S., Grego, T., Kandasaamy, S., Mitchell, A., Nuka, G., Paysan-Lafosse, T., Qureshi, M., Raj, S., Richardson, L., Salazar, G. A., Williams, L., Bork, P., Bridge, A., Gough, J., Haft, D. H., Letunic, I., Marchler-Bauer, A., … Finn, R. D. (2021). The InterPro protein families and domains database: 20 years on. *Nucleic Acids Research*, *49*(D1), D344–D354. https://doi.org/10.1093/NAR/GKAA977

Bomblies, K., Lempe, J., Epple, P., Warthmann, N., Lanz, C., Dangl, J. L., & Weigel, D. (2007). Autoimmune response as a mechanism for a Dobzhansky-Muller-type incompatibility syndrome in plants. *PLoS Biology*, *5*(9), 1962–1972. https://doi.org/10.1371/JOURNAL.PBIO.0050236,

Bomblies, K., & Weigel, D. (2010). Arabidopsis and relatives as models for the study of genetic and genomic incompatibilities. *Philosophical Transactions of the Royal Society B: Biological Sciences*, *365*(1547), 1815–1823.

Botella, M. A., Parker, J. E., Frost, L. N., Bittner-Eddy, P. D., Beynon, J. L., Daniels, M. J., Holub, E. B., & Jones, J. D. G. (1998). Three Genes of the Arabidopsis RPP1 Complex Resistance Locus Recognize Distinct Peronospora parasitica Avirulence Determinants. *Source: The Plant Cell*, *10*(11), 1847–1860. https://www.jstor.org/stable/3870908

Buchfink, B., Ashkenazy, H., Reuter, K., Kennedy, J. A., & Drost, H.-G. (2023). Sensitive clustering of protein sequences at tree-of-life scale using DIAMOND DeepClust. *BioRxiv*, 2023.01.24.525373. https://doi.org/10.1101/2023.01.24.525373

Chae, E., Bomblies, K., Kim, S. T., Karelina, D., Zaidem, M., Ossowski, S., Martín-Pizarro, C., Laitinen, R. A. E., Rowan, B. A., Tenenboim, H., Lechner, S., Demar, M., Habring-Müller, A., Lanz, C., Rätsch, G., & Weigel, D. (2014). Species-wide genetic incompatibility analysis identifies immune genes as hot spots of deleterious epistasis. *Cell*, *159*(6), 1341–1351.

https://doi.org/10.1016/J.CELL.2014.10.049/ATTACHMENT/1B93A1DE-43E2-489C-84DB-A9394536DD73/MMC3.PDF
Cao, J., Schneeberger, K., Ossowski, S., Günther, T., Bender, S., Fitz, J., Koenig, D., Lanz, C., Stegle, O., Lippert, C., Wang, X., Ott, F., Müller, J., Alonso-Blanco, C., Borgwardt, K., Schmid, K. J., & Weigel, D. (2011). Whole-genome sequencing of multiple Arabidopsis thaliana populations. *Nature Genetics*, *43*(10), 956–965. https://doi.org/10.1038/NG.911;SUBJMETA=1870,1948,208,2491,514,631;KWRD=DNA+SEQUENCING,NATURAL+VARIATION+IN+PLANTS
Cheng, C. Y., Krishnakumar, V., Chan, A. P., Thibaud-Nissen, F., Schobel, S., & Town, C. D. (2017). Araport11: a complete reannotation of the Arabidopsis thaliana reference genome. *The Plant Journal*, *89*(4), 789–804. https://doi.org/10.1111/TPJ.13415
Chou, S., Krasileva, K. V., Holton, J. M., Steinbrenner, A. D., Alber, T., & Staskawicz, B. J. (2011). Hyaloperonospora arabidopsidis ATR1 effector is a repeat protein with distributed recognition surfaces. *Proceedings of the National Academy of Sciences of the United States of America*, *108*(32), 13323–13328. https://doi.org/10.1073/PNAS.1109791108/SUPPL_FILE/SM01.AVI
Consortium, T. 1001 G. P., Alonso-Blanco, C. C., Ashkenazy, H., Baduel, P., Bao, Z., Becker, C., Caillieux, E., Colot, V., Crosbie, D., Oliveira, L. De, Fitz, J., Fritschi, K., Grigoreva, E., Guo, Y., Habring, A., Henderson, I., Hou, X.-H., Hu, Y., Igolkina, A., … Xian, W. (2024). The 1001G+ project: A curated collection of Arabidopsis thaliana long-read genome assemblies to advance plant research. *BioRxiv*, 2024.12.23.629943. https://doi.org/10.1101/2024.12.23.629943
Du, X., Miao, M., Ma, X., Liu, Y., Kuhl, J. C., Martin, G. B., & Xiao, F. (2012). Plant Programmed Cell Death Caused by an Autoactive Form of Prf Is Suppressed by Co-Expression of the Prf LRR Domain. *Molecular Plant*, *5*(5), 1058–1067. https://doi.org/10.1093/MP/SSS014
Exposito-Alonso, M., Becker, C., Schuenemann, V. J., Reiter, E., Setzer, C., Slovak, R., Brachi, B., Hagmann, J., Grimm, D. G., Chen, J., Busch, W., Bergelson, J., Ness, R. W., Krause, J., Burbano, H. A., & Weigel, D. (2018). The rate and potential relevance of new mutations in a colonizing plant lineage. *PLOS Genetics*, *14*(2), e1007155. https://doi.org/10.1371/JOURNAL.PGEN.1007155
Fick, A., Swart, V., & van den Berg, N. (2022). The Ups and Downs of Plant NLR Expression During Pathogen Infection. *Frontiers in Plant Science*, *13*, 921148. https://doi.org/10.3389/FPLS.2022.921148
Ghifari, A. S., Teixeira, P. F., Kmiec, B., Pružinská, A., Glaser, E., & Murcha, M. W. (2020). A mitochondrial prolyl aminopeptidase PAP2 releases N-terminal proline and regulates proline homeostasis during stress response. *Plant Journal*, *104*(5), 1182–1194. https://doi.org/10.1111/TPJ.14987,
Goritschnig, S., Krasileva, K. V., Dahlbeck, D., & Staskawicz, B. J. (2012). Computational prediction and molecular characterization of an oomycete effector and the cognate arabidopsis resistance gene. *PLoS Genetics*, *8*(2). https://doi.org/10.1371/JOURNAL.PGEN.1002502
Goritschnig, S., Steinbrenner, A. D., Grunwald, D. J., & Staskawicz, B. J. (2016). Structurally distinct Arabidopsis thaliana NLR immune receptors recognize tandem WY domains of an oomycete effector. *New Phytologist*, *210*(3), 984–996. https://doi.org/10.1111/NPH.13823
Gassmann, W., Hinsch, M. E., & Staskawicz, B. J. (1999). The Arabidopsis RPS4 bacterial-resistance gene is a member of the TIR-NBS-LRR family of disease-resistance genes. *Plant Journal*, *20*(3), 265–277. https://doi.org/10.1046/J.1365-313X.1999.T01-1-00600.X,
Hackl, T., Duponchel, S., Barenhoff, K., Weinmann, A., & Fischer, M. G. (2021). Virophages and retrotransposons colonize the genomes of a heterotrophic flagellate. *ELife*, *10*. https://doi.org/10.7554/ELIFE.72674
Hall, A., Donohue, T., & Peters, J. (2023). Complete sequences of conjugal helper plasmids pRK2013 and pEVS104. *MicroPublication Biology*, *2023*, 10.17912/micropub.biology.000882. https://doi.org/10.17912/MICROPUB.BIOLOGY.000882
Hanahan, D. (1983). Studies on transformation of Escherichia coli with plasmids. *Journal of Molecular Biology*, *166*(4), 557–580. https://doi.org/10.1016/S0022-2836(83)80284-8,
Holub, E. B., & Beynon, J. L. (1997). Symbiology of Mouse-Ear Cress (Arabidopsis Thaliana) and Oomycetes. *Advances in Botanical Research*, *24*(C), 227–273. https://doi.org/10.1016/S0065-2296(08)60075-0
Huh, S. U., Cevik, V., Ding, P., Duxbury, Z., Ma, Y., Tomlinson, L., Sarris, P. F., & Jones, J. D. G. (2017). Protein-protein interactions in the RPS4/RRS1 immune receptor complex. *PLOS Pathogens*, *13*(5), e1006376. https://doi.org/10.1371/JOURNAL.PPAT.1006376
Jiao, W. B., & Schneeberger, K. (2020). Chromosome-level assemblies of multiple Arabidopsis genomes reveal hotspots of rearrangements with altered evolutionary dynamics. *Nature Communications 2020 11:1*, *11*(1), 1–10. https://doi.org/10.1038/s41467-020-14779-y

Kang, M., Wu, H., Liu, H., Liu, W., Zhu, M., Han, Y., Liu, W., Chen, C., Song, Y., Tan, L., Yin, K., Zhao, Y., Yan, Z., Lou, S., Zan, Y., & Liu, J. (2023). The pan-genome and local adaptation of Arabidopsis thaliana. *Nature Communications 2023 14:1*, *14*(1), 1–14. https://doi.org/10.1038/s41467-023-42029-4

Katoh, K., Misawa, K., Kuma, K. I., & Miyata, T. (2002). MAFFT: A novel method for rapid multiple sequence alignment based on fast Fourier transform. *Nucleic Acids Research*, *30*(14), 3059–3066. https://doi.org/10.1093/NAR/GKF436,

Kee, H. S., Lei, R., Nemri, A., & Jones, J. D. G. (2007). The Downy Mildew Effector Proteins ATR1 and ATR13 Promote Disease Susceptibility in Arabidopsis thaliana. *The Plant Cell*, *19*(12), 4077. https://doi.org/10.1105/TPC.107.054262

Kolesnikova, U. K., Scott, A. D., Van de Velde, J. D., Burns, R., Tikhomirov, N. P., Pfordt, U., Clarke, A. C., Yant, L., Seregin, A. P., Vekemans, X., Laurent, S., & Novikova, P. (2023). Transition to Self-compatibility Associated With Dominant S-allele in a Diploid Siberian Progenitor of Allotetraploid Arabidopsis kamchatica Revealed by Arabidopsis lyrata Genomes. *Molecular Biology and Evolution*, *40*(7), msad122. https://doi.org/10.1093/MOLBEV/MSAD122

Krasileva, K. V., Dahlbeck, D., & Staskawicz, B. J. (2010). Activation of an Arabidopsis Resistance Protein Is Specified by the in Planta Association of Its Leucine-Rich Repeat Domain with the Cognate Oomycete Effector. *The Plant Cell*, *22*(7), 2444. https://doi.org/10.1105/TPC.110.075358

Krasileva, K. V., Zheng, C., Leonelli, L., Goritschnig, S., Dahlbeck, D., & Staskawicz, B. J. (2011). Global Analysis of Arabidopsis/Downy Mildew Interactions Reveals Prevalence of Incomplete Resistance and Rapid Evolution of Pathogen Recognition. *PLoS ONE*, *6*(12), e28765. https://doi.org/10.1371/JOURNAL.PONE.0028765

Larsson, A. (2014). AliView: a fast and lightweight alignment viewer and editor for large datasets. *Bioinformatics*, *30*(22), 3276. https://doi.org/10.1093/BIOINFORMATICS/BTU531

Lapin, D., Bhandari, D. D., & Parker, J. E. (2020). Origins and Immunity Networking Functions of EDS1 Family Proteins. *Annual Review of Phytopathology*, *58*, 253–276. https://doi.org/10.1146/ANNUREV-PHYTO-010820-012840,

Lee, R. R. Q., & Chae, E. (2020). Variation Patterns of NLR Clusters in Arabidopsis thaliana Genomes. *Plant Communications*, *1*(4). https://doi.org/10.1016/J.XPLC.2020.100089/ATTACHMENT/563A9114-FAE2-4CF7-A0CC-D8E0C253BE61/MMC3.PDF

Leister, D. (2004). Tandem and segmental gene duplication and recombination in the evolution of plant disease resistance genes. *Trends in Genetics*, *20*(3), 116–122. https://doi.org/10.1016/j.tig.2004.01.007

Letunic, I., & Bork, P. (2021). Interactive tree of life (iTOL) v5: An online tool for phylogenetic tree display and annotation. *Nucleic Acids Research*, *49*(W1), W293–W296. https://doi.org/10.1093/NAR/GKAB301,

Li, L., & Weigel, D. (2021). One Hundred Years of Hybrid Necrosis: Hybrid Autoimmunity as a Window into the Mechanisms and Evolution of Plant-Pathogen Interactions. *Annual Review of Phytopathology*, *59*, 213–237. https://doi.org/10.1146/ANNUREV-PHYTO-020620-114826,

Li, H. (2021). New strategies to improve minimap2 alignment accuracy. *Bioinformatics*, *37*(23), 4572–4574. https://doi.org/10.1093/BIOINFORMATICS/BTAB705

Li, H. (2023). Protein-to-genome alignment with miniprot. *Bioinformatics*, *39*(1). https://doi.org/10.1093/BIOINFORMATICS/BTAD014,

Li, X., Chanroj, S., Wu, Z., Romanowsky, S. M., Harper, J. F., & Sze, H. (2008). A distinct endosomal Ca2+/Mn2+ pump affects root growth through the secretory process. *Plant Physiology*, *147*(4), 1675–1689. https://doi.org/10.1104/PP.108.119909,

Lian, Q., Huettel, B., Walkemeier, B., Mayjonade, B., Lopez-Roques, C., Gil, L., Roux, F., Schneeberger, K., & Mercier, R. (2024). A pan-genome of 69 Arabidopsis thaliana accessions reveals a conserved genome structure throughout the global species range. *Nature Genetics 2024 56:5*, *56*(5), 982–991. https://doi.org/10.1038/s41588-024-01715-9

Ma, S., Lapin, D., Liu, L., Sun, Y., Song, W., Zhang, X., Logemann, E., Yu, D., Wang, J., Jirschitzka, J., Han, Z., Schulze-Lefert, P., Parker, J. E., & Chai, J. (2020). Direct pathogen-induced assembly of an NLR immune receptor complex to form a holoenzyme. *Science*, *370*(6521). https://doi.org/10.1126/SCIENCE.ABE3069/SUPPL_FILE/ABE3069_REPRODUCIBILITY_CHECKLIST.PDF

Martin, E. C., Sukarta, O. C. A., Spiridon, L., Grigore, L. G., Constantinescu, V., Tacutu, R., Goverse, A., & Petrescu, A. J. (2020). Lrrpredictor—a new LRR motif detection method for irregular motifs of plant NLR proteins using an ensemble of classifiers. *Genes*, *11*(3). https://doi.org/10.3390/GENES11030286,

McDowell, J. M., Dhandaydham, M., Long, T. A., Aarts, M. G. M., Goff, S., Holub, E. B., & Dangl, J. L. (1998). Intragenic recombination and diversifying selection contribute to the evolution of downy mildew resistance at the RPP8 locus of Arabidopsis. *The Plant Cell*, *10*(11), 1861. https://doi.org/10.1105/TPC.10.11.1861

Meng, E. C., Goddard, T. D., Pettersen, E. F., Couch, G. S., Pearson, Z. J., Morris, J. H., & Ferrin, T. E. (2023). UCSF ChimeraX: Tools for structure building and analysis. *Protein Science*, *32*(11), e4792. https://doi.org/10.1002/PRO.4792

Meyers, B. C., Kozik, A., Griego, A., Kuang, H., & Michelmore, R. W. (2003). Genome-Wide Analysis of NBS-LRR–Encoding Genes in Arabidopsis. *The Plant Cell*, *15*(4), 809. https://doi.org/10.1105/TPC.009308

Minh, B. Q., Schmidt, H. A., Chernomor, O., Schrempf, D., Woodhams, M. D., Von Haeseler, A., Lanfear, R., & Teeling, E. (2020). IQ-TREE 2: New Models and Efficient Methods for Phylogenetic Inference in the Genomic Era. *Molecular Biology and Evolution*, *37*(5), 1530–1534. https://doi.org/10.1093/MOLBEV/MSAA015,

Nemri, A., Atwell, S., Tarone, A. M., Huang, Y. S., Zhao, K., Studholme, D. J., Nordborg, M., & Jones, J. D. G. (2010). Genome-wide survey of Arabidopsis natural variation in downy mildew resistance using combined association and linkage mapping. *Proceedings of the National Academy of Sciences of the United States of America*, *107*(22), 10302–10307. https://doi.org/10.1073/PNAS.0913160107/SUPPL_FILE/PNAS.200913160SI.PDF

Noël, L., Moores, T. L., Van Der Biezen, E. A., Parniske, M., Daniels, M. J., Parker, J. E., & Jones, J. D. G. (1999). Pronounced Intraspecific Haplotype Divergence at the RPP5 Complex Disease Resistance Locus of Arabidopsis. *The Plant Cell*, *11*(11), 2099–2111. https://doi.org/10.1105/TPC.11.11.2099

Ordon, J., Martin, P., Erickson, J. L., Ferik, F., Balcke, G., Bonas, U., & Stuttmann, J. (2021). Disentangling cause and consequence: genetic dissection of the DANGEROUS MIX2 risk locus, and activation of the DM2h NLR in autoimmunity. *The Plant Journal*, *106*(4), 1008–1023. https://doi.org/10.1111/TPJ.15215

Parker, J. E., Coleman, M. J., Szabò, V., Frost, L. N., S~hmidt, R., Van Der Biezen, E. A., Moores, T., Dean, C., Daniels, M. J., & Jonesal4, J. D. G. (1997). The Arabidopsis Downy Mildew Resistance Gene RPPS Shares Similarity to the Toll and Interleukin-I Receptors with N and L6. *The Plant Cell*, *9*, 879–894. https://academic.oup.com/plcell/article/9/6/879/5986402

Rehmany, A. P., Gordon, A., Rose, L. E., Allen, R. L., Armstrong, M. R., Whisson, S. C., Kamoun, S., Tyler, B. M., Birch, P. R. J., & Beynon, J. L. (2005). Differential recognition of highly divergent downy mildew avirulence gene alleles by RPP1 resistance genes from two Arabidopsis lines. *Plant Cell*, *17*(6), 1839–1850. https://doi.org/10.1105/TPC.105.031807,

Reignault, P., Frost, L. N., Richardson, H., Daniels, M. J., Jones, J. D. G., & Parker, J. E. (1996). Four Arabidopsis RPP loci controlling resistance to the Noco2 isolate of Peronospora parasitica map to regions known to contain other RPP recognition specificities. *Molecular Plant-Microbe Interactions*, *9*(6), 464–473. https://doi.org/10.1094/MPMI-9-0464

Robinson, J. T., Thorvaldsdottir, H., Turner, D., & Mesirov, J. P. (2023). igv.js: an embeddable JavaScript implementation of the Integrative Genomics Viewer (IGV). *Bioinformatics*, *39*(1). https://doi.org/10.1093/BIOINFORMATICS/BTAC830,

Schreiber, K. J., Bentham, A., Williams, S. J., Kobe, B., & Staskawicz, B. J. (2016a). Multiple Domain Associations within the Arabidopsis Immune Receptor RPP1 Regulate the Activation of Programmed Cell Death. *PLOS Pathogens*, *12*(7), e1005769. https://doi.org/10.1371/journal.ppat.1005769

Schreiber, K. J., Bentham, A., Williams, S. J., Kobe, B., & Staskawicz, B. J. (2016b). Multiple Domain Associations within the Arabidopsis Immune Receptor RPP1 Regulate the Activation of Programmed Cell Death. *PLoS Pathogens*, *12*(7), e1005769. https://doi.org/10.1371/JOURNAL.PPAT.1005769

Seeholzer, S., Tsuchimatsu, T., Jordan, T., Bieri, S., Pajonk, S., Yang, W., Jahoor, A., Shimizu, K. K., Keller, B., & Schulze-Lefert, P. (2010). Diversity at the Mla powdery mildew resistance locus from cultivated barley reveals sites of positive selection. *Molecular Plant-Microbe Interactions*, *23*(4), 497–509. https://doi.org/10.1094/MPMI-23-4-0497/SUPPL_FILE/MPMI-23-4-0497E6.PDF

Simão, F. A., Waterhouse, R. M., Ioannidis, P., Kriventseva, E. V., & Zdobnov, E. M. (2015). BUSCO: assessing genome assembly and annotation completeness with single-copy orthologs. *Bioinformatics*, *31*(19), 3210–3212. https://doi.org/10.1093/BIOINFORMATICS/BTV351

Shirsekar, G., Devos, J., Latorre, S. M., Blaha, A., Dias, M. Q., Gonz Alez Hernando, A., Lundberg, D. S., Burbano, H. A. A., Fenster, C. B., & Weigel, D. (n.d.). *Multiple Sources of Introduction of North American Arabidopsis thaliana from across Eurasia*. https://doi.org/10.1093/molbev/msab268

Shumate, A., & Salzberg, S. L. (2021). Liftoff: accurate mapping of gene annotations. *Bioinformatics*, *37*(12), 1639–1643. https://doi.org/10.1093/BIOINFORMATICS/BTAA1016

Stirnweis, D., Milani, S. D., Brunner, S., Herren, G., Buchmann, G., Peditto, D., Jordan, T., & Keller, B. (2014). Suppression among alleles encoding nucleotide-binding–leucine-rich repeat resistance proteins interferes with resistance in F1 hybrid and allele-pyramided wheat plants. *The Plant Journal*, *79*(6), 893–903. https://doi.org/10.1111/TPJ.12592

Stuttmann, J., Peine, N., Garcia, A. V., Wagner, C., Choudhury, S. R., Wang, Y., James, G. V., Griebel, T., Alcázar, R., Tsuda, K., Schneeberger, K., & Parker, J. E. (2016). Arabidopsis thaliana DM2h (R8) within the Landsberg RPP1-like Resistance Locus Underlies Three Different Cases of EDS1-Conditioned Autoimmunity. *PLoS Genetics*, *12*(4), e1005990. https://doi.org/10.1371/JOURNAL.PGEN.1005990

Tahir, J., Watanabe, M., Jing, H. C., Hunter, D. A., Tohge, T., Nunes-Nesi, A., Brotman, Y., Fernie, A. R., Hoefgen, R., & Dijkwel, P. P. (2013). Activation of R-mediated innate immunity and disease susceptibility is affected by mutations in a cytosolic O-acetylserine (thiol) lyase in Arabidopsis. *Plant Journal*, *73*(1), 118–130. https://doi.org/10.1111/TPJ.12021,

Teasdale, L. C., Murray, K. D., Collenberg, M., Contreras-Garrido, A., Schlegel, T., van Ess, L., Jüttner, J., Lanz, C., Deusch, O., Fitz, J., Mencia, R., van Velthoven, R., Drost, H.-G., Weigel, D., Shirsekar, G., & Fe, S. (2024). Pangenomic context reveals the extent of intraspecific plant NLR evolution. *BioRxiv*, 2024.09.02.610789. https://doi.org/10.1101/2024.09.02.610789

Thomas, W. J., Thireault, C. A., Kimbrel, J. A., & Chang, J. H. (2009). Recombineering and stable integration of the Pseudomonas syringae pv. syringae 61 hrp/hrc cluster into the genome of the soil bacterium Pseudomonas fluorescens Pf0-1. *Plant Journal*, *60*(5), 919–928. https://doi.org/10.1111/J.1365-313X.2009.03998.X,

Todesco, M., Kim, S. T., Chae, E., Bomblies, K., Zaidem, M., Smith, L. M., Weigel, D., & Laitinen, R. A. E. (2014). Activation of the Arabidopsis thaliana Immune System by Combinations of Common ACD6 Alleles. *PLOS Genetics*, *10*(7), e1004459. https://doi.org/10.1371/JOURNAL.PGEN.1004459

Tran, D. T. N., Chung, E. H., Habring-Müller, A., Demar, M., Schwab, R., Dangl, J. L., Weigel, D., & Chae, E. (2017). Activation of a Plant NLR Complex through Heteromeric Association with an Autoimmune Risk Variant of Another NLR. *Current Biology*, *27*(8), 1148–1160. https://doi.org/10.1016/j.cub.2017.03.018

Van De Weyer, A.-L., Monteiro, F., Furzer, O. J., Dangl, J. L., Weigel, D., & Bemm, F. (2019). A Species-Wide Inventory of NLR Genes and Alleles in Arabidopsis thaliana. *Cell*, *178*, 1260-1272.e14. https://doi.org/10.1016/j.cell.2019.07.038

Wan, W.-L., Kim, G., Kim, N., Tan, Y. Y., Watari, M., Charoennit, N., Lee, R. R. Q., Phang, I. R. K., Wang, J., Liew, Y. Y., Hu, D., Ng, S. K., Zhang, Y., Jang, I.-C., Song, J.-J., & Chae, E. (2025). Structural determinants of DANGEROUS MIX 3, an alpha/beta hydrolase that triggers NLR-mediated genetic incompatibility in plants. *Molecular Cell*, *85*(14), 2776-2795.e8. https://doi.org/10.1016/J.MOLCEL.2025.06.021

Williams, S. J., Sohn, K. H., Wan, L., Bernoux, M., Sarris, P. F., Segonzac, C., Ve, T., Ma, Y., Saucet, S. B., Ericsson, D. J., Casey, L. W., Lonhienne, T., Winzor, D. J., Zhang, X., Coerdt, A., Parker, J. E., Dodds, P. N., Kobe, B., & Jones, J. D. G. (2014). Structural basis for assembly and function of a heterodimeric plant immune receptor. *Science*, *344*(6181), 299–303. https://doi.org/10.1126/SCIENCE.1247357/SUPPL_FILE/WILLIAMS_SM.PDF

Wirthmueller, L., Zhang, Y., Jones, J. D. G., & Parker, J. E. (2007). Nuclear Accumulation of the Arabidopsis Immune Receptor RPS4 Is Necessary for Triggering EDS1-Dependent Defense. *Current Biology*, *17*(23), 2023–2029. https://doi.org/10.1016/j.cub.2007.10.042

Wlodzimierz, P., Rabanal, F. A., Burns, R., Naish, M., Primetis, E., Scott, A., Mandáková, T., Gorringe, N., Tock, A. J., Holland, D., Fritschi, K., Habring, A., Lanz, C., Patel, C., Schlegel, T., Collenberg, M., Mielke, M., Nordborg, M., Roux, F., … Henderson, I. R. (2023). Cycles of satellite and transposon evolution in Arabidopsis centromeres. *Nature 2023 618:7965*, *618*(7965), 557–565. https://doi.org/10.1038/s41586-023-06062-z

Yang, L., Wang, Z., & Hua, J. (2021). A Meta-Analysis Reveals Opposite Effects of Biotic and Abiotic Stresses on Transcript Levels of Arabidopsis Intracellular Immune Receptor Genes. *Frontiers in Plant Science*, *12*, 625729. https://doi.org/10.3389/FPLS.2021.625729/BIBTEX

Yang, S., & Hua, J. (2004). A haplotype-specific Resistance gene regulated by BONZAI1 mediates temperature-dependent growth control in Arabidopsis. *Plant Cell*, *16*(4), 1060–1071. https://doi.org/10.1105/TPC.020479,

Zhang, C., Shine, M., Pyle, A. M., & Zhang, Y. (2022). US-align: universal structure alignments of proteins, nucleic acids, and macromolecular complexes. *Nature Methods*, *19*(9), 1109–1115. https://doi.org/10.1038/S41592-022-01585-1;SUBJMETA=114,631,663,794;KWRD=PROTEIN+ANALYSIS,SOFTWARE

Zhou, T., Wang, Y., Chen, J. Q., Araki, H., Jing, Z., Jiang, K., Shen, J., & Tian, D. (2004). Genome-wide identification of NBS genes in japonica rice reveals significant expansion of divergent non-TIR NBS-LRR genes. *Molecular Genetics and Genomics*, *271*(4), 402–415. https://doi.org/10.1007/S00438-004-0990-Z

4. Concluding remarks

4.1 Outlook

This thesis presents an analysis of *RPP1* diversity and *ATR1* variation, leveraging a large collection of *A. thaliana* long-read genome assemblies for the host, extensive receptor annotation, phylogenetic clustering, and heterologous expression assays with ATR1 variants isolated from a new European-wide collection of *H. arabidopsidis* strains. At the locus level, *RPP1* exhibits extensive presence/absence polymorphisms**,** structural rearrangements, and frequent truncated variants, reflecting enormous genomic complexity and dynamic evolutionary behavior.

Using phylogenetic clustering and AlphaFold-based structural prediction, I selected representative RPP1 variants and tested them for their ability to recognize diverse ATR1 variants. Functional assays revealed that although specific RPP1 variants can recognize ATR1 variants in heterologous systems, these interactions do not necessarily result in clear disease resistance *in planta*. This gap suggests that recognition alone is not sufficient, and additional regulatory or signaling components likely modulate effective immunity, for example, through other effectors or interactions among RPP1 proteins.

While this study reveals substantial diversity in both RPP1 and ATR1, a major unresolved question is how much of this variation is functionally relevant versus evolutionarily neutral. The frequent occurrence of truncated RPP1 variants, structural rearrangements, and presence/absence polymorphisms raises the possibility that a significant portion of the observed diversity may not contribute to pathogen recognition or resistance. Some variants may represent evolutionary byproducts of rapid gene duplication and diversification, without direct functional consequences (Leister 2004; Wang et al., 2011; Bailey et al., 2018). Alternatively, such variants could act as regulatory buffers, dominant-negative modulators, or scaffolds for future adaptive innovation (Yang & Hua, 2004; Cesari et al., 2014). Disentangling functional from neutral diversity will require further work, such as fine-scale expression profiling, mutant analysis, or long-term co-evolution experiments.

The widespread presence of truncated RPP1 variants suggests that full reliance on RPP1-mediated immunity may carry evolutionary costs (Chae et al., 2014; Barragan et al., 2019; Tran et al., 2017). Given the multiple known activation

mechanisms of the DM2/RPP1 resistosome (Tahir et al., 2013; Stuttmann et al.,2016; Lei & Weigel, 2021; Krasileva et al., 2010; Rehmany et al., 2005; Bomblies et al., 2007; Chae et al., 2014; Tran et al., 2017) and the high allelic diversity within the locus, it is plausible that negative regulatory mechanisms may have evolved to minimize fitness costs from inappropriate activation (Figure 4.1).

One hypothesis is that truncated RPP1 variants act as regulators or decoys, suppressing autoimmunity in a manner analogous to the RPS4/RRS1-R NLR pair, where RRS1-R suppresses weak autoactivity of RPS4 (Wirthmueller et al., 2007; Huh et al., 2017). Similarly, examples from wheat demonstrate that co-expression of certain *Pm3* alleles can lead to suppression of resistance, highlighting how NLR interactions can modulate immune responses (Stirnweis et al., 2014). Another hypothesis, given the unknown host target of ATR1, is that ATR1 variants may specifically suppress certain RPP1 variants or interfere directly with their activation. This aligns with findings in other systems, such as the *Phytophthora infestans* effector AVRcap1b, which suppresses the helper NLR SINRC3 in tomato (Seager et al., 2025).

Together, these findings emphasize the complexity of the RPP1–ATR1 immune interaction and illustrate how natural variation**,** domain-specific conservation, and functional redundancy or specialization contribute to plant immunity. This work demonstrates the value of combining comparative genomics**,** structural prediction, and functional assays to dissect immune receptor diversity. Ultimately, it provides a framework for studying complex NLR loci and offers long-term potential to identify productive allele combinations capable of conferring robust resistance through integrated immune responses.

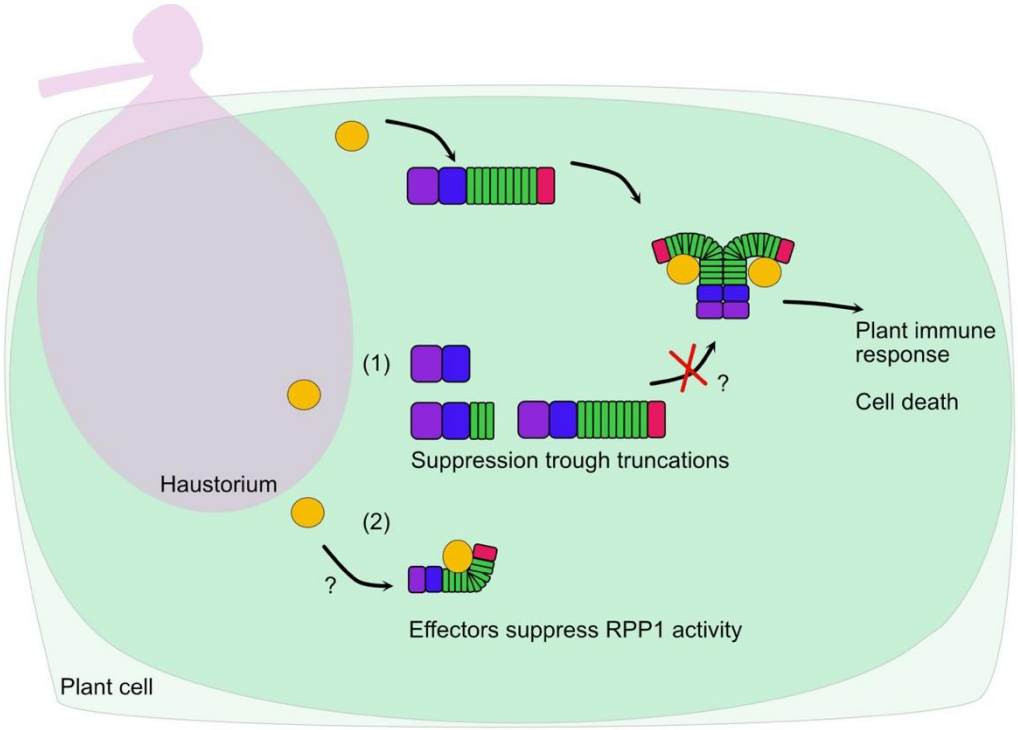

Figure 4.1: Suggested model of ATR1/RPP1 interaction suppression. Upon ATR1 recognition, RPP1 tetramerizes. Induced cell death response is masked through accumulation of RPP1 truncations (1) which could have suppressor roles, via altered RPP1-variants in the downstream response. (2) ATR1 may target RPP1 and therefore suppress the immune receptor.

4.2 Strengths and opportunities

With the currently available genomic resources for both *Hyaloperonospora arabidopsidis* and *Arabidopsis thaliana*, I identified a set of highly polymorphic effector candidates. These candidates can be structurally modeled *in silico* and potentially tested for direct interactions with a broader range of NLR proteins. On the RPP1 side, I presented a panel of representative alleles that can be further investigated for their ability to tetramerize, recognize ATR1 variants, and contribute to pathogen resistance through targeted genetic modification. Additionally, I assembled a geographically local set of *A. thaliana* accessions and corresponding *H. arabidopsidis* isolates, providing a valuable resource for focused studies of *RPP1* locus diversity and its potential trajectories over short evolutionary distances.

4.3 Pitfalls and shortcomings

After identifying potential effector candidates with key roles in plant immune suppression, efficiently testing their functions across a large number of *A. thaliana* accessions remains challenging. While co-expressing different pathogen and host proteins in a heterologous system such as *Nicotiana* species, as demonstrated in this thesis, is feasible, the scale of experiments required can be substantial; for example, my study involved 240 combinations (which was just looking at 15 receptors and 16 effectors), demanding many replicates to achieve robust results. Alternative high-throughput methods have been developed. One such approach uses single plant cells in the form of protoplasts, as described by Arndell and colleagues (Arndell et al., 2024). However, routinely generating protoplasts from diverse *A. thaliana* accessions is difficult due to substantial variation in leaf physiology and architecture across accessions. In my experience, protoplast yield can vary significantly depending on the accession (data not shown), complicating assay standardization.

Another commonly employed method is spray inoculation with *Pseudomonas syringae* pv. tomato (*Pst*) DC3000 derivatives, which allows higher throughput screening with reduced manual labor. Nevertheless, spray inoculation has its limitations; for instance, post-translational modifications in heterologous expression systems can alter the accuracy and functionality of expressed proteins, potentially confounding results (Fabro et al., 2011). Taken together, these considerations highlight the trade-offs between throughput, reproducibility, and biological relevance. Consequently, findings from these assays generally require further validation through complementary approaches. Generally, initial high throughput assays are useful to later focus more specifically on the actual function.